Dear Participants of

15th Conference
INTEGRATED OPTICS - Sensors, Sensing Structures and Methods
IOS'2020

Organizers welcome All of You very cordially in Szczyrk, in the beautiful scenery of the Beskidy Mountains.

We wish all Participants of the Conference IOS'2020 plenty of scientific satisfactions and many professional and social impressions.

Organizers

President of the Conference:	Prof. Tadeusz Pustelny
Treasurer:	Dr eng. Aneta Olszewska
Secretary:	Dr eng. Sabina Drewniak
Members:	Dr eng. Kamil Barczak
	Dr eng. Marcin Procek
	Dr eng. Barbara Pustelny
	Dr eng. Przemysław Struk
	M. Sc. Piotr Kałużyński

This book includes the Program of IOS'2020 and Abstracts of presentations and posters sent by their Authors

CONFERENCE PROGRAMME

INTEGRATED OPTICS - SENSORS, SENSING STRUCTURES and METHODS

Szczyrk 24.02-28.02.2020

24.02.2020 Monday

13:00	***Dinner***
14:30-14:35	**OPENING CEREMONY of the Conferences** **15th IOS'2020** **49th WSW&QA** **48th WSEA&V**
14:35-15:00	**Jubilee Session**
15:00-15:30	*Plenary lecture:* **Integrated Photonics – yesterday, today and tomorrow** <u>R. PIRAMIDOWICZ</u>, S. STOPIŃSKI, A. PAŚNIKOWSKA, M. SŁOWIKOWSKI, A. KAŹMIERCZAK, A. JUSZA, K. ANDERS, W. PLESKACZ, P. SZCZEPAŃSKI
15:30-16:00	*Plenary lecture:* **Nanoparticles-doped photonic liquid crystal fibers for enhanced efficiency of electric field tunability** <u>T. R. WOLIŃSKI</u>, K. BEDNARSKA, D. BUDASZEWSKI, M. CHYCHŁOWSKI, P. LESIAK, B. BARTOSEWICZ, Z.JANKIEWICZ, R.DĄBROWSKI
16:00-16:30	*Plenary lecture:* **Nonlocal Solitons** <u>W. KRÓLIKOWSKI</u>
16:30-17:00	***Coffee break***
17:00-17:20	*Plenary lecture:* **Vortex solitons propagation in planar nematic liquid crystals structures** U. A. LAUDYN, M. KWAŚNY, <u>M. A. KARPIERZ</u>
17:20-17:40	*Invited lecture* **Single-mode ytterbium doped nanostructured core optical fibers for high power laser applications** <u>M. FRANCZYK</u>, D. PYSZ, K. STAWICKI, J. LISOWSKA, A. FILIPKOWSKI, D. MICHALIK, R. STĘPIEŃ, T. OSUCH, M. BIDUŚ, M.DŁUBEK, R. BUCZYŃSKI
17:40-18:00	**Silicon nitride based building blocks for integrated photonics - design, technology and characterization** <u>M. LELIT</u>, M. SŁOWIKOWSKI, A. KAŹMIERCZAK, K. ANDERS, S. STOPIŃSKI, M. JUCHNIEWICZ, B. STONIO, B. MICHALAK, M. FILIPIAK, K. PAVŁOV, P. WIŚNIEWSKI , R. B. BECK, R. PIRAMIDOWICZ
18:30	***Supper***
19:30	**MUSIC GLANCE**

25.02.2020 Tuesday

8:00	***Breakfast***
13:00	***Dinner***
14:30-15:00	*Plenary lecture:* **Twist induced mode confinement in partially open ring of holes** <u>G. STATKIEWICZ-BARABACH</u>, M. NAPIÓRKOWSKI, K. ŻOŁNACZ, M. BERNAŚ, A. KICZOR, P. MERGO, W. URBAŃCZYK
15:00-15:20	*Invited lecture* **Integrated multichannel transmitters for telecom and datacom applications** <u>A. PAŚNIKOWSKA</u>, S. STOPIŃSKI, A. KAŹMIERCZAK, R. PIRAMIDOWICZ
15:20-15:40	**Elimination of outliear and uncertain data in sensing devices aimed for in-situ and environmental use** M. BORECKI, P. PRUS, A. OLEJNIK, J. SZMIDT
15:40-16:00	**Generation optical vortex beam in Liquid media using novel nanostuctured vortex phase masks** <u>H.T NGUYEN</u>, K. SWITKOWSKI, R. KASZTELANIC, A. ANUSZKIEWICZ, A. FILIPKOWSKI, H.V LE, D. PYSZ, R. STEPIEN, W. KROLIKOWSKI, R. BUCZYNSKI
16:00-16:20	**Modeling of self-organized, one-dimensional periodic structures in a gold nanoparticle-doped nematic liquid crystal composite** <u>P. LESIAK</u>, K. BEDNARSKA, A. FRONCZAK, P. FRONCZAK, T. R. WOLIŃSKI
16:20-17:00	***Coffee break***
17:00-17:20	*Invited lecture* **Application of Artificial Intelligence for Optimization of Organic Solar Cells Production Process** <u>G. LO SCIUTO</u>
17:20-17:40	*Invited lecture* **Light depolarization by nematic liquid crystals** <u>P. MARĆ</u>, N. BENNIS, R. WĘGŁOWSKI, A. SPADŁO, K. GARBAT, D. WĘGŁOWSKA, E. PAWLIKOWSKA, A. PAKUŁA, L. R. JAROSZEWICZ
17:40:18:00	**Pattern formation in a gold nanoparticles-doped nematic liquid crystal composite by optical methods** <u>K.BEDNARSKA</u>, P. LESIAK, A.SITKIEWICZ, T.WOLIŃSKI
18:00-18:20	**The practice of accepting gas sensors for commercial purposes** <u>A.PACHOLE</u>
18:20-18:35	**Analysis of energy characteristics of the UV communication system based on LED matrices** <u>G. S. VASILYEV</u>, D. I. SURZHIK, O. R. KUZICHKIN
18:35-18:50	**Performance analysis of MIMO communication system with NLOS UV channel** <u>D. I. SURZHIK</u>, G. S. VASILYEV, O. R. KUZICHKIN
19:30	***Festive Supper (Banquet)***

26.02.2020 Wednesday

8:00	***Breakfast***
13:00	***Dinner***
14:30-15:00	*Plenary lecture:* **Optical properties of achromatic flat-surface gradient index microlenses** R. BUCZYNSKI, A. FILIPKOWSKI, H. T. NGUYEN, D. PYSZ, R. STEPIEN, A. WADDIE, M. R. TAGHIZADEH, R. KASZTELANIC
15:00-15:20	*Invited lecture* **Improvement properties of optical fibers for distributed sensors** P. MERGO, A. PAŹDZIOR, M. MAKARA, K. POTURAJ, G. WÓJCIK, L. CZYŻEWSKA
15:20-15:40	*Invited lecture* **Effect of thermal annealing on sensing properties of optical fiber sensors coated with indium tin oxide nano-overlays** B.MICHALAK, P. SEZEMSKY, V. STRANAK, M. SMIETANA
15:40-16:00	*Invited lecture* **Applicable ultrafast all-optical switching by soliton self-trapping in high index contrast dual-core fiber** M. LONGOBUCCO, P. STAJANČA, L. ČURILLA, D. PYSZ, R. BUCZYŃSKI, I. BUGÁR
16:00-16:20	**Response of a broadband differential interferometer to a change in waveguide thickness** K. GUT
16:20-17:00	***Coffee break***
17:00-17:20	*Invited lecture* **Ultra-dense endoscopic bundles** R. KASZTELANIC, D. PYSZ, R. STEPIEN, R. BUCZYNSKI
17:20-17:40	**Experimental analysis of axial stress distribution in nanostructured core fused silica fibers** A. ANUSZKIEWICZ, M. BIDUS, A. FILIPKOWSKI, D. PYSZ, M. DLUBEK, R. BUCZYNSKI
17:40-18:00	**Methodology for extraction of thin film properties based on semi-analytical optical parameters extraction approach** M. KIELISZCZYK, B. JANASZEK, P. SZCZEPAŃSKI
18:00-18:20	**Optical properties of realistic hyperbolic metamaterials** B. JANASZEK, M. KIELISZCZYK, A. TYSZKA-ZAWADZKA, P. SZCZEPAŃSKI
18:30	***Supper***
19:30-21:00	**POSTER SESSION**

27.02.2020 Thursday

8:00	***Breakfast***
13:00	***Dinner***
14:30-15:00	*Plenary lecture:* **Soft sensor design for measuring liquid volume** <u>K. MURAWSKI</u>
15:00-15:20	*Invited lecture* **The endomicroscopy probe based on micro-interferometer Mirau and 2-axis microscanner fabricated in MOEMS/MEMS technology for SS-OCT imaging** <u>P. STRUK</u>, F. E. GRACIA-RAMIREZ, S. BARGIEL, Q. TANGUY, O. GAIFFE, R. CHUTANI, N. PASSILLY, P. LUTZ, J-M. COTE, H. XIE, C GORECKI
15:20-15:40	**Photonic integrated circuits for portable OTDR systems** <u>S. STOPIŃSKI</u>, K. ANDERS, S. SZOSTAK, R. PIRAMIDOWICZ
15:40-16:00	**Direct ink writing of water-sensitive glass: towards optical application** <u>P.GOŁĘBIEWSKI</u>, B. NAN, R. BUCZYŃSKI, F.J. GALINDO-ROSALES, J.M.F. FERREIRA
16:00-16:20	**ASPIC-based photonic system for monitoring breath/respiratory rate of patient under MRI diagnosis** <u>M. SŁOWIKOWSKI</u>, A. KAŹMIERCZAK, M. BIENIEK, S. SZOSTAK, T. OSUCH, M. KREJ, Ł. DZIUDA, S. STOPIŃSKI, R. PIRAMIDOWICZ
16:20-17:00	***Coffee break***
17:00-17:20	*Invited lecture* **Methodology for measuring the size of gaps with an optical proximity sensor on the example of a centrifugal blood pump** <u>M. GAWLIKOWSKI</u>, P. KURTYKA, J. ZALEWSKI, M. ZARWAŃSKA-DOFFEK, A. KAPIS
17:20-17:40	**Analysis of neural networks parameters for improved face recognition performance** <u>A. GRUDZIEŃ</u>, M. KOWALSKI, N. PAŁKA
17:25-17:40	**Optoelectronic motion tracking system for virtual reality shooting symulator** <u>M. MACIEJEWSKI</u>, M. PISZCZEK, M. POMIANEK, N. PAŁKA
18:00-18:20	**Measurement setup for determination of spectral characteristics of leaves** <u>A. MAZIKOWSKI</u>, M. FELDZENSZTAJN
18:20	***Closing ceremony***
18:30	***Supper***

POSTER SESSION

Application of optical sensor for measurements of lightning strike currents
K. BARCZAK, D. DUDA

Model of the broadband interferometric optical biosensor in the planar configuration
M. BŁAHUT

Optical properties of achromatic flat-surface gradient index microlenses
R. BUCZYNSKI, A. FILIPKOWSKI, H. T. NGUYEN, D. PYSZ, R. STEPIEN, A. WADDIE, M. R. TAGHIZADEH, R. KASZTELANIC

Spectral properties of photonic crystal fibers infiltrated with nanoparticles-doped ferroelectric liquid crystals
D.BUDASZEWSKI, K. WOLIŃSKA, B. JANKIEWICZ, B. BARTOSEWICZ, T. R. WOLIŃSKI

Influence of electric field frequency on optical response of photonic crystal fibers infiltrated with NP-doped liquid crystals
M.S. CHYCHŁOWSKI, B. BARTOSEWICZ, B. JANKIEWICZ, T.R. WOLIŃSKI

Organic lanthanide complexes obtained from the recycling of nickel metal hydride batteries for active optical fiber technology
L. CZYŻEWSKA, M. GIL-KOWALCZYK, D.KOŁODYŃSKA, Z. HUBICKI, P. MERGO

The influence of selected gases on reduced graphene oxides
S. DREWNIAK, M. PROCEK, R. MUZYKA

Purification of tellurite glasses for mid-infrared applications
X. FORESTIER, M. KLIMCZAK, R. BUCZYŃSKI

Optimization of PMMA and PS granulates extrusion process for polymer optical fiber technology
M. JÓŹWICKI, **M. GIL-KOWALCZYK**, M. GARGOL, P. MERGO

The direct laser writing system for mask-based lithography based on confocal microscopy
K. GUT, S. STUDENT

Novel directional coupler utilizing hyperbolic metamaterial: coupled mode formulation by reciprocity
A. TYSZKA-ZAWADZKA, **B. JANASZEK**, M. KIELISZCZYK, P. SZCZEPAŃSKI

Study of sensing properties of UV activated organic-inorganic blend of graft comb copolymer and ZnO nanomaterial for room temperature NO_2 gas sensing applications in ppm and sub-ppm range
P. KAŁUŻYŃSKI, M. PROCEK, A. STOLARCZYK

Optical fiber sensors for rotational seismology – field measurements for data comparability analysis
A. T. KURZYCH, L. R. JAROSZEWICZ, M. DUDEK, J. K. KOWALSKI

Bending loss analysis in silica hollow core antiresonant fibers fabricated with single capillary or nested capillary claddings
B. LOU, G. STĘPNIEWSKI, D. PYSZ, L. ZHAO, R. BUCZYŃSKI, M. KLIMCZAK

Perimeter protection of east EU border rivers

N. PAŁKA, J. MŁYŃCZAK, M. ŻYCZKOWSKI, M. KAROL, **M. MACIEJEWSKI**, M. KOWALSKI, P. MARKOWSKI, M. SZUSTAKOWSKI, K. CICHULSKI, S. BRAWATA, G. GRZECZKA, A. ADAMCZYK

Design of displacement sensor based on Fiber Bragg Grating for long-range extension measurements of pipeline compensators

E. MACIAK, W. KOSTOWSKI, G. GŁUSZEK, D. ADAMECKI, Z. OPILSKI, T. PUSTELNY

Optical fiber distributed sensors in objects subject to conservation protection

A. PAŹDZIOR, **M.Z MAKARA**, J. KOPEĆ, P. MERGO

Fusion splicing and termination of silica hollow core anti-resonant fibers with single mode fibers

Y. MIN, A. FILIPKOWSKI, G. STĘPNIEWSKI, M. KLIMCZAK, L. ZHAO, R. BUCZYŃSKI

Effects of cladding modification tapered optical fiber on optical properties of propagated light

J.MOŚ, K. A. STASIEWICZ, L.R. JAROSZEWICZ

The use of silk fibroin in a fiber optic humidity sensor

Z. OPILSKI, M. PROCEK, M. MAQUEDA, M. BARBEL, S. AZNAR-CERVANTES

The importance of monitoring the vergence eye movements for solutions using virtual technologies

M. PISZCZEK, **M. POMIANEK**, M. MACIEJEWSKI, L. JODŁOWSKI, P. KRUKOWSKI

The stability of the MEMS 2D mirror's operating point in terms of eye tracking systems

M. POMIANEK, M. PISZCZEK, M. MACIEJEWSKI, L. JODŁOWSKI, P. KRUKOWSKI

Sensing applications of LC:PDMS photonic systems

K.A. RUTKOWSKA, P. SOBOTKA, SZ. BACZYŃSKI, K. MARCHLEWICZ, A. DYBKO

Methodology for assessing near-infrared absorption properties of historical materials and microorganisms from objects in the collections of the Auschwitz-Birkenau State Museum in Oświęcim

D. RYBITWA, E. MACIAK, M. PROCEK, P. KAŁUŻYŃSKI, A. WAWRZYK

Fabrication aspects of silicon nitride photonics integrated circuits

M. SŁOWIKOWSKI, M. LELIT, M. JUCHNIEWICZ, B. STONIO, B. MICHALAK, M. FILIPIAK, K. PAVŁOV, P. WIŚNIEWSKI, S. STOPIŃSKI, R. PIRAMIDOWICZ, R. B. BECK

Optical properties of one-dimensional tin oxide nanostructures

W.SMOK, W.MATYSIAK, T. TAŃSKI

Numerical analysis of integrated photonics structures obtained by FDTD method

P. STRUK

Evanescent wave transducers based on grating couplers embossed in silica-titania waveguide films

C. TYSZKIEWICZ, P. KARASIŃSKI, A. KAŹMIERCZAK

Chromatic dispersion engineering in nanostructured graded-index silica fiber tapers for supercontinuum generation

J. ZHOU, A. FILIPKOWSKI, G. STĘPNIEWSKI, D. MICHALIK, M. KLIMCZAK, L. ZHAO, R. BUCZYŃSKI

ABSTRACTS
OF
ORAL PRESENTATIONS

Experimental analysis of axial stress distribution in nanostructured core fused silica fibers

A. ANUSZKIEWICZ[1], M. BIDUS[2], A. FILIPKOWSKI[1], D. PYSZ[1], M. DLUBEK[2], R. BUCZYNSKI[1,3]

[1] Department of Glass, Institute of Electronic Materials Technology, Wolczynska 133, 01-919 Warsaw, Poland

[2] FIBRAIN Sp. z o.o., Zaczernie 190F, 36-062 Zaczernie, Poland

[3] Faculty of Physics, University of Warsaw, Pasteura 5, 02-093 Warsaw, Poland

e-mail address: alicja.anuszkiewicz@itme.edu.pl

Stress present in the optical fiber after drawing is very important parameter as it changes refractive index of glass, which thus has impact on optical properties of the fiber. It also can change mechanical properties and durability of the fiber causing i.e. surface crack growth [1]. The frozen-in stress have disadvantageous impact and is unwanted because of uncontrollable dispersion and bending losses change [2]. It causes also undesired frequency shift in Brillouin scattering media [3] and has adverse impact on long-period grating inscription process [4]. On the other hand, intentionally introduced and well controlled stress is advantageous for highly birefringent optical fibers, widely used for sensing [5] and for telecom, i.e. for polarization-maintaining fibers [6]. To meet the increasing performance demands for the telecommunication, the stress has to be controlled during fiber draw and refractive index changes due to stress presence have to be studied.

The axial stress is well recognized in all-solid fibers. It strongly depends on drawing force [3], resulting in typical stress distributions with tensile stress in the cladding and compressive stress in the core [4]. To the best of our knowledge, the axial stress was not measured for photonic crystal fibers (PCFs), as PCFs are made usually of one glass material and there is no thermal stress caused by differences in glass properties. What is more, hole assisted cladding of PCF is not suitable for typical axial stress measurement methods, which use the immersion. The axial stress also has not been studied for all-solid PCFs with internal microstructure made of at least two glass materials.

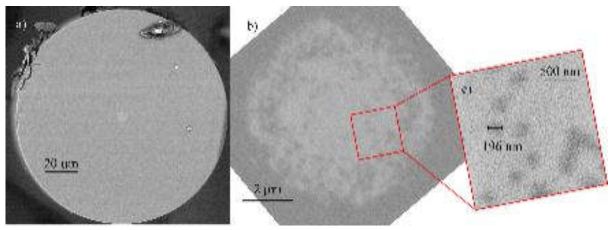

Fig. 1. SEM images of nGRIN fiber: a) full diameter, b) core and c) zoomed core area.

Recently we introduced new type of fiber with nanostructured graded-index core (nGRIN fiber), Fig. 1. This fiber is made of pure fused silica and germanium doped silica rods arranged as to create effectively parabolic refractive index profile [7]. Nanostructuration technique allows to modify with the high degree of freedom the propagation properties of optical fiber with preserved compatibility to optical systems working on conventional telecom fibers, i.e. SMF-28 Corning®.

The core of nGRIN fiber is composed of 2107 rods made of glasses with different refractive indices and different thermal properties. The core structure here is then complex and may introduce unrevealed axial stress distribution after fiber drawing, which may induce change of expected refractive index value and thus influence the performance of the fiber.

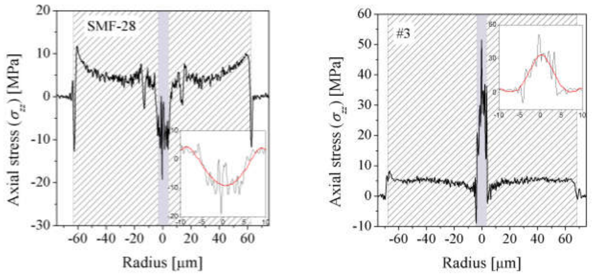

Fig. 2. Axial stress distribution in SMF-28 and in #3 nGRIN fiber. Insets show smoothed compressive stress in the core of SMF-28 and tensile stress in the core of nGRIN fiber.

In this work we present for the first time experimental analysis of axial stress distribution in recently introduced nGRIN fiber [7]. Transverse interferometric method [8] was used to measure stress distribution. Obtained results were compared with reference fiber SMF-28. For nGRIN fibers we proved that the axial stress is purely thermal with negligible contribution of mechanical stress, Fig. 2. In result we observed presence of tensile stress in the fiber core, which is in contrary to a standard telecom fiber, where a compressive stress in the core exists.

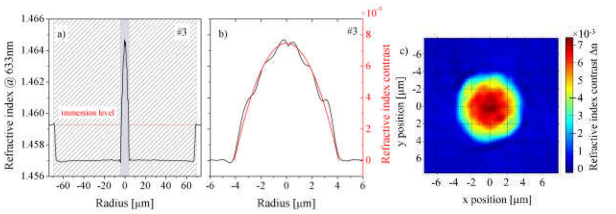

Fig. 3. Refractive index distribution measured at a wavelength of 633 nm in the fiber #3: (a) total profile, (b) zoomed core area and (c) 2D map of RI contrast in the central part of the fiber.

We also showed that measured axial stress has negligible impact on refractive index distribution of nanostructured fibers (Fig. 3), thus it does not affect its performance.

Within this work the origin of an axial stress present in nGRIN fibers was revealed. The obtained results confirm that even for such a complex structure in the core there is no unexpected phenomena causing disadvantageous change in performance of the nGRIN fiber.

As there is no additional limitations caused by residual stress, this kind of structures can be considered for future research and development, which would open new directions for progress in telecom fibers and fiber optics-based devices.

Acknowledgments: This work was supported by Foundation for Polish Science (FNP) (POIR.04.04.00-1C74/16).

References:

[1] P. L. Chu et al., Electronic Letters 20, 11 (1984).
[2] W. Hermann et al., Applied Optics 28, 11 (1989).
[3] Y. Sikali Mamdem et al., Proceedings of IEEE 37th ECOC (2011).
[4] P. Wang et al., Applied Optics 55, 9, (2016).
[5] A. Anuszkiewicz et al., Optics Express 21, 10 (2013).
[6] D. Dobrakowski et al., Journal of Optics 21, 1 (2019).
[7] A. Anuszkiewicz et al., Scientific Reports 8, 1 (2018).
[8] A. D. Yablon, Journal of Lightwave Technology 28, 4 (2010).

Pattern formation in a gold nanoparticles-doped nematic liquid crystal composite by optical methods

K.BEDNARSKA[1], P. LESIAK[1], A.SITKIEWICZ[1],T.WOLIŃSKI[1]

[1] Faculty of Physics, Warsaw University of Technology, Koszykowa 75, 00-662 Warsaw
e-mail address: *karolina.bednarska.dokt@pw.edu.pl*

In our previous work [1] we showed a mechanism of periodic structures formation in nematic liquid crystals doped with gold nanoparticles through the phase transition process. We explained that initial fluctuations of nanoparticles in liquid crystals lead to discrete segregation of domains, thus creating a photonic structure. In this work we employ our findings to purposely create patterns in such composites (Fig. 1). Our approach is based on the use of a light source and amplitude masks to induce a local phase transition in the composite.

Fig. 1. Star patterns formed in a cell filled with gold nanoparticles-doped nematic liquid crystal

References:

[1] P. Lesiak et al., ACS Nano, 13, 10154-10160, 2019

Optical properties of achromatic flat-surface gradient index microlenses

R. BUCZYNSKI[1,2], A. FILIPKOWSKI[1,2], H. T. NGUYEN [1,2], D. PYSZ[2], R. STEPIEN[2], A. WADDIE[3], M. R. TAGHIZADEH[3], R. KASZTELANIC[1,2]

[1]University of Warsaw, Faculty of Physics, Pasteura 5, 02-093 Warszawa
[2]Łukasiewicz -Institute of Electronic Materials Technology, Wólczynska 133, 01-919 Warszawa
[3]Heriot-Watt University, Department of Physics, School of Engineering and Physical Sciences, Scottish Universities Physics Alliance, Edinburgh, EH14 4AS, UK.
e-mail address: *ryszard.buczynski@fuw.edu.pl*

Achromatic lenses are highly desirable for both imaging systems and beam manipulation tasks. It is well known that singlet refractive lenses cannot be achromatic (Fig. 1(a)) due to the dispersive nature of all known glass materials the chromatic aberrations cannot be compensated by any shape of lens. The standard solutions to eliminate chromatic aberrations are based on multi-element lens systems. However, a few works have discussed methods to create singlet-type achromatic lenses. Flynn et al. proposed to fabricate a hybrid diffractive-refractive achromatic lens, where a refractive lens made of homogenous material, is combined with an additional diffractive Fresnel lens [1]. Other solutions show a feasibility of development lenses made of 2 materials with spherical surfaces [2] or lenses made of 3 components with spherical or flat surfaces [3].

We proposed a fully flat-parallel gradient index (GRIN) microlens, which can be easily integrated as part of the optical fiber line. In order to design and fabricate a nanostructured GRIN lenses, it is necessary to use pair of glasses with good rheological properties and similar expansion coefficients as well as thermal properties, which allow joint thermal processing in a fiber drawing tower. To ensure achromatic properties of lenses, the first derivative of the difference between the material dispersion of the glasses has to cross a zero. We have developed in-house a pair of borosilicate glasses labelled as NC34 and NC21A which fulfils these requirements for the development of achromatic nGRIN microlenses.

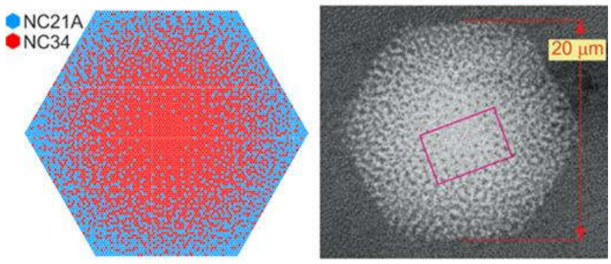

Fig. 1. Internal structure of the achromatic nanostructured GRIN microlens composed of NC21A and NC34 glass nanorods: a cross-section of design and fabricated component.

The NC21A/NC34 pair of glasses has an expansion coefficient difference of Δα=0.4×10-7·K-1, which is sufficiently small for joint thermal processing. During the drawing in the fiber drawing tower the glasses are kept at a temperature between the curvature and sphere points. For NC21A/NC34 the difference in the curvature temperature is ΔTc=50°C and difference in sphere temperature is ΔTsph=35°C.

The nanostructure of the proposed GRIN lens has been designed so the effective refractive index would change parabolically between these two refractive indices, from the maximum at the optical axis to the minimum on the edge of the aperture. We have used a standard stack and draw method commonly used for photonic crystal fiber fabrication to develop achromatic nGRIN microlenses. The preform was formed with 0.6 mm diameter NC21A and NC34 glass rods. A hexagonal structural preform was then stacked layer by layer, according to the calculated pattern (Fig. 1). A total of 7651 glass rods were used and the final element had 101 rods on the diagonal. The preform was drawn into sub-preforms of diameters 5 mm. A 30 mm outer diameter NC21A glass tube was used to create sub-preform and finally achieve a 125 µm diameter fiber with a 20 µm nanostructured lens structure in the middle [4,5].

The light propagation through the lens has been characterized using the imaging setup. It was illuminated by a collimated beam from continuous-wave laser sources at wavelengths in the range 532 nm - 1550 nm. The beam formed by the nanostructured lens was imaged by a microscope lens onto a camera. For each laser source, CCD, CMOS, and phosphate enhanced CCD cameras with appropriate sensitivities were used. The images of the beam cross-sections were collected on the CCD continuously by the translation of the structured lens. A series of images were taken at different distances from the lens facet with the distance changing with a step of 1 µm and then combined to give the plot of the beam FWHM and the longitudinal profile of the beam formed by the measured lens.

The focal spot was observed at a distance of 34.1 – 35.6 µm over a wavelength range of an octave between 600 nm and 1550 nm. It is nearly wavelength independent, however axial achromatic behavior is clearly observed. A maximum working distance, defined as the distance from the final lens facet to the focal plane, of 35.6 µm was observed for 980 nm illumination. For the remaining longer and shorter wavelengths the working distance is shorter. The measured beam diameter at the focal plane with FWHM criterion is equal to 2.1 µm – 4.1 µm in the considered wavelength range.

Acknowledgments: This work was supported by This work was supported by the project TEAM TECH/2016-1/1 (POIR.04.04.00-1C74/16) operated within the Foundation for Polish Science Team Programme co-financed by the European Regional Development Fund under Smart Growth Operational Programme (SG OP), Priority Axis IV.

References:

[1] N. Davidson et al., Appl. Opt. 32(25), 4770–4774 (1993).
[2] J. N. Mait et al., Opt. Express 23(17), 243268 (2015).
[3] G. Beadie at al., Proc. SPIE 10181, 1018108 (2017).
[4] A. Filipkowski et al., Opt. Lett. 40(22), 5200–5203 (2015).
[5] R. Buczynski et al., Opt. Express 27(7), 9588-9600 (2019).

Single-mode ytterbium doped nanostructured core optical fibers for high power laser applications

M. FRANCZYK[1], D. PYSZ[1], K. STAWICKI[1], J. LISOWSKA[1], A. FILIPKOWSKI[1], D. MICHALIK[1,2], R. STĘPIEŃ[1], T. OSUCH[3,4], M. BIDUŚ[5], M. DŁUBEK[5], R. BUCZYŃSKI[1,2]

[1] Lukasiewicz Research Network - Institute of Electronic Materials Technology, Glass Department, Wolczynska 133, 01-919 Warsaw, Poland

[2] University of Warsaw, Faculty of Physics, Pasteura 5, 02-093 Warsaw, Poland

[3] Warsaw University of Technology, Department of Electronics and Information Technology, Institute of Electronic Systems, Nowowiejska 15/19, 00-665 Warsaw, Poland

[4] National Institute of Telecommunications, 1 Szachowa, 04-894 Warsaw, Poland

[5]Fibrain, 36-062 Zaczernie 190F, Poland

e-mail address: marcin.franczyk@itme.edu.pl

High power single mode fiber lasers are of great interest, due to many industrial, defense and scientific application. Since double-clad structure was demonstrated over last three decades [1] actually the basic design of all-solid fiber applicable for single mode high power laser performance has not changed significantly. The fibers for high power applications still have the “step-index” profile and more irregular internal cladding for effective mode scrambling of pump radiation. The dramatic power scaling in recent years up to several kilo Watts we owe to silica material improvements and outstanding progress in pumping diodes technology. Although researchers presented several fiber designs including photonic crystal fibers (PCF) or leaky-channel fibers (LCF) with large mode areas, the significant share of high power fiber lasers have been achieved with conventional all-solid step-index large mode area (LMA) fibers due to their compatibility with standard fiber splicing techniques and superior heat dissipation, thus they are still favored in the industry [2].

In this paper we present the novel approach in a development of optical fibers. The nanostructurization is the new generic method, which applied within the fiber core, allows to control precisely optical properties of the fibers including the opportunity of development of large mode area fibers with breakthrough performance.

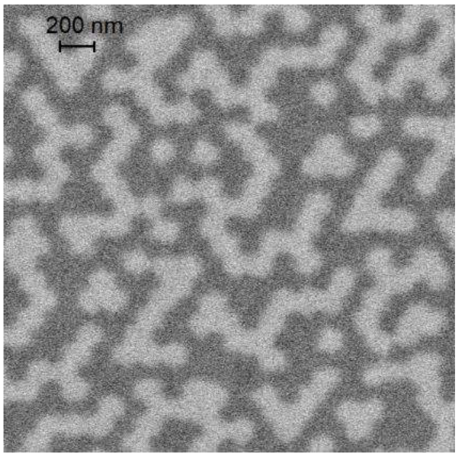

Fig. 1. The cross-section SEM of manufactured “mosaic” nanostructured core with 160nm in diameter elements: the bright area is Yb doped glass, the dark area is undoped glass.

The nanostructured core is composed of two or more kind of glasses with the size of a fraction of the light wavelength (feature size smaller than $\lambda/5$), which create the “mosaic” structure along the fiber (Fig.1). The effective refractive index of that “mosaic” material can be treated as a compound of refractive indices of each glass area averaged over a certain neighborhood inside the material [3]. It results in any continuous-like refractive index profile according to the design. This method allows to design and develop very large mode area single mode fibers for high power applications with optimized gradient refractive index profiles like triangular or parabolic with, respectively, 110 µm and 70 µm fiber core diameter, which show breakthrough performance in comparison with up-to-date solutions [4].

We present proof-of-concept fibers that show the outstanding performance of nanostructurization as a method applicable for very high power applications.

We report development of nanostructured ytterbium doped silica fiber with uniformity of 1.3×10-4 refractive index unit (RIU), which exceed results achieved with standard MCVD method. We also demonstrate the single-mode laser based on that developed fiber with 61.8% of slope efficiency [5].

Nanostructurization also allows to merge optical properties of glasses with different dopants, which is often not feasible or limited with standard methods. We present active and photosensitive nanostructured silica core fiber with the Bragg grating inscribed within the ytterbium doped core area resulting with splice-free laser cavity.

Acknowledgments: This work was supported by the project POIR.04.04.00-1C74/16 operated within the Foundation for Polish Science Team Programme co-financed by the European Regional Development Fund under Smart Growth Operational Programme (SG OP), Priority Axis IV.

References:

[1] E. Snitzer, H. Po, F. Hakimi, R. Tumminelli, and B. C McCollum. Double clad, offset core Nd fiber laser. Paper PD5
in Proc. Opt. Fib. Sensors 2 (1988).

[2] IPG Photonics, Oxford, MA, USA, 2018, http://www.ipgphotonics.com/

[3] R. Buczyński, M. Klimczak, T. Stefaniuk, R. Kasztelanic, B. Siwicki, G. Stępniewski, J. Cimek, D. Pysz, and R. Stępień, “Optical fibers with gradient index nanostructured core,” Opt. Express 23(20), 25588-25596 (2015).

[4] M. Franczyk, K. Stawicki, J. Lisowska, D. Michalik, A. Filipkowski and R. Buczynski, “Numerical studies on large mode area fibers with nanostructured core for fiber lasers,” J. Lightwave Technol. 36,23 (2018).

[5] M. Franczyk, D. Pysz, P. Pucko, D. Michalik, M. Biduś, M. Dłubek, and R. Buczyński, "Yb3+ doped silica nanostructured core fiber laser," Opt. Express 27,24 (2019)

Methodology for measuring the size of gaps with an optical proximity sensor on the example of a centrifugal blood pump

M. GAWLIKOWSKI, P. KURTYKA, J. ZALEWSKI, M. ZARWAŃSKA-DOFFEK, A. KAPIS

[1] Silesian University of Technology, Faculty of Biomedical Engineering, Department of Biosensors and Biomedical Signals, 40 Roosevelta Str. 41-800 Zabrze, Poland, maciej.gawlikowski@polsl.pl

[2] Foundation of Cardiac Surgery Development, Artificial Heart Laboratory, 345a Wolnosci Str. 41-800 Zabrze, Poland

e-mail address: *maciej.gawlikowski@polsl.pl*

Introduction: The modern constructions of centrifugal, rotary blood pumps (RBP) are based on bearing-less impeller suspension systems:. In passive systems the impeller levitation is achieved by balance of magnetic force (generated by a permanent magnets) and hydrodynamic force (generated by rotating impeller). In such pumps, the size of the gap between the impeller and the housing is about 50 µ m. The gap size is crucial for the shear stress affecting the blood as it flows through hydrodynamic bearing. The gap size may be estimated by means of CFD modeling however results depend on blood rheology model, mesh quality etc. The aim of work was to make physical measurement of micrometric gap size by means of fiber-optic, reflectance proximity sensor.

Material and methods: The RC19 (Philtec, USA) sensor was used. The 0.8mm in diameter sensor tip consists of two parallel group of optical fibers, which allows to compensate differences in light reflection from various types of surfaces. The sensor resolution given by manufacturer is 0.2 µm at 100Hz of band. Sensor operating range is 760 µm and the near-field range is 150 µm. The sensor tip was mounted in Polish construction of centrifugal RBP called ReligaHeart ROT via hole drilled in zirconium pump housing. The reflective surface was titanium impeller covered by TiN layer with roughness R_a=0.08. In orger to avoid operation in the near-field the sensor tip was moved deeper into the pump housing. The diameter of the hole in the zirconium layer has been chosen in such way so - for the sensor tip located 120 µm from the housing surface and the beam convergence angle of 60o - as to avoid the light beam shadowing by the edge of the hole. The system was calibrated using a flat sample made of the same material as the impeller and placed parallel to the pump housing surface. The sample was raised to a given height which was measured with an electronic micrometer. Space between pump housing and sample was filled in 40% water – glycerin solution. After calibration, the pump was assembled with a rotor whose levitation height was to be measured. Measurements was carried out for various pump speed as well as various pump load.

Results: The geometry of hydrodynamic bearing made on rotor surfaces was known and previously measured by means of coordinate machine (reference) with accuracy 0.5 µm. Hydrodynamic bearing blades depth was 17 µm. During optical distance measurements this geometry was reproduced with accuracy 0.5 µm. Moreover, differences between individual blades was measured and confirmed by reference method. In line with theoretical expectations the impeller levitation height was depended on pump speed and was in the range of 7.5-28.0 µm.

Conclusions: The reflectance method and fiber-optic sensor RC19 may be used to measure the gaps size with excellent accuracy. The limitation of the applicability of the method is optical transparency of the environment in the gap.

Acknowledgements: This work has been supported by NCBiR (RH-ROT/266798/STRATEGMED-II)

Direct ink writing of water-sensitive glass: towards optical application.

P.GOŁĘBIEWSKI[1,2], B. NAN[3,4], R. BUCZYŃSKI[1,2], F.J. GALINDO-ROSALES[5], J.M.F. FERREIRA[3]

[1] Institute of Electronic Materials Technology, Wólczyńska 133, 01-919 Warsaw, Poland
[2] Faculty of Physics, University of Warsaw, Pasteura 5, 02-093 Warsaw, Poland
[3]Department of Materials and Ceramic Engineering, University of Aveiro, CICECO – Aveiro Materials Institute, 3810-193 Aveiro, Portugal
[4]CEITEC - Central European Institute of Technology, Brno University of Technology, Purkynova 656/123, 612 00 Brno, Czech Republic
[5]CEFT, Department of Chemical Engineering, Faculty of Engineering of the University of Porto, 4200-465 Porto, Portugal
e-mail address: *pgolebiewski@fuw.edu.pl*

Additive manufacturing (AM), commonly known as three-dimensional printing (3D printing), has already gained much attention in both scientific and industrial communities. It is a group of moldless, shaping techniques which enables quick fabrication of fully customized products with a complex structure. While most of researchers have been focused on printing materials such as metals, ceramics and polymers [1-4] there is still need to increase efforts in printing glass. However, due to specific properties of this group of materials, application of AM is demanding, as glass is brittle and often sensitive to thermal shock. Moreover, it can be difficult to apply shaping techniques based on powder densification, as glass starts to flow as a viscous material after reaching transition temperature. Therefore, it is challenging to retain shape of already formed product. If the temperature is not adjusted correctly, printing process can also result in cracked or porous structure as it was already reported in [5,6] when Selective Laser Melting (SLM) technique was used. Besides dry processing also colloidal processing is possible. However, if glass contains alkali and alkaline earth oxides, it may undergo preferential ionic leaching as a result of hydrolysis. Accordingly, rheological parameters of suspensions/inks are not predictable. Nevertheless, recent reports [7,8] demonstrated that production of transparent glass is possible, thus research should be continued with the aim of application of AM in e.g. fabrication of optical fibers preforms or optical components production.

In this work, preliminary study regarding direct ink writing of water-sensitive glasses is presented on the example of borosilicate glass with high content of alkali and alkaline earth oxides. Glass powder was prepared by milling glass frit until desired particle size distribution was obtained. Inks were made of glass powder suspended in Pluronic F-127 hydrogel. According to the results presented by Bromberg et al. [9] and Park et al. [10], it was assumed that glass hydrolysis which occurs in this system does not affect rheological properties significantly, unlike standard dispersant-thickener-coagulant system. Obtained inks were subjected to rheological measurements and subsequently used to print small rings. After printing differential scanning calorimetry measurements of pure polymer, pure glass and printed sample were performed.

Fig. 1. Photograph of printed samples

Based on obtained results, samples were debinded (burnout of organic compounds) at 500°C for 8 h and sintered at 720°C for 30 min (Fig. 1.). As a result opaque samples were acquired. In the following steps XRD and SEM analyses were carried out in order to find the sources of scattering. Diffraction patterns did not exhibit any additional, crystalline phases. SEM (Fig. 1) micrographs of the sintered samples revealed the presence of closed porosity which is assumed to be the main source of scattering.

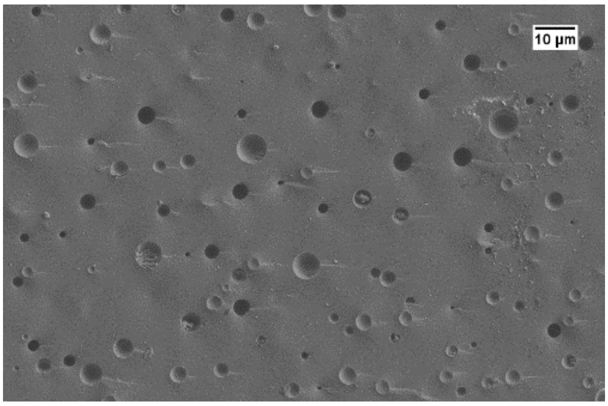

Fig. 2. SEM micrograph of sintered sample

To summarize, developed manufacturing process is suitable for preparation of water-sensitive glass inks. However, due to the closed porosity of obtained samples it still needs improvement. On one hand the composition of inks may be changed with a view to increase the amount of glass powder while other parameters are preserved. On the other hand sintering process can be further developed either by changing temperatures and holding times or instead of sintering in the air atmosphere vacuum may be applied.

Acknowledgments:
This research was funded by The Polish National Agency for Academic Exchange, grant number PN/BIL/2018/1/00253, Foundation for Polish Science, grant number POIR.04.04.00-00-1C74/16 (TEAM TECH/2016-1/1) and FCT grant Ref. UID/CTM/50011/2019, financed by national funds through the FCT/MCTES.

References:
[1] J.Y. Lee et al., Appl. Mater. Today 7, 120-133, (2017)
[2] J.Y. Lee et al., J. Memb. Sci. 499, 480–490, (2016)
[3] K.V. Wong et al., ISRN Mech. Eng. 2012, 1-10, (2012)
[4] T.D. Ngo et al., Compos. B Eng. 143, 172-196, (2018)
[5] C.E. Protasov et al., Int. J. Heat Mass Transf. 104, 665-674, (2017)
[6] M. Fateri et al., Int. J. Appl. Ceram. Technol. 12(1), 53-61, (2015)
[7] F. Kotz et al., Nature 544, 337, (2017)
[8] D.T. Nguyen et al., Adv. Mater. 29, 1701181, (2017)
[9] L. Bromberg et al., Int. J. Pharm. 282, 45-60, (2004)
[10]S.Y. Park et al., Macromol. Rapid Commun. 28, 1172-1176, (2007)

Analysis of neural networks parameters for improved face recognition performance

A. GRUDZIEŃ[1], M. KOWALSKI[1], N. PAŁKA[1]

[1]Military University of Technology, Institute of Optoelectronics, Gen. S. Kaliskiego 2, 00-908 Warsaw
e-mail address: *artur.grudzien@wat.edu.pl*

Face recognition is used in many aspects, such as business, security, crime detection. Therefore, face recognition technology has become wide developed research field [1].
The currently explored approaches strongly focus on using neural networks for face recognition.
While face recognition algorithms based on neural networks outperform other existing methods, this study concerns residual neural networks, which are state-of-the-art algorithms. We consider these models in view of two properties. The first concerns different number of layers while the second the increasing number of learning parameters. The aim of this study is to investigate various parameters that may strongly affect performance of the face recognition. In order to find optimal algorithm configuration batch size and learning rate [2] have been investigated.
All deep learning neural networks learn from large set of images, thus this paper also addresses the aspect of size of the database as well as data entropy.
In order to assess the impact of parameters on networks' performance the training time, recognition rates, FMR1000, ZeroFMR, EER are used for evaluation purposes.

Acknowledgments: This project has received funding from the European Union's Horizon 2020 research and innovation programme under grant agreement No 833704.

References:

[1] Jain, A.K., Ross, A.A. and Nandakumar, K., Introduction to Biometrics, Springer, London & New York, 2011
[2] M. Wang and W. Deng, Deep Face Recognition: A Survey, CVPR, 2019

Response of a broadband differential interferometer to a change in waveguide thickness

K.GUT[1]

[1] Department of Optoelectronics, Silesian University of Technology, Krzywoustego 2, 44-100 Gliwice, POLAND

e-mail address: *kazimierz.gut@polsl.*

The work presents an analysis of planar broadband waveguide interferometers in the case of a change in layer thickness. The analysis was performed for the wavelength range of 450nm-1200nm. The TE_0 and TM_0 orthogonal modes which propagate in this wavelength range are considered. At the output of the system, an interference signal behind a polarizer can be recorded. If a spectrometer is used as a detector, the recorded signal is a function of the wavelength. Change in the change thickness of the waveguide layers results in a change of the recorded signal shape.

Optical properties of realistic hyperbolic metamaterials

B.JANASZEK[1], M. KIELISZCZYK[2], A. TYSZKA-ZAWADZKA[1], P.SZCZEPAŃSKI[1,2]

[1] Warsaw University of Technology, Faculty of Electronics and Information Technology, Institute Microelectronics and Optoelectronics, Koszykowa 75, 00-662 Warszawa, Poland
[2] National Institute of Communications, Szachowa 1, 04-894 Warszawa, Poland
e-mail address: *b.janaszek@imio.pw.edu.pl*

Over the last decade, hyperbolic metamaterials (HMMs) have been recognized as a promising class of photonic nanostructures. Due to their unique dispersion properties and potentially unbounded photonic density of states, such structures reveal a multitude of potential applications from biosensing [1] to quantum information processing [2, 3]. Until now, several methods dedicated to HMM description have been developed, including effective model applicable for structures fulfilling local approximation condition $a/\lambda \rightarrow 0$, where a is a characteristic dimension of the structure and λ is wavelength [4]. However, the performance of the realistic HMM structures, violating the local approximation condition, tend to differ significantly from behavior anticipated by means of local treatment. In our analysis, we employ nonlocal effective medium theory (EMT) to design HMM structures and precisely predict their behavior, including effects arising from temporal as well as spatial dispersion.

Our analysis is based on nonlocal EMT treatment developed by Chern [5] as well as original transfer matrix method dedicated to anisotropic media. This approach allows us to anticipate behavior of HMM structures of realistic dimensions for which local approximation is not satisfied, i.e., $a/\lambda > 0$ To compare differences between local and nonlocal treatment as well as to determine strength of spatial dispersion, an exemplary HMM structure has been selected. As we can see, spectral behavior of a multilayer nanostructure with a basic cell consisted of single graphene sheet and 150 nm HfO_2 layer differs drastically depending whether local (Fig. 1a) or nonlocal treatment (Fig. 1b) has been applied. Such strong nonlocality is caused by substantial deviation from local approximation, i.e., $a/\lambda \rightarrow 0$.

(a)

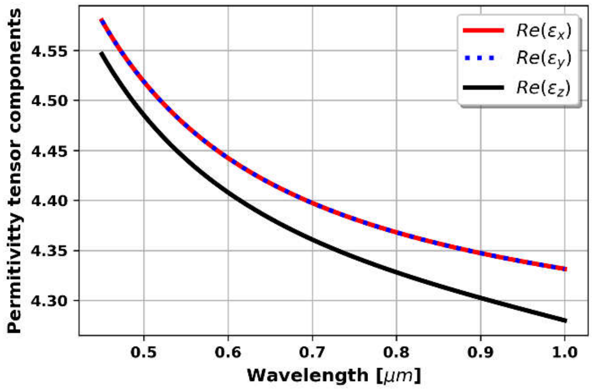

(b)

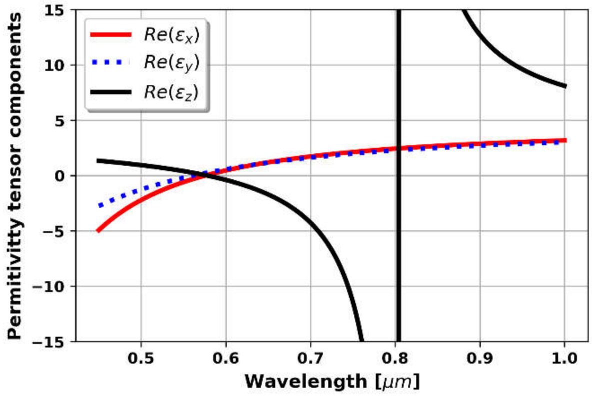

Fig. 1. Effective dispersion characteristic for a single HMM structure described by local (a) and nonlocal treatment (b).

In this case, local approximation condition is violated, i.e., $a/\lambda > 0$, which lead to change in effective optical properties. For a better insight, calculation of transmittance and reflectance for previously considered single structure described by local and nonlocal treatment have been performed, see Fig.2.

(a)

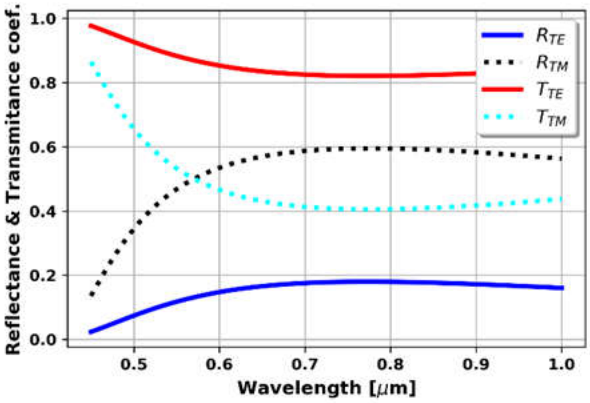

(b)

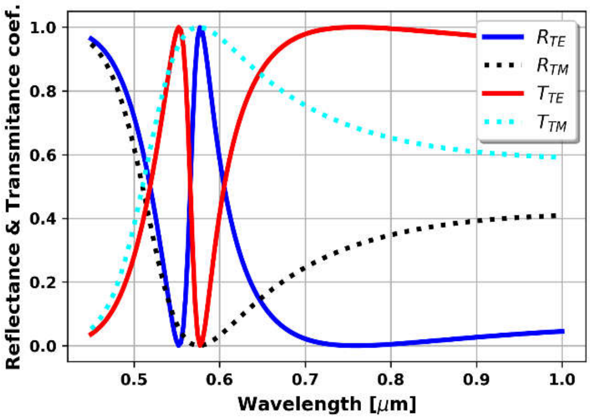

Fig. 2. Reflectance and transmittance spectra of a single HMM structure described by local (a) and nonlocal treatment (b).

As we can see, such drastic change in dispersion characteristic also lead to substantial change in effective optical properties, which can be observed especially for shorter wavelenghts where ratio a/λ is higher, compare Fig. 2a and 2b. Thus, an accurate design of a realistic HMM structure requires consideration of nonlocality by means of appropriate effective treatment (nonlocal EMT).

Within this work, we discuss influence of spatial dispersion on effective optical properties of an HMM structure and its possible outcomes, such as strong wavevector dependency. Moreover, we show that proper geometry engineering can lead not only to elimination [6,7], but also to enhancement of nonlocality, which can serve as a new degree of freedom in shaping effective properties of an HMM structure.

Acknowledgments: This work has been supported by The National Centre for Research and Development (NCBiR) under grant No. TECHMATSTRATEG1/347012/3/NCBR/2017 (HYPERMAT)

References:

[1] K. V. Sreekanth et al., Nat. Mater. 15, 621–627 (2016).
[2] M. Kieliszczyk, B. Janaszek, A. Tyszka-Zawadzka, R. P. Mroczyński, P. Szczepański, "Tunable Hyperbolic Metamaterials for Novel Photonic Devices" (paper presented, 2018).
[3] C. L. Cortes, W. Newman, S. Molesky, Z. Jacob, J. Opt. 14, 063001 (2012).
[4] B. Janaszek, M. Kieliszczyk, A. Tyszka-Zawadzka, P. Szczepański, Appl. Opt. 57, 2135 (2018).
[5] R.-L. Chern, Opt. Express. 21, 16514 (2013).
[6] A. I. Căbuz, D. Felbacq, D. Cassagne, Phys. Rev. A. 77 (2008), doi:10.1103/physreva.77.013807.
[7] A. Demetriadou, J. B. Pendry, J. Phys. Condens. Matter. 20, 295222 (2008).

Ultra-dense endoscopic bundles

R.KASZTELANIC[1,2], D. PYSZ[2], R. STEPIEN[2], R. BUCZYNSKI[1,2]

[1]University of Warsaw, Physics Department, ul. Pasteura 5, 02-093 Warszawa

[2]Institute of Electronic Materials Technology, ul. Wolczynska 133, 01-919 Warszawa

e-mail address: kasztel@*igf.fuw.edu.pl*

At the end of the 20th century, the medical community began to move from conventional ‘open’ operations to minimally invasive procedures (MIP) [1]. The philosophy behind MIP is to access the organs or tissues of interest through natural holes or small incisions in the body, while achieving the same therapeutic or diagnostic result, but without the injury and postoperative pain inherent to conventional operations. For the purpose of MIP it is necessary to use small diameter endoscopes. Modern endoscopes are generally available in many versions but the two basic are: video endoscopes [2] and glass fiber endoscopes [3]. The most popular one – the video endoscope – uses a miniaturized video chip and several additional microoptic devices such as lenses at the distal end to capture images in combination with optical fibers or LEDs that provide white light illumination [4]. However, due to the size of available cameras, these systems are used only to penetrate a part of the organs.

The second group of endoscopes includes all kinds of fiber optic systems, and in particular endoscopes based on multi-core fibers – optical bundles [3] (Fig. 1). In such systems, each core in the fiber corresponds to a single image 'pixel'. Thus, the image quality and spatial resolution of the endoscope is therefore highly dependent on the packing densities of the cores. Unfortunately, in the case of closely located cores, the effect of crosstalk [16,29,30] limits the spatial resolution of multi-core imaging bundles. That is why commercially available high-resolution optical bundles have cores with a diameter of about 2 µm distant from each other by more than 3 µm [5]. The way to minimize this problem is to increase the difference in refraction indexes between the core and the cladding and increase the distance between the cores, which reduces the spatial resolution. To solve the problem we have developed a special pair of glasses which, on the one hand, have a very large difference in refractive indexes and, on the other hand, are thermally matched and can be drawn together on the optical tower.

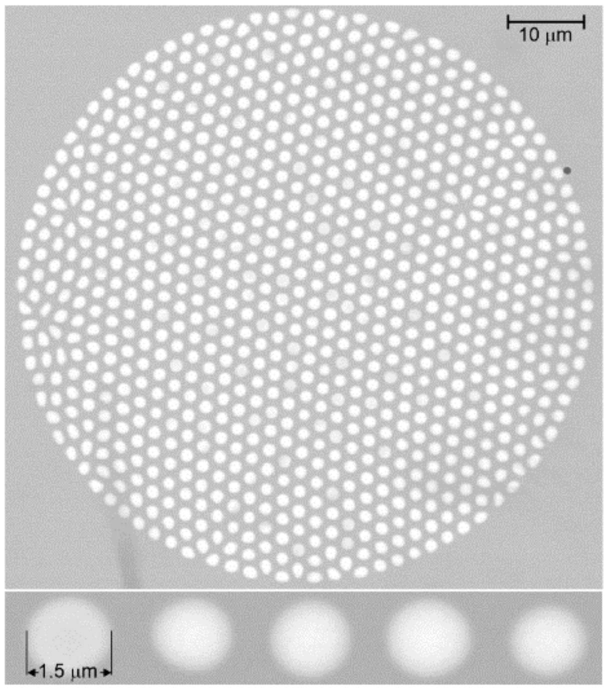

Fig. 1. An example of an optical bundles with a record close distance between cores of 2 um.

The refractive index of PBG08 and UV710 glasses differs by approximately 0.4 in the range from visible to near infrared light. Theoretically, in this case, the numerical aperture for a single core is greater than 1 (NA≈1.16). This allows to fabricate an optical bundle with record-small pixels, smaller than 2 µm, i.e. with a record-high spatial resolution (Fig. 1). However, when the size of the core diameter is reduced to less than 2 µm, the diffusion of glasses begins to play a major role. This results in a blurring of the interface between the two glasses, which decreases the contrast of the refractive indexes and leads to increased crosstalk between the cores. Therefore, it is also important to choose the right parameters for drawing out the optical bundles, which will minimize the diffusion (Fig. 2).

The presentation will focus on the results of the work on the test to fabrication of the optical bundles with the highest possible spatial resolution while controlling the diffusion process. We will present optical bundles with cores up to 1.5 um diameter and a distance between the centers of cores up to 2 um, which corresponds to a record spatial resolution of 500 'pixels' per mm. It will also present the results of the examination of the optical properties of the fabricated optical bundles.

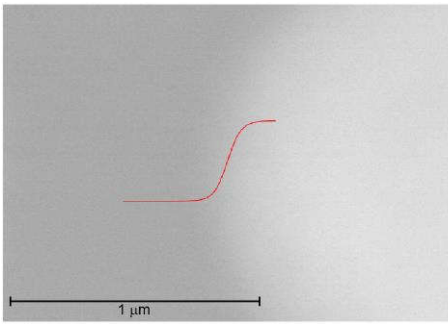

Fig. 2. Diffusion of glass on the edge of a single core.

Acknowledgments: This work was supported by the project TEAM TECH /2016-1/1 (POIR.04.04.00-1C74/16) operated within the Foundation for Polish Science Team Programme co-financed by the European Union under the European Regional Development Fund and National Science Centre project HARMONIA 8 (UMO-2016/22/M/ST2/ 00261)

References:

[1] J.E.A. Wickham, British Medical Bulletin 42(3), (1986).
[2] R.D. Ellis et. al. Int. J. Med. Rob. Comp. Ass. Surg. 12, (2016).
[3] B. Morova et. al., Opt. Express 27(7), (2019).
[4] S.F. Elahi et. al., J. Biophotonics 4(7-8), (2011).
[5] Z.A. Steelman et. al., Appl. Optics 57(6), (2018).

Methodology for extraction of thin film properties based on semi-analytical optical parameters extraction approach

M. KIELISZCZYK[1], B. JANASZEK[1], P. SZCZEPAŃSKI[1,2]

[1]Institute of Microelectronics and Optoelectronics WUT, Koszykowa 75, 00-662 Warsaw, Poland
[2]National Institute of Telecommunications, Szachowa 1, 04-894 Warsaw, Poland
e-mail address: *m.kieliszczyk@imio.pw.edu.pl*

Thin films have been a matter of interest for several decades now. Over the years, nanostructures based on thin metallic and/or dielectric films have found several applications as media to generate electromagnetic wave propagation or control its propagation (solid-state lasers, anti-reflection or high reflection coatings, filters of various kinds, see e.g. [1]). Recent advances in photonics, among which employment of hyperbolic metamaterials can be distinguished, allow to obtain properties previously unattainable with the use of conventional thin film structures. With the advent and development of advanced deposition techniques such as magnetron sputtering, electron-beam physical vapor deposition (EBPVD), ion-assisted deposition or atomic layer deposition (ALD), continually thinner and thinner layers are feasible and being employed.

The design of photonic structures demands precise knowledge of the dispersion properties of the constituent materials used. Addressing this need, we will present a methodology for extraction of thin film properties based on a transmissive-reflective spectrophotometric measurement and an improved semi-analytical approach, whereby simultaneous extraction of both the optical constants (refraction and extinction coefficients) and thickness of a thin film deposited on a substrate of known optical and physical parameters is possible. In contrast to methodologies presented so far, where algebraic or optimization-based techniques have been employed [2]–[4], our approach is based on a full-wave solution to Maxwell's equations (Transfer Matrix Method) and yields a model-free dispersion characteristic of a thin film along with its physical thickness, given that the measurement band / optical thickness of the layer remains in the subwavelength regime. No further assumptions are made as to the physical nature of the film or the properties of its optical dispersion characteristics. In particular, no assumption is made as to the mathematical model, which might accurately describe the dispersion of a material of a particular thin film.

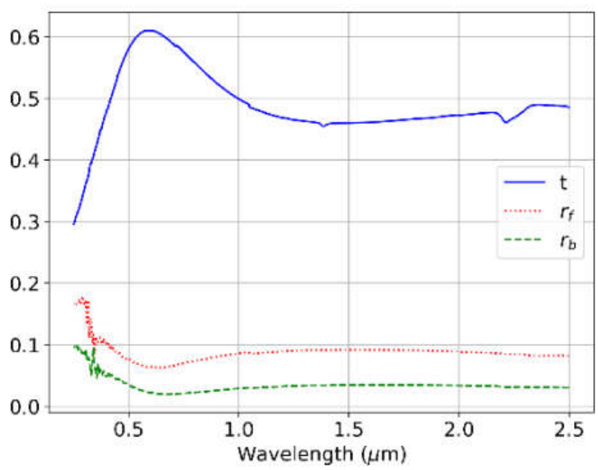

Fig. 1. Measured characteristics of transmission (t), reflection from the coated side (r_f), and reflection from the side of the substrate (uncoated, r_b,).

Fig. 1 presents measurement results for a thin layer of titanium nitride (TiN, 10 nm) deposited on a polished silica substrate of 2mm using magnetron sputtering technique. Spectrophotometric transmission / reflection measurement has been performed using Digilab FTS3000 Excalibur FTIR spectrometer over the range of 0.3 – 2.5 µm.

Fig. 2. presents results of extraction, which qualitatively closely correspond to the comparable literature data available on titanium nitride properties (see e.g. [5]).

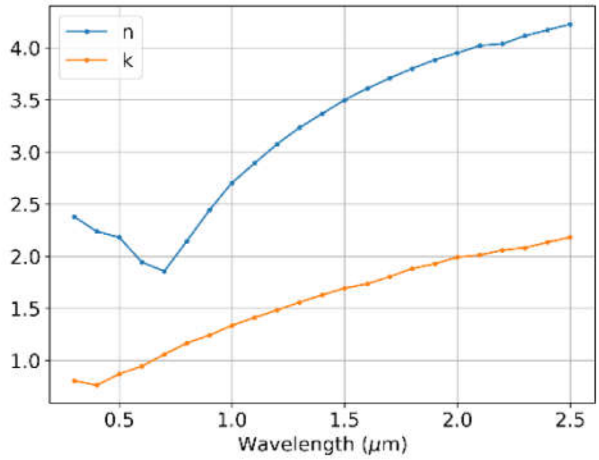

Fig. 2. Extracted optical constants of 10 nm thick titanium nitride thin film. Extracted results qualitatively correspond to comparable data available in the literature.

Note that the noticeable discontinuities of characteristics presented in Fig. 1. are a result of the measurement error and are not representative of the properties of the extraction algorithm itself (which, as shall be discussed, does not contribute additional error).

Within this work, we shall discuss main assumptions and benefits of our methodology, including problem of perceptibility of refractive index and extinction coefficient for ultrathin films, practical aspects of the choice and preparation of the substrate and the advantages that this methodology has over previously undertaken approaches.

Acknowledgements: This work has been supported by The National Centre for Research and Development (NCBiR) under grant No. TECHMATSTRATEG1/347012 /3/NCBR/2017 (HYPERMAT) in the course of "Novel technologies of advanced materials – TECHMATSTRATEG".

References:

[1] M. Kieliszczyk et. al., Appl. Opt., vol. 57, no. 5, pp. 1182–1187, 2018, doi: 10.1364/AO.57.001182.

[2] D. Poelman et. al., J. Phys. Appl. Phys., vol. 36, no. 15, pp. 1850–1857, Aug. 2003, doi: 10.1088/0022-3727/36/15/316.

[3] N. H. Jakatdar et. al., presented at the Optoelectronics and High-Power Lasers & Applications, San Jose, CA, 1998, p. 163, doi: 10.1117/12.304402.

[4] Md. G. Saber, et. al., Silicon, vol. 8, no. 2, pp. 245–250, Apr. 2016, doi: 10.1007/s12633-014-9267-2.

[5] H. Reddy et. al., ACS Photonics, vol. 4, no. 6, pp. 1413–1420, Jun. 2017, doi: 10.1021/acsphotonics.7b00127.

Nonlocal Solitons

W. KROLIKOWSKI

Science Program, Texas A&M University at Qatar, Doha, Qatar
Laser Physics Centre, Australian National University, Canberra, Australia
e-mail: *wieslaw.krolikowski@qatar.tamu.edu*

Spatial optical solitons are formed when the natural process of light diffraction which tends to spread the finite beams is counteracted by the nonlinear response of the material (typically its refractive index change) which focuses the beam. When the dynamic balance between spreading and self-focusing is achieved the beam may propagate without changing its amplitude as spatial soliton. [1]

Typically, the light-induced nonlinear response of the material is spatially local, i.e. the response in a specific point is determined solely by the light intensity in the very same point. Common example involves standard Kerr media. However, there is a wide class of materials, the so- called nonlocal media, in which the nonlinear response in particular location is determined by wave intensity distribution in a certain neighborhood of this location. The extend of this neighborhood determines the degree of nonlocality. In the extreme case of infinite nonlocality, the nonlinear refractive index becomes almost parabolic with its amplitude determined by solely the power of the beam and not its intensity profile [2,3].

It appears that nonlocality is a generic feature of various nonlinear systems ranging from optics to matter waves. It may result from certain transport processes such as atom diffusion, heat transfer, drift of electric charges etc., or the long range of the inter-particle interaction. It turns out that nonlocality may dramatically affect propagation of waves and their stability.

In this talk I review the role of spatial nonlocality of nonlinearity light propagation and its localization. In particular, I discuss here the impact of nonlocality on the modulational instability of plane waves, the collapse of finite-size beams, and the formation, stability and interaction of spatial solitons.

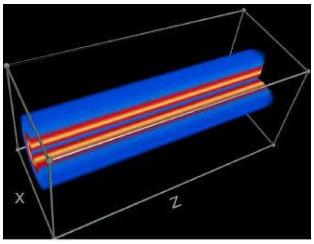

Fig. 1. Stable propagation of vortex soliton in highly nonlocal nonlinear medium

Acknowledgement: This work was supported by the Qatar National Research Fund: NPRP12S-0205-190047

References:

[1.]Yu. Kivshar, G. Agarwal, Fibers to Photonic Crystals, Academic Press, San Diego (2003).

[2]. A. Snyder M. Mitchell, Science, 276 1538 (1997).

[3]. O. Bang, W. Krolikowski, J. Wyller, JJ. Rasmussen Phys. Rev. E 66, 046619 (2002).

Silicon nitride based building blocks for integrated photonics - design, technology and characterization

M. LELIT[1,2], M. SŁOWIKOWSKI[1,2], A. KAŹMIERCZAK[2], K. ANDERS[2], S. STOPIŃSKI[2], M. JUCHNIEWICZ[1], B. STONIO[1,2], B. MICHALAK[1], M. FILIPIAK[1], K. PAVŁOV[1], P. WIŚNIEWSKI[1,2], R. B. BECK[1,2], R. PIRAMIDOWICZ[2]

[1]Warsaw University of Technology, Centre for Advanced Materials and Technologies CEZAMAT, Poleczki 19, 02-822 Warsaw, Poland
[2]Warsaw University of Technology, Institute of Microelectronics and Optoelectronics, Koszykowa 75, 00-662 Warsaw, Poland
e-mail address: *marcin.lelit@pw.edu.pl*

Nowadays, photonic integrated circuits (PICs) are commonly deployed in several ICT-related fields including telecom and datacom, data processing, sensing and metrology [1]. Silicon nitride (Si_3N_4) has been proved to be one of the most promising materials for developing a versatile passive photonic platform mainly due to its wide transparency window (ranging from 380 nm to over 6.7 µm) and CMOS compatibility [2]. These characteristics make the Si_3N_4 platform applicable in areas such as communication, biophotonics, sensing and are also suitable for hybrid photonic devices [3].

In this work we show the first results of our recent work on development of the library of Si3N4-based building blocks for PICs and their technological implementation. In particular, a series of waveguides (WGs), multimode interferometer (MMI) devices [4] and arrayed waveguide gratings (AWGs) [5] has been designed and developed to verify the potential of technological lines disposed by CEZAMAT with respect to manufacturing the integrated photonic elements.

The Film Mode Matching (FMM) and Finite Difference (FD) methods/algorithms have been used for simulation and a freeware Python-based package has been used to design the layout of building blocks and photonic integrated circuits.

The integrated devices presented in this work have been manufactured on 4'' silicon wafers with the material layers stack: 2.3 µm SiO_2 / 0.32 µm Si_3N_4 / 2.3 µm SiO_2. An exemplary development flow is presented in Fig. 1.

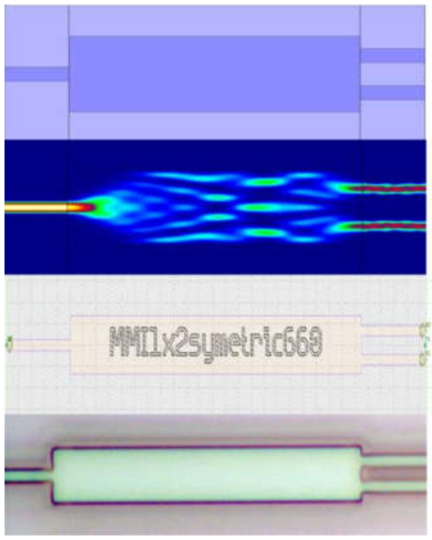

Fig. 1. 1×2 MMI optimized for 660 nm wavelength development flow. From top: design, field distribution simulation, GDS layout of building block, microscopic image of manufactured element.

The development flow started with simulations and design of straight and curved waveguides. The measurements of manufactured test samples confirmed a good stability and repeatability of waveguide losses. The average loss values are 3.3 dB/cm for delay line with 100 µm bending radius and 1.7 dB/cm for a delay line with a 400 µm bending radius. An average measured loss of a single 90° bend (100 µm radius) is as low as 0.2 dB.

Based on these results, a series of symmetrical MMIs 1×2, 1×4 and 1×8 and

AWGs 1×4 and 1×8 with the channel spacing of 0.8 nm (100 GHz), optimized for operation in the visible part of optical spectrum has been designed and manufactured. Good match of design and measured performance parameters of MMIs has been proven by optical characterization of developed structures.

AWGs are the most complex photonic passive elements due to several geometrical parameters, which have to be finetuned, and extremely high sensitivity to manufacturing errors. Two 1×8 AWGs optimized for the central wavelength (λ_c) of 590 nm and 610 nm have been manufactured and characterized using the setup equipped with tunable dye-laser as the excitation source (see Fig. 2). The obtained results show a moderate offset of the central wavelength with respect to the design value. The measured channel spacing and free spectral range (FSR) correspond well to the design values.

It should be noted, that the reported development flow comprises only a single production run on the CEZAMATs technological line. Considering above, achieving a fair performance of AWGs with a large potential for further optimization is a promising step in development of a passive photonic platform.

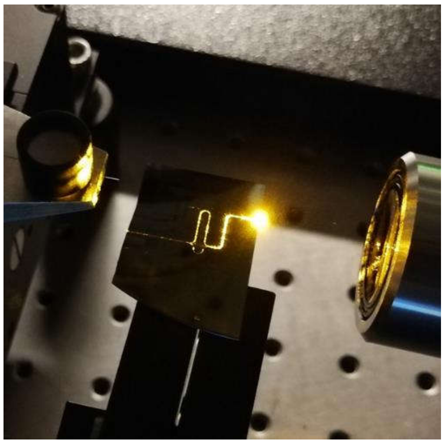

Fig. 2. Fabricated PICs guiding light of 575 nm wavelength.

References:

[1] Q. Wilmart et al., Applied Sciences 9, 2, p. 255 (2019)

[2] D. J. Blumenthal et al., Proceedings of the IEEE 106, 12, pp. 2209–2231 (2018)

[3] Z. Shao et al., Opt. Express, OE 24, 3, pp. 1865–1872 (2016)

[4] R. Halir et al., IEEE Photonics Technology Letters 21, 21, pp. 1600–1602, (2009)

[5] M. K. Smit and C. V. Dam, IEEE Journal of Selected Topics in Quantum Electronics, 2, 2, pp. 236–250 (1996)

Modeling of self-organized, one-dimensional periodic structures in a gold nanoparticle-doped nematic liquid crystal composite

P. LESIAK, K. BEDNARSKA, A. FRONCZAK, P. FRONCZAK, T. R. WOLIŃSKI

Faculty of Physics, Warsaw University of Technology, Koszykowa 75, 00-662 Warsaw
e-mail address: *piotr.lesiak@pw.edu.pl*

The world around us is full of various types of structures and patterns that one can attempt to model mathematically. Particularly interesting class of models are the reaction-diffusion systems, which allow to describe the formation of spatial patterns encountered in nature at every step. Systems of this type have been studied since the pioneering work of Alan Turing [1]. Their wide application in various areas of science makes this field lively and developing dynamically. In this work, we will limit ourselves to analyzing the possibilities of explaining the emergence of periodic phase separation in a mixture of liquid crystal and gold nanoparticles (Fig. 1) [2].

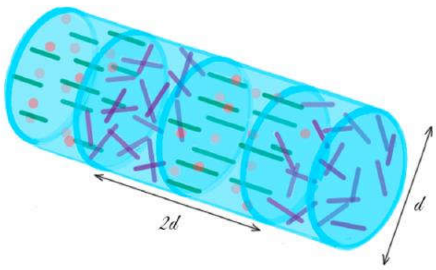

Fig. 1. Schematic representation of a periodic structure in a gold nanoparticle-doped nematic liquid crystal composite

We expect that the spontaneous pattern formation observed in this experiment can be imitated and reproduced within the formalism of reaction-diffusion systems. This formalism (introduced by Turing in 1952) aims to explain the phenomenon of morphogenesis. Such approach has been successfully applied to generate patterns found on seashells, fish, zebras, leopards, giraffes etc. The proposed methodology could allow to understand the impact of the system parameters on the properties of periodic structures in quasi-1D capillaries. In addition, it could also help to find conditions for obtaining more complex patterns in 2D media.

References:

[1] Turing, A. M. Philosophical Transactions of the Royal Society of London B. 237 (641): 37–72, 1952
[2] P. Lesiak et al., ACS Nano, 13, 10154-10160, 2019

Application of Artificial Intelligence for Optimization of Organic Solar Cells Production Process

G. LO SCIUTO

Department of Electrical, Electronic and Informatics Engineering,
University of Catania, Viale Andrea Doria 6, 95125 Catania, Italy
e-mail address: *glosciuto@dii.unict.it*

The production chain of the organic solar cells (OSC) can take advantage of application of artificial intelligence(AI). Indeed the integration into the production workflow makes solar cells more competitive and efficient. This paper presents some applications of the AI for optimization of OSCs production processes.

Geometric Shape Optimization of OSC by Neural Networks

The efficiency of organic solar cells is primarily limited by the ability of the active layer to absorb all the sunlight. The typical architecture of a polymer solar cell is shown in Fig. 1 and it consists of different layers including active layer sandwiched between the anode and the cathode with different work functions. Many effects tend to reduce the efficiency of the organic solar cells as the variation in the length devices.In this application, a back propagation neural network is developed to disclose the link between device length and its maximum power output. Simulations show that the device length influences the efficiency to be considered in manufacturing processes. The polymer solar cells analyzed have been made and tested in the laboratory of organic semiconductor devices Optoelectronic Organic Semiconductor Device Laboratory (OOSDL), department of electrical and computer engineering at Ben-Gurion University of the Negev in Beer Sheva,

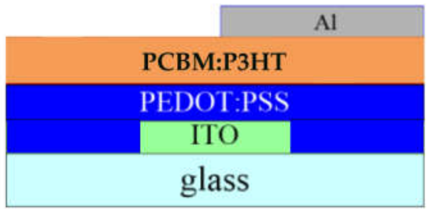

Fig. 1. Structure of the investigated OSC.

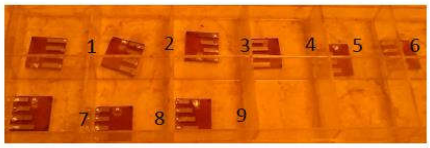

Fig. 2. The realized devices.

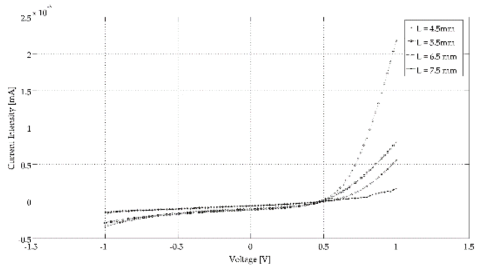

Fig. 3. Current density vs voltage characteristics of organic solar cells with different lengths under 1 sun ($100\ mW/cm^2$) simulated AM1.5 irradiation.

realizing 9 devices, each of which contains 4 organic solar cells. All devices have the same sizes (width and length of 12 mm),

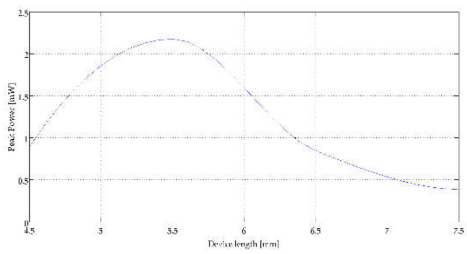

Fig. 4. The relationship between length and maximum power output of the organic solar cells obtained by the selected neural network

while the organic solar cells have a width of 1.5 mm and a length ranging from 4.50 to

7.50 mm. Fig. 2 shows the realized devices. The current density vs voltage characteristics of some organic solar cells with different lengths are shown in Fig. 3. The inputs to the neural network are the different lengths of organic solar cells and the targets are the maximum power outputs associated to each solar cell. The simulation results obtained show that the devices length has a great influence on their efficiency (see Fig. 4) and that only for a limited subset of organic cell lengths the electric performances for the cells (in this case: in the subset 5.2 mm ÷ 5.8 mm) are satisfactory.

Fig. 5. The defects on top surface of OSCs.

OSC Defects Detection by using an Elliptical Basis Function Network Classifier

The degradation mechanisms of the active inter-layers are fast induced by diffusion of molecular oxygen and water causing chemical reactions into the device, electrode reaction with the organic materials, morphological changes due to temperature, and macroscopic changes such as delamination, formation of particles, bubbles, cracks and scratches due to fabrication process at the interfaces of OSCs, as shown in Fig. 5.

The investigation of defects on surface morphology of OSCs examined by Microscopy was conducted acquiring 240 images with resolution of 1280 × 1024. In order to describe the texture, the color mapping co-occurrence matrix (GLCM) is adopted usually, however leading to a course of dimensionality, so that the singular value decomposition to reduce the redundancy arising of description of the texture is used by means GLCM. The experimental results show that the algorithm achieves a high accuracy of recognition of 96%.

References:

[1] BRABEC, Christoph Joseph, et al. (ed.). Organic photovoltaics: concepts and realization. Springer Science & Business Media, 2013.

[2] Erb, Tobias, et al. "Correlation between structural and optical properties of composite polymer/fullerene films for organic solar cells." Advanced Functional Materials 15.7 (2005): 1193-1196.

[3] Lo Sciuto, Grazia, et al. "Exploiting OSC Models by Using Neural Networks with an Innovative Pruning Algorithm." International Conference on Artificial Intelligence and Soft Computing. Springer, Cham, 2018

Applicable ultrafast all-optical switching by soliton self-trapping in high index contrast dual-core fiber

M. LONGOBUCCO[1,2], P. STAJANČA[3], L. ČURILLA[4], D. PYSZ[1], R. BUCZYŃSKI[1,2], I. BUGÁR[1,5]

[1] Department of Glass, Łukasiewicz Research Network - Institute of Electronic Materials Technology, Wólczyńska 133, 01-919 Warsaw, Poland
[2]Faculty of Physics, University of Warsaw, Pasteura 5, 02-093 Warsaw, Poland
[3]BAM Bundesanstalt für Materialforschung und -prüfung, Unter den Eichen 87, 12205 Berlin, Germany
[4]Optics11, De Boelelaan 1081, 1081 HV Amsterdam, the Netherlands
[5]International Laser Centre, Ilkovičova 3, 841 04 Bratislava, Slovakia
e-mail addresses: *mattia.longobucco@itme.edu.pl, mlongobucco@fuw.edu.pl*

Dual-core (DC) fiber-based nonlinear directional coupler is a classical approach for a compact all-optical switching device, however, up to now, without applicable demonstration [1]. A high-contrast switching of femtosecond pulses in solitonic regime in a soft glass DC photonic crystal fiber (PCF) was predicted at the excitation wavelength of 1550 nm [2]. However, the experimental demonstration failed due to the asymmetry of the used air-glass DC PCF [3]. Therefore, we proposed recently a solution by development of an all-solid dual-core fiber (DCF), which enables both high level of dual-core symmetry and advantageous solitonic propagation for the effective all-optical switching.

The applicable ultrafast all-optical switching in DCF stems from the principle of controllable self-trapping of high-order soliton in the both fiber cores [2]. In order to establish it for case of all-solid DCF, special soft glasses were in-house synthetized. The two glasses selected for the cores and for the cladding were the highly nonlinear lead–bismuth-gallium-silicate (PBG-08) glass, already used in the case of the air-glass DC PCF structure, and the complementary low index borosilicate glass (UV-710). Detailed values of refractive index (n) at 1500 nm and thermal expansion coefficient (α_{th}) are showed in Tab. 1. The combination of these two glasses provided a refraction index contrast at the level of 0.4 over a wide spectral region (1400 nm - 2000 nm).

Tab. 1. Properties of the in-house synthesized glasses for the all-solid DC fibers fabrication.

	PBG-08	**UV-710**
n @ 1500 nm	1.945	1.523
αth [μK^{-1}]	81.7	77.8

The study of the femtosecond nonlinear propagation was performed considering three fiber architectures: homogeneous simple cladding all-solid DC fiber (Fig. 1. center), air-glass PCF (same as Fig. 1 left), and all-solid PCF (Fig. 1 right). The structural geometries of all three architectures were optimized in order to satisfy the following requirements: high anomalous dispersion in the area of optical communication S, C, L, U-bands, sufficient nonlinearity for picojoule pulse energies with duration at level of 100 fs, minimization of TOD effect.

Fig. 1. Hexagonal array of the three DC fibers architectures: air-glass PCF with circular rods (left), simple cladding DCF (center) and all-solid PCF (right), both with hexagonal rods.

The optimization process was realized numerically by proper choice of the PCF lattice pitch Λ and outer radius r ratio (Λ/r). A structure with hexagonal-shaped rods with ratio Λ/r of 1.65 μm/0.85 μm was identified for the all-solid PCF as best from point of view of dispersion characteristics.

Nonlinear propagation of picojoule level femtosecond pulses was then compared numerically to identify the best switching performance at common input parameters, as 1700 nm central wavelength and 70 fs pulse width. The results revealed, that homogeneous cladding DCF supports the highest switching contrasts (SC) at the level of 12.1 dB regarding the integral energy at the lowest switching energies (67 – 73 pJ).

In the next step, combined optimization of excitation wavelength in range of 1400 – 1800 nm and pulse width in range 75 – 150 fs was performed in the case of the simple cladding DCF. This study resulted in lower switching energies (53 – 65 pJ) and simultaneous improvement of the SC at the level of 17.2 dB at combination of 1500 nm, 75 fs pulses and at 43 mm fiber length.

From the spectral point of view, Fig. 2 shows, that the best SC performance, under excitation of the simple all-solid structure by pulses with 75 fs width at 1500 nm, exceeds the level of 10 dB for most of the wavelengths. There are some peaks with exceptional SC at 1420 nm, 1480 nm and 1515 nm, expressing values of 39 dB, 39 dB and 30 dB, respectively.

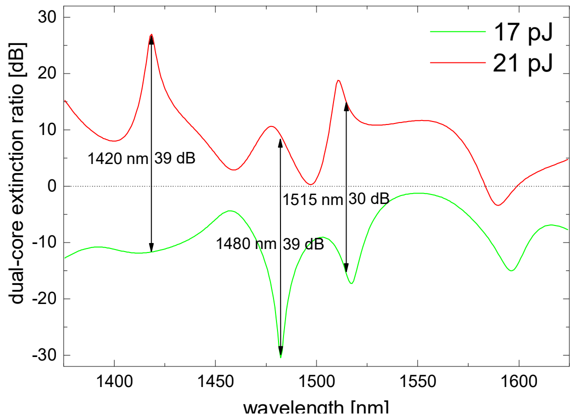

Fig. 2. DC SC of the spectral intensities. Homogeneous cladding, high index contrast DC fiber excited by 1500 nm, 75 fs pulses.

The predicted incoupled switching energies are at the level of 20 pJ only, which is a significant progress in comparison to similar works. The suggested approach is promising also from the application point of view, because of the easily manufacturable and simple cladding structure from readily available glasses.

Acknowledgments: This work was supported by the National Science Centre, Poland (project No. 2016/21/B/ST7/02249 under the OPUS 11 program).

References:

[1] A. Betlej et al, Optics Letters, 31 (2006) 1480–2

[2] P. Stajanca et al, Laser Physics Letters, 13 (2016) 116-201

[3] L. Curilla et al, Optical Fiber Technology, 42 (2018) 39-49

[4] M. Longobucco et al, Laser Physics Letters, 17 (2020) 025102

Optoelectronic motion tracking system for virtual reality shooting simulator

M. MACIEJEWSKI[1], M. PISZCZEK[1], M. POMIANEK[1] N. PAŁKA[1]

[1]Institute of Optoelectronics, Military University of Technology, 2 Kaliski Str., 00-908 Warsaw, POLAND
e-mail address: *marcin.maciejewski@wat.edu.pl*

Shooting skills practice is an important aspect of military training. However, its realization in the form of field training exercises is expensive, especially in the case of rocket weapons. Significant cost reduction can be achieved by implementing part of the training in a virtual environment. The simulator that fulfills this task requires, among other things, an accurate and precise motion tracking system that will provide information about the pose (position and orientation) of the user's head and replica of a weapon. One of the systems that can be used is SteamVR Tracking, which provides relatively high accuracy and precision and at the same time is much cheaper than professional motion tracking systems. Compared to other solutions, it is also distinguished by an open license, thanks to which users can construct their own tracking devices called trackers, optimized to work in a specific application.

We describe the design process and the optimization of the SteamVR tracker model. As a result, a prototype of the device was build, which at the simulation stage was characterized by better parameters than its commercial counterparts. The device has been tested at measuring setup (Fig. 1) prepared for this purpose.

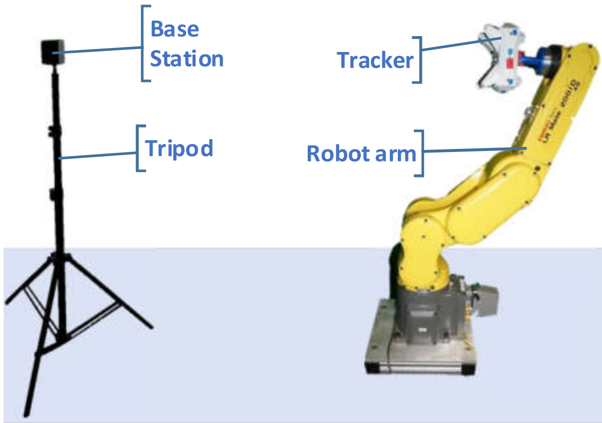

Fig. 1. Measuring setup

The results were analyzed to validate the software supporting the design process as well as to determine the accuracy and precision of position and orientation measurement of the developed device. The obtained results confirm that the simulation software used for designing allows to predict the parameters of the designed device. It can also be stated that the tracker parameters confirm that it can be used in the shooting simulator.

Light depolarization by nematic liquid crystals

P. MARĆ*, N. BENNIS, R. WĘGŁOWSKI, A. SPADŁO, K. GARBAT, D. WĘGŁOWSKA, E. PAWLIKOWSKA, A. PAKUŁA, L. R. JAROSZEWICZ

* Wojskowa Akademia Techniczna, gen. S. Kaliskiego 2, Warszawa, Poland
e-mail address: *pawel.marc@wat.edu.pl*

Liquid crystals are very extensively studied since many decades. Their application in display technology is one of the most important ones. However, electro-optic properties of the liquid crystal are still a very attractive subject of research. Basic form of a liquid crystal device is a liquid crystal cell in which liquid crystal is sandwiched between two glass plates. Each of them has ITO conducting layer and polymer arrangement layer. The latter one allows to predefine orientation of the liquid crystal director. In the presented work there were used nematic liquid crystals with specific polymer alignment layers for which the induced orientation of liquid crystal molecules is vertical. This type of orientation allows to induce spatial distribution of the birefringence. When such liquid crystal cell is illuminated by polarized light, the transmitted light measured by point detector is partially polarized. This effect is called pseud-depolarization. Due to the fact that electro-optic properties of a nematic liquid crystal are controlled by electric field, it is possible to tune degree of polarization of the transmitted light. During laboratory tests, there were selected materials which are driven not only by voltage but frequency, as well. In the presentation full optical properties of such liquid crystal cells described by losses, dichroism, phase shift and depolarization will be shown.

Measurement setup for determination of spectral characteristics of leaves

A.MAZIKOWSKI[1], M. FELDZENSZTAJN[1,2]

[1] Gdańsk University of technology, Faculty of Electronics, Telecommunications and Informatics, Narutowicza 11/12 , 80-233 Gdańsk, Poland

[2]NIVISS Sp. z o.o. Rdestowa 53D, 81-577 Gdynia, Poland

e-mail address: *adamazik@eti.pg.edu.pl*

Plant lighting systems are playing an increasingly important role in horticulture. The dynamic progress of lighting technology as well as significant increase in electricity prices necessitate researchers to increase the efficiency of these systems. Designing effective lighting for plant growing is a complex issue. One of the most important tasks is to match the spectral characteristics of designed lamp to the needs of the tested plant. Thus, the determination of spectral characteristics of leaves of the illuminated plant is required.

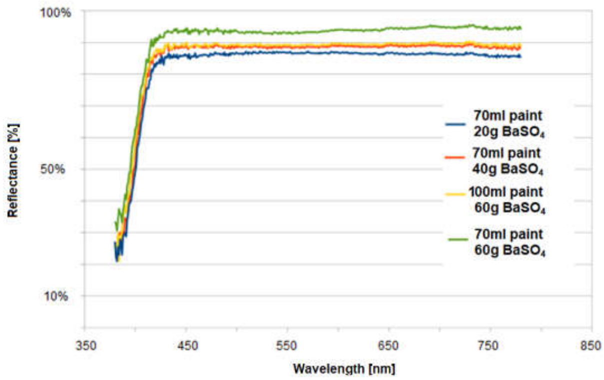

Fig. 1. Reflectance spectral characteristics of the developed painting mixture for different proportions of ingradients

The developed measurement setup consists of high-end spectroradiometer, moving stage with leaf mounting and illuminating lamp of broad and continuous spectrum. Additionally, high efficiency of lamp is required to provide an enough amount of light, while the leaf surface should not be overheated. Thus, the developed lamp is based on a selection of power LEDs.

To properly mix light from several different LEDs, a dedicated low-cost integration sphere was applied. It was made of two metal hemispheres (one with output hole) pained inside with developed paint based on barium sulfate and white latex paint.

Several compositions of barium sulfate powder and white latex paint have been tested (Fig.1). The best results (highest reflectance, over 90%) was achieved for the composition of 70 ml of latex paint mixed with 60 g of barium sulfate. Such mixture is suitable for painting the sphere, however it is recommended to paint in thin layers several times.

Fig. 2. View of the tested leaf through the instrument viewfinder; small black dot represents the measurement fields

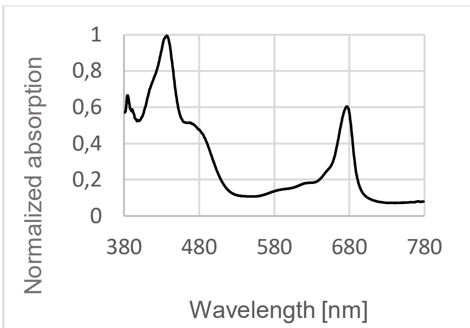

Fig. 3. Measured absorption characteristic of basil leaves

Based on the developed measurement setup, measurements of spectral characteristics of basil leaves were performed. View of the instrument observation field with tested leaf is presented in Fig. 2, while the measured characteristic on the basil leaf is shown in Fig. 3

Summarizing, the developed measurement setup allows for determination of characteristics of the leaves of various plants and, consequently, the proper selection of the spectrum of the illuminating lamp during cultivation.

Acknowledgments: This work is supported by the DS funds of the Faculty of Electronics, Telecommunications and Informatics of the Gdańsk University of Technology.

References:

[1] R.M. Metallo, D.A. Kopsell, C.E. Sams, N.R. Bumgarner, “Influence of blue/red vs. white LED light treatments on biomass, shoot morphology, and quality parameters of hydroponically grown kale” , Scientia Horticultura, 235, 189-197, 2018.

[2] Mazikowski A., Feldzensztajn M., "Lamp of adjustable spectrum for photographic usage", Proc. SPIE 10445, 2017.

[3] DiLaura D. L., Houser K. W., Mistrick R. G., Steffy G. R, “The lighting handbook”, Illuminating Engineering Society, 2011.

[4] “Measurement of LEDs”, Central Bureau of the CIE, Publication No. 127 Vienna, Austria, 2007.

Effect of thermal annealing on sensing properties of optical fiber sensors coated with indium tin oxide nano-overlays

B.MICHALAK[1,2], P. SEZEMSKY[3], V. STRANAK[3], and M. SMIETANA[1]

[1] Warsaw University of Technology, Institute of Microelectronics and Optoelectronics, Koszykowa 75, 00-662, Warsaw Poland
[2] Warsaw University of Technology, Centre for Advanced Materials and Technologies CEZAMAT, Poleczki 19, 02-822, Warsaw, Poland
[3] University of South Bohemia, Institute of Physics, Branisovska 1760, 370 05 Ceske Budejovice, Czech Republic
e-mail address: *b.michalak@cezamat.eu*

In this work we discuss an effect of thermal annealing on optical properties of indium tin oxide (ITO) deposited on short section of core of multimode polymer-clad optical fiber (see Fig. 1.). Due to high refractive index sensitivity, this type of structures can be used for biosensing.

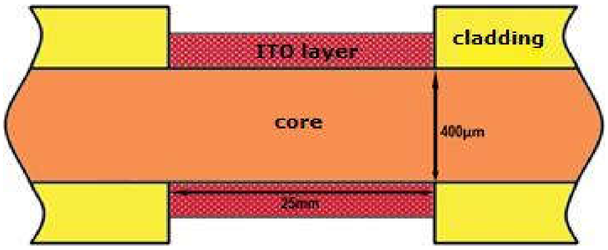

Fig. 1. Schematically shown cross section of optical fiber with deposited ITO layer.

For these structures it is possible to observe a lossy-mode resonance (LMR) optical effect [1] and, due to electrochemical activity of ITO they can be used for simultaneous optical (LMR) and electrochemical measurement what makes cross-verification of the results possible [2].

ITO layers were deposited using high power impulse magnetron sputtering (HiPIMS) and radio frequency magnetron sputtering (RF MS) [3]. A various position of sputtered target led to different thickness of the overlays. Optical transmission of the ITO-LMR samples was measured when they were submerged in liquids of refractive index in range nD=1.334-1.466 (Fig. 2). We analysed properties of LMR shift observed in the spectrum as an effect of thermal annealing.

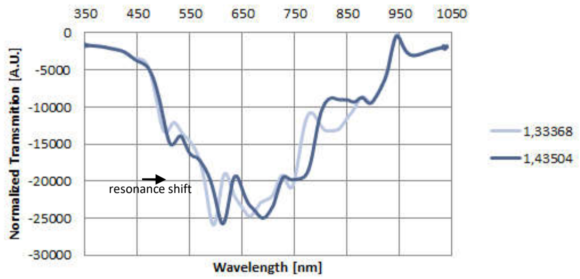

Fig. 2. Transmission of an ITO-LMR sample before thermal annealing when immersed in liquids of different refractive index.

Electrical resistance of the ITO overlays was also measured on 25 mm length of sensor area (see Tab. 1.) After both measurements samples were annealed at 200°C in a tube furnace in nitrogen atmosphere. Optical and electrical measurements were repeated after the thermal annealing. Results of the measurements are shown in Tab.1 and Fig 3.

Tab. 1. ITO-LMR samples resistance for specific position of sputter target before and after thermal annealing

RB160 sample series	Resistance before annealing	Resistance after annealing
Run A	450 Ω	230 Ω
Run B	275 Ω	210 Ω
Run C	335 Ω	240 Ω

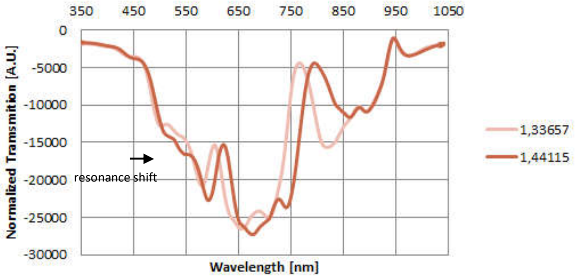

Fig. 3. Transmission of an ITO-LMR sample after thermal annealing when immersed in liquids of different refractive index.

Obtained data indicates that thermal annealing changed the optical response of the sensor. Observed LMRs are shifted towards longer and shorter wavelengths for thinner and thicker ITO thickness, respectively. Thermal annealing also decreased electrical resistance of the deposited ITO. Understanding of both effects can lead to finding optimal ITO deposition parameters and also optimal annealing temperature for optical fiber sensors used in simultaneous optical and electrochemical measurements [4][5].

Acknowledgments: This work was supported by National Science Centre of Poland within the research project 2014/14/E/ST7/00104 and also The National Centre for Research and Development of Poland within the research project TECHMATSTRATEG1/347324/12/NCBR/2017

References:

[1] I. Del Villar et al., J. Opt., vol. 12, no. 9, p. 95503, 2010,
[2] M. Sobaszek et al., 25th Int. Conf. Opt. Fiber Sensors, vol. 10323, p. 103234W, 2017,
[3] P. Niedziałkowski et al., Sensors and Actuators B - Chemical, vol. 301, no. 12 December, pp. 1–10, 2019.
[4] M. Śmietana et al., J. Light. Technol., vol. 36, no. 4, pp. 954–960, 2018.
[5] M. Śmietana et al., Electroanalysis 2019, 31, 398.

Soft sensor design for measuring liquid volume

Krzysztof Murawski

S. Kaliskiego 2, Warszawa, Warszawa 01-489 Poland
e-mail address: *krzysztof.murawski@wat.edu.pl*

The paper presents the construction and application of a soft sensor developed for measuring liquid volume. A characteristic feature of the device is the measurement of liquid volume based on the image from a miniature camera. The paper presents the design of the soft sensor and its calibration results. The results of measurements tests are also presented in the paper. During the tests, tle volume of liquid was measured in the range of 0 to 80 ml with an absolute error of 0.31ml.

Generation optical vortex beam in Liquid media using novel nanostuctured vortex phase masks

H.T NGUYEN[1,2], K. SWITKOWSKI[3], R. KASZTELANIC[1,2], A. ANUSZKIEWICZ[2,7], A. FILIPKOWSKI[2], H.V LE[6], D. PYSZ[,2], R. STEPIEN[2], W. KROLIKOWSKI[4,5], R. BUCZYNSKI[1,2]

[1] Faculty of Physics, University of Warsaw, Pasteura 5, 02-093 Warsaw, Poland
[2] Department of Glass, Institute of Electronic Materials Technology, Wolczynska 133, 01-919 Warsaw, Poland
[3] Faculty of Physics, Warsaw University of Technology, Koszykowa 75, 00-662 Warsaw, Poland
[4] Science Program, Texas A&M University at Qatar, Doha, Qatar
[5] Laser Physics Centre, Research School of Physics and Engineering, Australian National university, Canberra, ACT 0200, Australia
[6] Institute of Research and Development, Duy Tan University, Da Nang 550000, Vietnam
[7] Institute of Electronic Systems, Warsaw University of Technology, Nowowiejska 15/19, 00-665 Warsaw, Poland
e-mail address: *hue.nguyen@fuw.edu.pl*

We report on a theoretical and experimental study of a single nano-structured gradient index vortex phase mask (nVPM). The nVPM is composed of an designed array of sub-wavelength rods which were made of two glass types with low and high refractive indices. The refractive index distribution of a masks was calculated using the effective medium theory (EMT) [1] using simulated annealing approach [2]. Accordingly with the EMT the binary nano-rod structure, while discrete, will behave as a continuous effective medium with effective index distribution equal to spatial average of neighboring refractive indices.

A cost-effective modified stack-and-draw technique was utilized for nVPM development [3]. This approach is commonly applied in development of photonic crystal fibers and nanostructured optical micro-components as nGRIN microlens, microaxicon [4,5]. The fabricated nVPMs have a diameter of 20 µm and length of 25 µm, which, according to the theory, should generate optical vortex beam charge l = 1 at 632.8 nm wavelength of the input beam. We numerically and experimentally investigated optical performance of the nVPM in different liquid media like water and ethanol. Our measurement setups with the use of He-Ne laser sources allow observing a vortex beam.

A few different techniques were used to study phase properties of the vortex beams. We used a astigmatic vortex transformation to Hermite-Gaussian modes by cylindrical lens [6] and formation of interference patterns between vortex and the Gaussian reference beam realized in Mach-Zehnder interferometer configuration [7]. The astigmatic vortex transformation pattern proved that the vortex is of topological charge l = 1 because there are two distinct bright elongated regions separated by a dark stripe. That is also confirmed by results obtained by interferometric measurements involving collimated and slightly divergent reference waves. The presence of one extra fringe in the fork pattern as well as single spiral arm in the phase form indicating generation of single charge optical vortex (l = 1).

The experimental results are in good agreement with the theoretical predictions. Importantly, the optical performance of nVPMs is unaffected by the refractive index of the surrounding media no matter in air [3] or in water or in ethanol media. This confirms that nanostructurization technique allows obtaining nano-structured masks suitable for work well either in the air or liquid media making it an excellent candidate for microfluidic applications.

Acknowledgments: This work was supported by the project POIR.04.04.00-1C74/16 operated within the Foundation for Polish Science Team Programme co-financed by the European Regional Development Fund under Smart Growth Operational Programme (SG OP), Priority Axis IV. W.K. acknowledges support from Qatar National Research Fund (NPRP 9-020-1-006). W.K. acknowledges support from Qatar National Research Fund (grant# NPRP 9-020-1-006).

References:

[1] A. Sihvola, Electromagnetic Mixing Formulas and Applications (IET, The Institution of Engineering and Technology, UK, 1999).

[2] S. Kirkpatrick et al., Science, 80, (1983).

[3] K. Switkowski et al., Opt. Express 25, 31443 (2017).

[4] F. Hudelist et al., Opt. Express 17, 3255 (2009).

[5] A. Filipkowski et al., Opt. Lett. 40, 5200 (2015).

[6] V. Denisenko et al., Opt. Express 17, 23374 (2009).

[7] G. Bogatiryova et al., Semicond. Phys. Quantum Electron. Optoelectron. 6, 254 (2003).

The practice of accepting gas sensors for commercial purposes

A.PACHOLE

Atest-Gaz A. M. Pachole sp. j., ul. Spokojna 3, 44-109 Gliwice, Poland
e-mail address: *a.pachole@atestgaz.pl*

One of the Conference topics is "Integrated Optics - Sensors". Atest Gaz is a company which uses optoelectronic gas sensors in its everyday business practice.

As the appropriate gas sensor is the most crucial component of our products, our Company have worked out and implemented our own procedures for the tests of the sensors prior to its acceptance in practical use. So we have a rich portfolio of the experience with different sensor technologies, models, its quality, performance and make. We also perceive particular flaws in the commercial approach of the sensors manufacturers product strategy, which very often eliminates them from the use. In the presentation we would like to present and share our experience in this field with the Audience.

Integrated multichannel transmitters for telecom and datacom applications

A. PAŚNIKOWSKA, S. STOPIŃSKI, A. KAŹMIERCZAK AND R. PIRAMIDOWICZ

Warsaw University of Technology, Institute of Microelectronics and Optoelectronics,
Koszykowa 75, 00-662 Warszawa, Poland
e-mail address: *aleksandra.pasnikowska.dokt@pw.edu.pl*

The continuous development of optical communications and specifically access technologies like Fiber-To-The-Home (FTTH) has fuelled an increasing attention on local optical links. This, in turn, stimulates the dynamic development of integrated transmitters and receivers. As the technology of photonic integrated circuits (PICs) is progressing very fast, it becomes possible to develop photonic chips for those applications. PICs offer the same advantages as electronic integration technologies, including cost and energy efficiency, high reliability of the devices and tremendous size reduction.

Although the widely investigated and matured silicon (Si) platform seems ideal for development of photonic devices, it suffers from indirect bandgap of silicon forbidding efficient light generation. The solution for this limitation is the use of the indium phosphide (InP) platform, supporting light propagation, amplification, detection and fast phase modulation in a monolithic chip. Nowadays the InP platform provides basic building blocks like deeply and shallow etched waveguides, semiconductor optical amplifiers (SOA), electro-optic phase modulators, PIN photodiodes and DBR gratings. The combination of these enables constructing photonic devices of various functionality [1].

In this work we present and discuss the properties of the line of integrated multichannel transmitters designed and characterized in the Eastern Europe Design Hub of Warsaw University of Technology. The chips were manufactured using a generic InP technology in two different foundries: SMART Photonics and Fraunhofer Heinrich Hertz Institute (HHI).

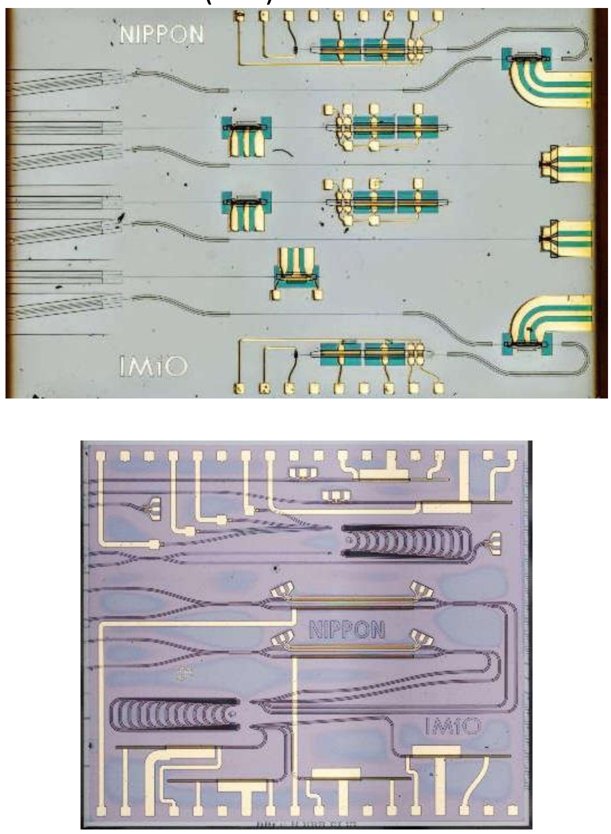

Fig. 1. Microscope photographs of transmitters fabricated in HHI (top) and SMART (bottom).

Fig. 1. presents microscope photographs of exemplary cases of integrated transmitters designed as optical network unit (ONU), operating in an experimental access network. All of the designed and manufactured chips were carefully characterized with respect of their optical properties, which enabled discussion on their potential deployment in commercial optical access systems and data communication as well.

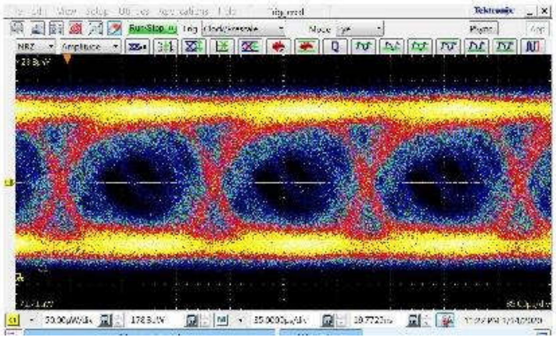

Fig. 2 Eye-diagram of a 10 Gb/s optical signal recorded in the back-to-back configuration.

The output power of transmitters is around 0.5 mW, static extinction ratio of the modulators is above 15 dB, side mode suppression ratio of the lasers is above 30 dB. These parameters satisfy ITU recommendations for 10G-PON access networks [2]. Fig. 2. shows an example of an eye diagram, measured for 10 Gb/s transmission of transmitter fabricated in HHI. The error-free operation at -17 dBm was recorded.

The obtained results, especially open eye diagrams, prove that InP photonic integrated circuits can be successfully deployed in telecom and datacom applications.

Acknowledgments: This work was supported by the National Centre for Research and Development (project NIPPON of the 3rd Applied Research Programme, grant agreement PBS3/A3/21/2015).

References:

[1] M. Smit et al., "An introduction to InP based generic integration technology," Semicond. Sci. Technol., vol. 29, no. 8, p. 083001, Jun. 2014.

[2] G.987.2, "10-Gigabit-capable passive optical networks (XG-PON): Physical media dependent (PMD) layer specification," 2010.

Integrated Photonics – yesterday, today and tomorrow

R. PIRAMIDOWICZ, S. STOPIŃSKI, A. PAŚNIKOWSKA, M. SŁOWIKOWSKI, A. KAŹMIERCZAK, A. JUSZA, K. ANDERS, W. PLESKACZ, P. SZCZEPAŃSKI

Warsaw University of Technology, Institute of Microelectronics and Optoelectronics, Koszykowa 75, 00-662 Warsaw, Poland

e-mail address: r.piramidowicz@elka.pw.edu.pl

Starting from the turn of the 21st century a dynamic evolution of integrated photonic technologies has been observed, manifesting itself in continuous breaking records of number of photonic elements integrated within a single chip, as well in a fast route from the lab to the innovation-hungry ICT market.

Photonic integrated circuits (PICs) – miniaturized optoelectronic devices, consisting of multiple photonic components (active and passive), integrated on a single substrate are fully analogous to integrated electronic circuits, differing from these only in information carriers, which are photons instead of electrons.

The beginnings of integration of photonic components date back to years 70's of the former century and are closely connected with mastering the technology of semiconductor lasers. This resulted also in a dynamic progress in all semiconductor-based optoelectronic components and a natural tendency to their integration.

PICs offer the combination of unique advantages of miniaturization, low energy consumption, high reliability and reduction of manufacturing and packaging costs. These features are similar to those, which were decisive for the revolution that has been brought by integrated electronics, omnipresent in the entire world of information technologies. It seems that integrated photonics, complementary to electronic chips in its character, begins to revolutionize the market of photonic applications.

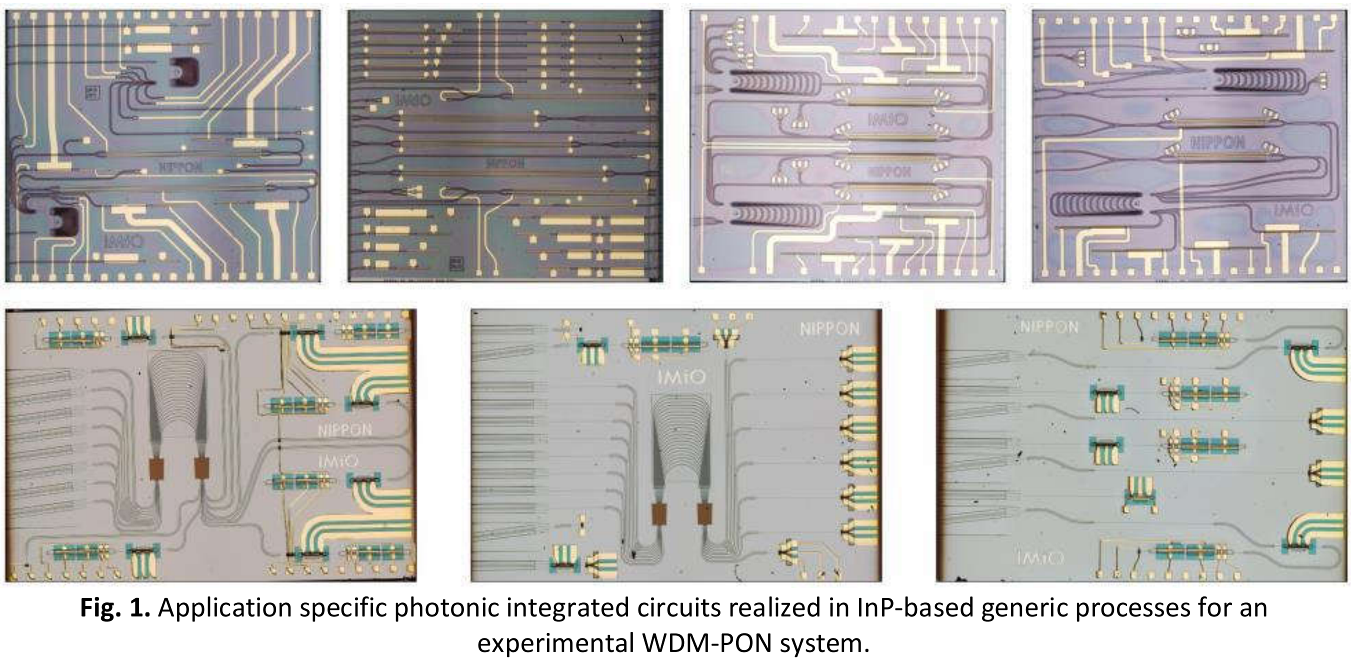

Fig. 1. Application specific photonic integrated circuits realized in InP-based generic processes for an experimental WDM-PON system.

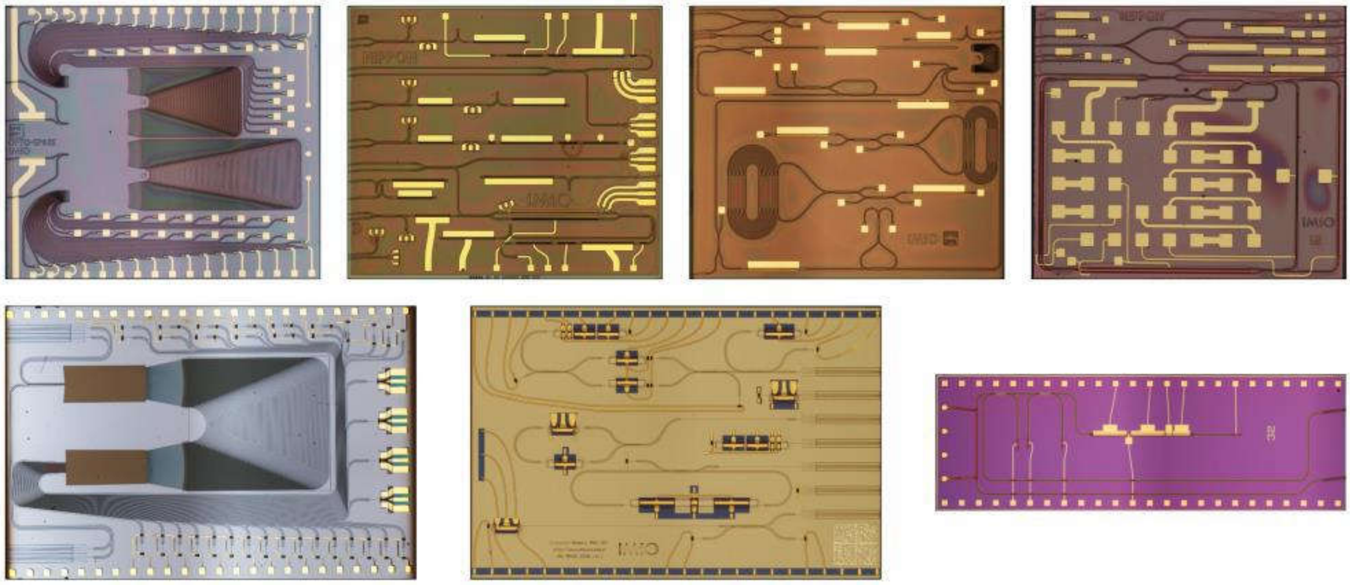

Fig. 2. Application specific photonic integrated circuits realized in InP-based generic processes for optical sensing and metrology applications.

In this work the history and current capabilities and potential of the major technological platforms (indium phosphide, silicon and silicon nitride) will be discussed in the context of applications in optical communications, sensing and metrology, which are considered as the main drivers of integrated photonics market. The results of the last few years of research on application specific photonic integrated circuits (ASPICs) conducted by the team of the Eastern Europe Design Hub (EEDH) of Warsaw University of Technology will be shown. In particular, two main ASPIC lines will be presented and discussed in detail. They address two abovementioned fields of applications – high-speed multichannel transmitters and receivers for fiber-optic access systems (based both on wavelength and spatial domain multiplexing techniques) and integrated photonic interrogators for fiber Bragg grating (FBG) sensor networks. Furthermore, a concept of photonic-electronic integration will be discussed, as well as other perspective directions of integrated photonics evolution.

Acknowledgments: This work has received support from the National Centre for Research and Development through projects NIPPON (PBS3/A3/21/2015), OPTO-SPARE (PBS3/B9/41/2015) and NMKM+ (TECHMATSTRATEG/1348438/ 16/NCBR/2018) and from the EU Horizon 2020 research and innovation programme under grant agreement No. 687777 (PICs4All).

ASPIC-based photonic system for monitoring breath/respiratory rate of patient under MRI diagnosis

M. SŁOWIKOWSKI[1,2], A. KAŹMIERCZAK[1], M. BIENIEK[1], S. SZOSTAK[1], T. OSUCH[3], M. KREJ[4], Ł. DZIUDA[4], S. STOPIŃSKI[1] AND R. PIRAMIDOWICZ[1]

[1] Warsaw University of Technology, Centre for Advanced Materials and Technologies CEZAMAT, Poleczki 19, 02-822 Warsaw, Poland
[2] Warsaw University of Technology, Institute of Microelectronics and Optoelectronics, Koszykowa 75, 00-662 Warsaw, Poland
[3] Warsaw University of Technology, Institute of Electronic Systems, Nowowiejska 15/19, 00-665 Warsaw, Poland
4 Military Institute of Aviation Medicine, Krasińskiego 54/56, 01-755 Warsaw, Poland
e-mail address: *mateusz.slowikowski@pw.edu.pl*

During a magnetic resonance imaging (MRI) examination, the experience of anxiety caused by a claustrophobic shape of an MRI chamber is quite common. Such an experience may lead to increased heart rate and respiratory rate of the patient. Monitoring of these two vital functions provides real-time basic information about the general condition of the patient undergoing MRI.

The measurement system presented in this work has been designed and manufactured for monitoring heart and respiratory rate of a patient undergoing an MRI examination. The system consists of a fiber optic sensor network and a dedicated photonic interrogator. Defined in that way the proposed solution has two elementary features essential during MRI examination: it does not interact with the strong electromagnetic field generated by the device and is imperceptible to the patient. The installed sensor network, containing a number (ranging from 3 up to 10) of fiber Bragg gratings (FBGs) is mounted in the overlay of the bed on which the patient is lying. During the MRI examination, the sensors record both current respiratory and heart rate, influencing Bragg wavelengths of FBGs. As the sensors are fabricated in all-fiber technology, not containing any metal parts, they do not interfere with the MRI system.

The entire readout unit of the measuring system is placed outside the MRI chamber and is based on an application specific photonic integrated circuit (ASPIC). This approach offers potential for system miniaturization, reduction of electric power demand, increased reliability and optimized costs of the whole measurement system. The concept of the interrogation is based on the use of a broadband light source, connected to sensors and reconstruction of the spectrum of the signals reflected from FBGs with a wavelength-selective element, followed by a matrix of photodetectors. The essential part of the developed integrated interrogator is an arrayed waveguide grating (AWG) wavelength demultiplexer. The designed ASPIC, which is the receiving part of the interrogator, has two AWGs with a channel spacing of 0.4 nm and 0.6 nm. Both demultiplexers have two inputs and 36 outputs, connected directly to an array of p-i-n photodiodes. One of the inputs of each circuit comprises a semiconductor optical amplifier (SOA) to increase the power level of the optical signal. To collect all 36 photocurrent signals simultaneously, a dedicated driver based on an STM microcontroller was designed and implemented. The driver was mounted on a printed circuit board (PCB), which enables assembling a packaged PIC. The receiving part of the interrogator is shown in Fig. 1.

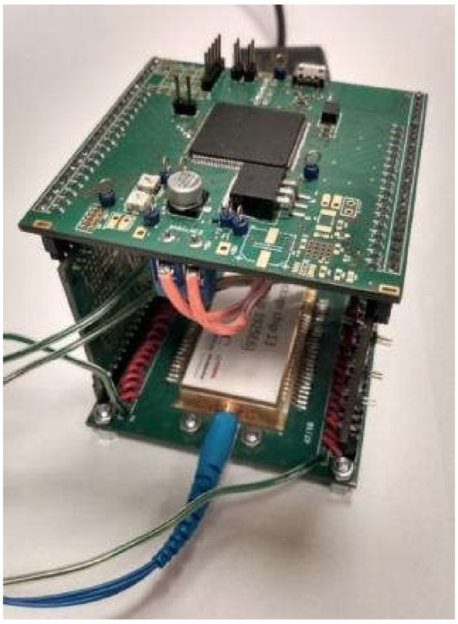

Fig. 1. Receiving part of interrogator consisting packaged PIC and electronics driver.

Superluminescent LED was used as a broadband signal source in the system. The sensor network consisted of 9 FBGs connected in series using a standard single mode optical fiber.

Fig. 2. presents the signals recorded from four consecutive photodiodes of the developed interrogator unit as a function of time. In the performed experiment a person was lying on the mattress and intentionally changing his/her respiratory rate. The plot indicates the breathing pattern with intervals of normal breathing, apnea and fast breathing.

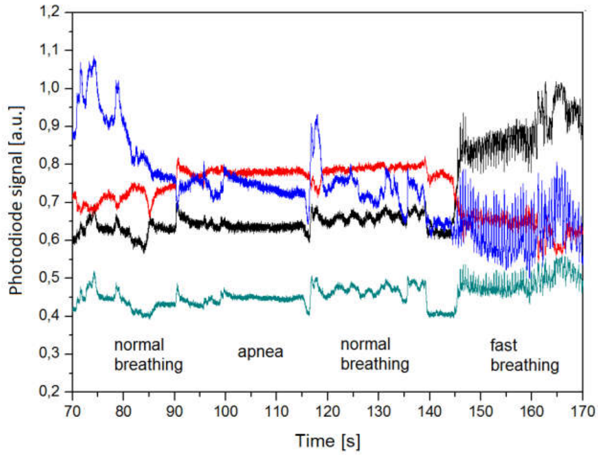

Fig. 2. Interrogator signals received according to the breath pattern.

Due to the variable pressure induced by the patient's body on the sensor network, the optical power detected by specific photodiodes fluctuates. It can be observed that the level of the received signal is changing in accordance to the breath pattern. Changes are most clearly noticed between neighboring detectors, transmission channels of which are the closest to the Bragg wavelength of the sensor.

The results confirm the potential of developing a fully functional system for monitoring the patient condition during MRI scanning with the use of an ASPIC-based interrogator and a network of FBG sensors. As a follow up of the presented work, further development of the system is envisaged including data analysis for precise readout of patient heart-beat and breath ratio as well as increasing the number of FBGs to be interrogated.

Acknowledgments: This work was supported by the National Centre for Research and Development (project OPTO-SPARE, grant agreement PBS3/B9/41/2015).

Twist induced mode confinement in partially open ring of holes

G. STATKIEWICZ-BARABACH[1], M. NAPIÓRKOWSKI[1], K. ŻOŁNACZ[1], M. BERNAŚ[1], A. KICZOR[2], P. MERGO[2], W. URBAŃCZYK[1]

[1] Department of Optics and Photonics, Faculty of Fundamental Problems of Technology, Wroclaw University of Science and Technology, Wybrzeze Wyspianskiego 27, 50-370 Wroclaw, Poland
[2] Laboratory of Optical Fiber Technology, Maria Curie-Sklodowska University, pl. M. Curie-Sklodowskiej 3, 20-031 Lublin, Poland
e-mail address: *gabriela.statkiewicz@pwr.edu.pl*

We report on a new phenomenon of light guidance in a fiber core created by an arrangement of holes making a partially open ring. In such structure there is no complete refractive index barrier to confine the light and therefore it cannot guide light if untwisted. However, if the open ring of holes is shifted off the symmetry axis of the twisted fiber then the mode confinement and low loss propagation is possible due to purely geometrical effect related to the increase in the optical path of light following the helical route. Properties of such structures, including confinement loss, modal field distribution, birefringence of fundamental modes were investigated both numerically and experimentally.

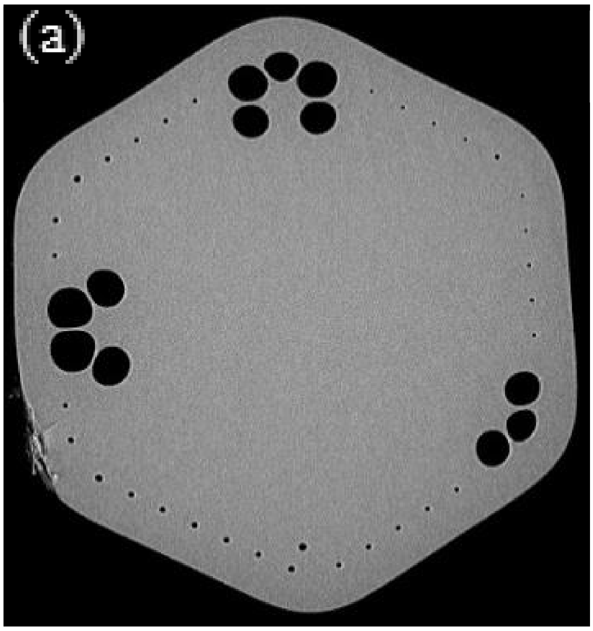

Fig. 1. Cross-section of a microstructured optical fiber with partially open ring of holes.

Acknowledgments: This work was supported by the National Science Centre of Poland, grant Maestro 8, DEC- 2016/22/A/ST7/00089

Photonic integrated circuits for portable OTDR systems

S. STOPIŃSKI, K. ANDERS, S. SZOSTAK AND R. PIRAMIDOWICZ

Warsaw University of Technology, Institute of Microelectronics and Optoelectronics, Koszykowa 75, 00-662 Warsaw, Poland

e-mail address: *stanislaw.stopinski@pw.edu.pl*

Optical time domain reflectometers (OTDR) enable performing a reasonably fast and versatile characterization of optical fiber links in terms of the attenuation of fibers, the loss and reflectivity of splices and junctions, and eventually the length of the fiber sections [1]. Nowadays, despite a tremendous development of various types of OTDR devices, they are still based on discrete photonic elements. In this work we present our recent results of the work focused on development of a novel OTDR system, concept of which is based on monolithic optical chips, realized using indium phosphide generic platforms. Such a solution may enable realizing compact reflectometers, which can be used by technicians in the field as the interface would be provided through smartphones, tablets or other portable devices.

Generally, the OTDR measurement technique is based on sending a series of light pulses to an optical fiber and analyzing the signals that propagate backwards. These are a result of Rayleigh backscattering and Fresnel reflections occurring within the fiber link.

Fig. 1. presents an operational scheme of the realized integrated OTDR interrogation units. The first device comprises a directly modulated DFB laser and two photodiodes connected to a multi-mode interference (MMI) coupler. The remaining port of the coupler is connected to the chip output.

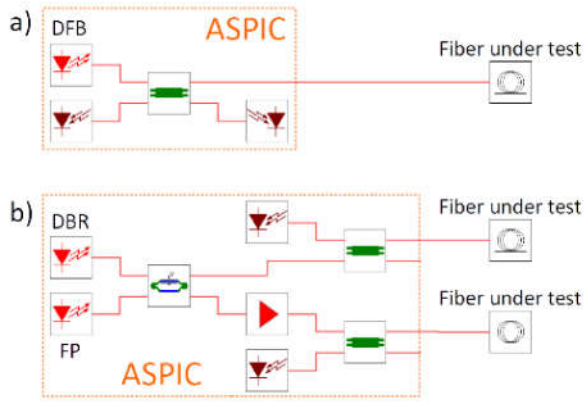

Fig. 1. Operational scheme of the integrated OTDR interrogator units.

The second investigated circuit uses continuous wave laser sources, either with a DBR or a Fabry-Perot resonator. Optical pulses are generated using a 2×2 Mach-Zehnder modulator (MZM). Depending on the parameters of the driving electrical signal, the pulses can be routed to either of the output ports of the MZM. One of the outputs is connected to a semiconductor optical amplifier to boost the power of the pulses and compensate the chip-fiber coupling loss and insertion losses of all passive components. However, as the generated ASE noise could disturb the performance of the receiving photodiodes (the recorded Rayleigh signal is typically very weak), the second part of the circuit is purely passive.

The optical chips have been manufactured in the framework of multi-project wafer runs using two different InP platforms – Heinrich Hertz Institute and SMART Photonics [2]. Fig. 2. presents microscope pictures of both fabricated chips. The first one has the dimensions of 6 mm × 1 mm, while the second 4.6 mm × 2.0 mm.

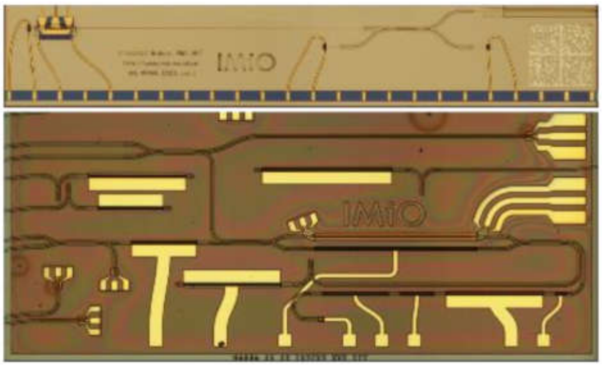

Fig. 2. Micrographs of OTDR interrogator units.

The fabricated devices have been initially characterized with respect to their applicability in real OTDR systems. Fig. 3 presents recorded time traces (averaged with 1024 samples) after injecting a series of optical pulses to a 10 km long section of a single mode fiber.

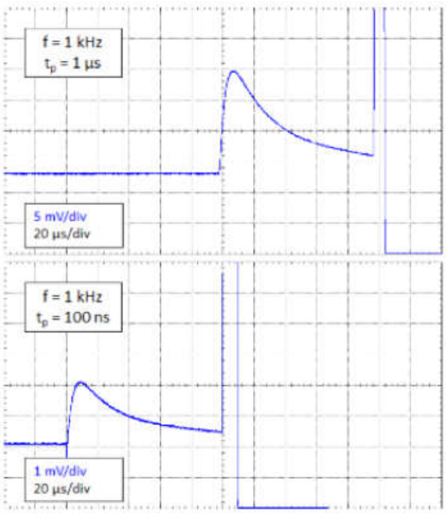

Fig. 3. Recorded time traces after injecting laser pulses to a 10 km section of a single mode fiber.

The obtained characterization results are promising – Rayleigh backscattering signal has been detected and reflection from the fiber end is clearly visible. However, further development of the interrogation unit requires dedicated and specialized electronic control units. Fig. 4. presents a scheme of the proposed electronic system. The circuits are designed to be compatible with both types of the photonic chips. The driver circuits will enable direct modulation of the DFB laser (switching from 10 mA to 150 mA) of the first ASPIC as well as provide DC power supply of the CW lasers and modulation of the Mach-Zehnder interferometer (switching between 0 V and 5 V of reverse bias). Thus, in both cases generation of optical pulses of a time duration between 20 ns and 100 μs will be supported. On the receiving side the control electronics comprises transimpedance amplifiers, with a controlled current-to-voltage gain, adjustable to the required level of the data acquisition (DAQ) system. The DAQ unit and the system controller are based on commercially available devices, dedicated to OTDR applications.

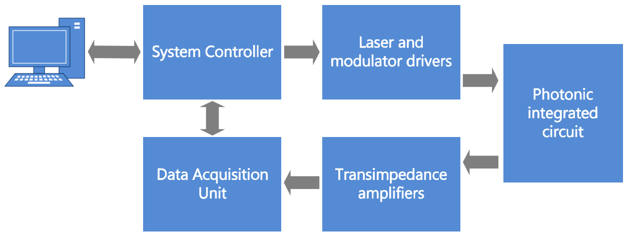

Fig. 4. Operational scheme of the OTDR electronic control system.

To sum up – the photonic integrated circuits for application in portable optical time domain reflectometers of a new type have been described and discussed. The basic capabilities of the devices such as detection of the Rayleigh backscattering signal and Fresnel reflections have been confirmed. A concept of further development of a complete opto-electronic system has been proposed.

References:

[1] M. K. Barnoski et al., Applied Optics, vol. 15, no. 9, pp. 2112-2115, 1976.
[2] M. Smit et. al., Semiconductor Science and Technology 2014, Volume 29, Number 8, p. 083001

The endomicroscopy probe based on micro-interferometer Mirau and 2-axis microscanner fabricated in MOEMS/MEMS technology for SS-OCT imaging

P. STRUK[2,1], F. E. GRACIA-RAMIREZ[1], S. BARGIEL[1], Q. TANGUY[1,3], O. GAIFFE[1], R. CHUTANI[1], N. PASSILLY[1], P. LUTZ[1], J-M. COTE[1], H. XIE[3], C. GORECKI[1],

[1]FEMTO-ST Institute (UMR CNRS 6174, Université Bourgogne Franche-Comté), 15B Avenue des Montboucons, 25030 Besançon, France.
[2]Department of Optoelectronics, Faculty of Electrical Engineering, Silesian University of Technology, 2 Krzywoustego Str., 44-100 Gliwice, Poland.
[3]University of Florida, Gainesville, Florida, USA.
e-mail address: *Przemyslaw.Struk@polsl.pl*

The most dangerous diseases in the human body directly life-threatening are cancerous lesions, particularly in stomach tissue. From this point of view early diagnosis of cancers in stomach tissue is very important to increase the chances of efficiency treatment of patient. Currently, diagnosis of cancers is mostly based on ultrasound scanning, biopsy and histopathological research of suspected part of tissue. However, this method is painful, time consuming and expensive. An alternative and interesting solution is a swept source optical coherence tomography imaging method combined with a endomicroscopic device, which allows to provide non-invasive, optical biopsy of tissue for cancer diagnosis, especially in upper digestive tract.

The Authors presents the SS-OCT imaging system with endomicroscopic micromachined probe fabricated in MOEMS/MEMS technology. The SS-OCT endomicroscopic probe is based on monolithically integrated MOEMS micro-interferometer Mirau and 2-axis electrothermal MEMS microscanner and GRIN lens collimator. The presented SS-OCT endomicroscopy probe can be fabricated in two version depending on diagnostic needs. The probe can 3D imaging of sample in two scanning regime. Regime of forward scanning of the sample is based on the probe consists of micro-interferometer Mirau and GRIN lens collimator. The 3D OCT image is obtained by moving of the probe by robotic arm. Regime of transverse scanning of the sample is based on the probe consist of Mirau micro-interferometer vertically integrated with the 2-axis electrothermal microscanner and with GRIN lens collimator [1,2]. The 3D imaging of sample is carried out by 2-axis electrothermal microscanner, which apply Lissajous scanning [1,3]. The scanning of the sample is carried out for wavelength λ_c=840nm (swept range $\Delta\lambda$= 60 nm), with axial and lateral resolution: L_A = 5.2 μm and L_R = 9.6 μm respectively.

Acknowledgments: This work was supported by Labex Action program, ANR-11-LABX-0001-01, the INSERM Plan Cancer program (ROBOT project), the French RENATECH network and its FEMTO-ST technological facility and by the Collegium SMYLE.

References:

[1] P. Struk et. al., Optics Letters, 43(19) (2018).
[2] P. Struk et. al., Proceedings of SPIE 10678,1067807 (2018).
[3] Q. A. A. Tanguy et. Al., 2017 19th International Conference on Solid-State Sensors, Actuators and Microsystems (TRANSDUCERS) (2017).

Performance analysis of MIMO communication system with NLOS UV channel

D. I. SURZHIK[1], G. S. VASILYEV[2], O. R. KUZICHKIN[3]

[1] Vladimir State University, Vladimir, 600000, Russia
[2] Belgorod State University, Belgorod, 308015, Russia
[3] Belgorod State University, Belgorod, 308015, Russia

e-mail address: *arzerum@mail.ru*

Abstract: analysis of the performance of the multiple input, multiple output (MIMO) UV communication system with non-line-of-sight (NLOS) UV channel is performed. The achievable bit error coefficient is calculated using three spatial multiplexing methods for different bitrate values, azimuthal deviation between the directional diagrams of the optical transmitter and the optical receiver, and different noise levels.
Keywords: UV communication, UV-C, NLOS, MIMO, ad-hoc networks.

Communication systems of the solar-blind UV-C range from 200 to 280 nm enable communication in the absence of direct visibility (non line-of-sight, NLOS) due to strong scattering of UV radiation in the atmosphere, including in the presence of high obstacles between the transmitter and receiver, when traditional radio communication is ineffective [1]. One of the ways to improve the performance of UV-C communication systems is to use the multiple input, multiple output (MIMO) technology. In addition, the use of an array of transmitters and an array of receivers oriented in different directions allows for communication when moving and turning communication nodes, which is typical for a mobile ad-hoc network with a UV-C channel [2]. To use MIMO technology in real UV communication systems, it is necessary to analyze the performance characteristics of the system in different operating conditions, determined by the channel state and the selected transmission mode.

Energy characteristics of the MIMO communication system with an abstract channel for three spatial multiplexing methods with 2 transmitter channels and 2 receiver channels have been calculated. Detection by a receiver is based on one of three criteria: 1) maximum-likelihood (ML); 2) Zero-Forcing Successful Interference Cancellation (ZF-SIC); 3) suppression of nonlinear interference based on minimization of the mean-square-error estimation (Minimum-Mean-Square-Error SIC, MMSE-SIC). To analyze the communication system with a real UV-C channel, it is necessary to determine the dependence of the signal-to-noise ratio (SNR) on the channel parameters.

The signal-to-noise ratio (SNR) of the UV channel is defined as the ratio of the number of detected signal photons to the number of noise photons. The number of signal photons depends on the power and bit rate of the transmission, the losses in the communication channel, the aperture, and the quantum efficiency of the receiver.

Typical frequencies for detecting noise photons at low, medium, and high noise levels are about 1000, 5000, and 15,000 Hz, respectively (when using a high-quality solar-blind filter and a photoelectronic multiplier with an aperture of 1.92 cm^2) [3].

The calculated energy characteristics of the MIMO UV communication system are shown in Fig. 1. Modeling of the amount of losses in the UV channel is performed on the basis of the Monte Carlo method. The following values of the UV channel parameters were accepted: communication range r=100 m, elevation angles of the transmitter and receiver ϑ_1 =30^0 and ϑ_2 =30^0, width of the radiation patterns of the transmitter and receiver φ_1=10^0 and φ_2=30^0, radiation wavelength λ=260 nm, the scattering and absorption coefficients for clear weather, the receiver aperture area Ar=1.92 cm^2). Also accepted P_T=50 mW, SNR=10 dB, and R=100 kbit/s.

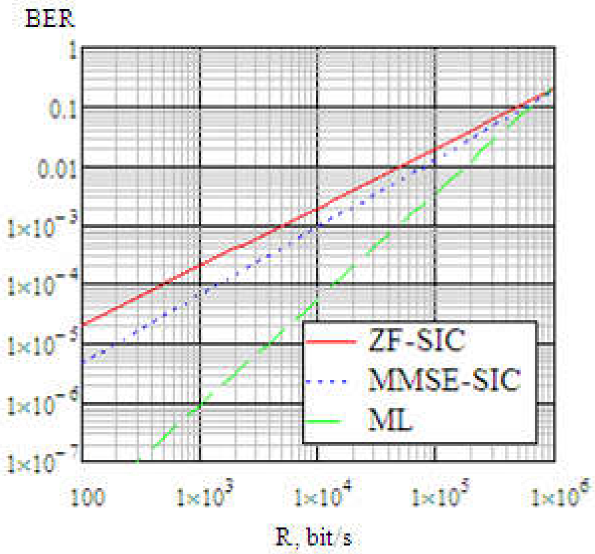

Fig. 1. Dependencies of BER on bitrate for different types of spatial encoding at high noise level

The multiplexing method based on the ML criterion provides the lowest bit error rate (BER), all other things being equal, but has the highest computational cost. Therefore, in real systems, it may be appropriate to use the MMSE-SIC method with better characteristics than ZF-SIC, but with lower computational costs than ML. The conducted research allows us to determine the performance characteristics of the MIMO UV communication system in various operating conditions (when changing the channel state, transmission mode, turns or movements of communication nodes).

Acknowledgements: the work was supported by RFBR grant 19-29-06030-MK "Research and development of wireless ad-hoc network technology between UAVs and smart city dispatch centers based on adaptation of transmission mode parameters at different levels of network interaction"

References:

Xu Z. and Sadler B. Ultraviolet communications: potential and state-of-the-art IEEE Commun. Mag.4667–73, 2009.

I.S. Konstantinov, G.S. Vasilyev, O.R. Kuzichkin, I.A. Kurilov, S.A. Lazarev. Modeling and Analysis of the Characteristics of UV Channels under Different Conditions of Radiation Propagation for the Organization of Wireless AD-HOC Network // JARDCS 2018.

Chen G., F. Abou-Galala, Z. Xu, and B. M. Sadler, “Experimental evaluation of LED-based solar blind NLOS communication links,” Optics Express, vol. 16, no. 19, pp. 15059-15068, Sep. 2008.

Analysis of energy characteristics of the UV communication system based on LED matrices

G. S. VASILYEV[1], D. I. SURZHIK[2], O. R. KUZICHKIN[3]

[1] Belgorod State University, Belgorod, 308015, Russia
[2] Vladimir State University, Vladimir, 600000, Russia
[3] Belgorod State University, Belgorod, 308015, Russia

e-mail address: *vasilievgleb@yandex.ru*

Abstract: energy characteristics of the UV-C communication system based on LED matrices are studied. The obtained results allow us to determine the energy characteristics of the UV communication system in various operating conditions (when changing the channel state, transmission mode, turns or movements of communication nodes).

Keywords: UV communication, UV-C, NLOS, ad-hoc networks

Laser communication systems of the solar-blind UV-C range from 200 to 280 nm are an alternative for traditional radio-frequency facilities and they enable communication in the absence of a line of sight (non line-of-sight, NLOS) due to the strong scattering of UV radiation in the atmosphere [1]. The use of lasers in mobile communication systems, in particular, in mobile ad-hoc networks based on the UV channel [2], is difficult, since lasers require a cumbersome pumping system. Therefore, instead of lasers on the optical transmitter side, it is more promising to use LEDs and LED matrices of the UV-C radiation range in mobile devices [3]. To use the components in real communication systems, it is necessary to analyze the energy characteristics of the system based on the properties of the UV channel.

The geometry of the NLOS UV communication channel includes following parameters: Tx - ground station transmitter, Rx – receiver of unmanned aerial vehicle (UAV), r - distance between Tx and Rx, $\vartheta_{1,2}$ and $\varphi_{1,2}$ - angle of location and width of the radiation pattern, index 1 refers to the transmitter, index 2 - to the receiver, $\psi_{T,R}$ - azimuths of the transmitter and receiver.

The signal-to-noise ratio (SNR) of the UV channel is defined as the ratio of the number of detected signal photons N_d to the number of noise photons N_n, where

$$N_d = \eta_f \eta_r N_r = \eta_f \eta_r N_r / Loss = \\ = \eta_f \eta_r P_T \lambda / (hcR \cdot Loss).$$

Here is indicated P_T - radiation power of the transmitter, η_f - transmission coefficient of the solar-blind filter, η_r - quantum efficiency of the detector (receiver), η_r – number of received photons, λ – wavelength of radiation, Loss – losses in the channel, R – bitrate, h - Planck constant, c – the speed of light in a vacuum. Typical frequencies for detecting noise photons at low, medium, and high noise levels are about 1000, 5000, and 15,000 Hz, respectively (when using a high-quality solar-blind filter and a photoelectronic multiplier with an aperture of 1.92 cm^2) [3]. The radiation power sufficient to achieve the specified SNR value is determined by the expression:

$$P_T(r,\theta_1,\theta_2,\psi_1,\psi_2) = \\ = \frac{SNR \cdot N_n \cdot hcR \cdot Loss(r,\theta_1,\theta_2,\psi_1,\psi_2)}{\eta_f \eta_r \lambda}$$

Modeling of losses in the UV channel is performed on the basis of the Monte Carlo method. The following values of the UV channel parameters were accepted: the communication range r=100 m, the elevation angles of the transmitter and receiver ϑ_1 =30^0 and ϑ_2 =30^0, the width of the radiation patterns of the transmitter and receiver $\varphi_1 = 10^0$ and $\varphi_2 = 30^0$, the radiation wavelength λ=260 nm, the scattering and absorption coefficients for clear weather, the receiver aperture area A_r=1.92 cm^2). Also accepted is SNR = 10 dB, R = 100 kbit/s.

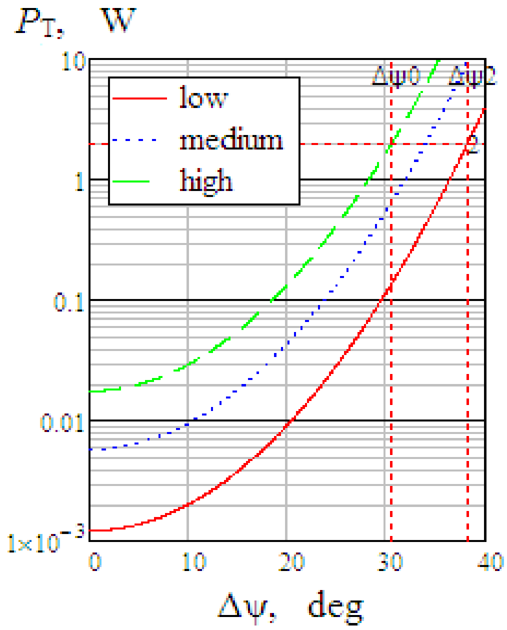

Fig. 1. Energy characteristics of the UV communication system at different noise levels from the azimuthal deviation

$$\Delta\psi = |\psi_1| + |\psi_2|$$

To increase the radiation power, it is advisable to use LED matrices with a radiated power of up to 2 W (FLS 6060 UVC SMD LED 5x5 Array). According to Fig. 1, with P_{Tmax} = 2 W, communication at a range of r =100 m is provided with an azimuthal deviation of no more than 30^0, 34^0, and 38^0 at high, medium, and low noise levels, respectively. The conducted research allows us to determine the energy characteristics of the UV communication system in various operating conditions (when changing the channel state, transmission mode, turns or movements of communication nodes).

Acknowledgements: The work was supported by RFBR grant 19-29-06030-MK "Research and development of wireless ad-hoc network technology between UAVs and smart city dispatch centers based on adaptation of transmission mode parameters at different levels of network interaction"

References:

Xu Z. and Sadler B. Ultraviolet communications: potential and state-of-the-art IEEE Commun. Mag.4667–73, 2009.

I.S. Konstantinov, G.S. Vasilyev, O.R. Kuzichkin, I.A. Kurilov, S.A. Lazarev. Modeling and Analysis of the Characteristics of UV Channels under Different Conditions of Radiation Propagation for the Organization of Wireless AD-HOC Network // JARDCS - 2018.

Chen G., F. Abou-Galala, Z. Xu, and B. M. Sadler, “Experimental evaluation of LED-based solar blind NLOS communication links,” Optics Express, vol. 16, no. 19, pp. 15059-15068, Sep. 2008.

Nanoparticles-doped photonic liquid crystal fibers for enhanced efficiency of electric field tunability

T. R. WOLIŃSKI*, BEDNARSKA, D. BUDASZEWSKI, M. CHYCHŁOWSKI, P. LESIAK, B. BARTOSEWICZ, Z. JANKIEWICZ, R. DĄBROWSKI

* Faculty of Physics, Warsaw University of Technology, 75 Koszykowa Str., 00-662 Warsaw
e-mail address: *tomasz.wolinski@pw.edu.pl*

A new class of highly tunable nanoparticles-doped photonic liquid crystal fibers for enhanced efficiency of electric field tunability has been studied. It has been shown that the presence of either gold or silver nanoparticles enhances sensitivity of the photonic liquid crystal fiber to an external electric field decreasing simultaneously the Fredericks threshold voltage as well reducing its switching times.

ABSTRACTS
OF
POSTERS

Application of optical sensor for measurements of lightning strike currents

K. BARCZAK[1], D. DUDA[2]

[1] Silesian University of Technology, Department of Optoelectronics, ul. Krzywoustego 2, 44-100 Gliwice, POLAND
[2] Silesian University of Technology, Department of Power System and Control, Krzywoustego 2, 44-100 Gliwice, POLAND
e-mail address: *kamil.barczak@polsl.pl*

Optical sensors are usually equivalent to existing classical sensors, which are the result of many years of experience, research and improvement. Optical sensors are often characterized by high resolution, reliability and stability. The main reason for the introduction of optical waveguide sensors (optical sensors in general) are their insulating properties, which allow for safe operation in high current and voltage environment. Another advantage is their immunity to electromagnetic disturbances. This advantage is very important in measurements of electric current made (produce) by lightning strike in lightning protection systems.

This work presents results and analysis of a prototype optical fiber current sensor with external conversion has been developed at the Department of Optoelectronics of Silesian University of Technology [1], which has been extensively tested. It is planned to use this sensor to measure lightning strike currents. Voltage strength tests proved good insulating properties of the tested prototype sensor. Presented results show good metrological properties in investigated area. The sensor could be used to measure the lightning strike currents in lightning protection systems.

References:

Barczak K., Optical fibre current sensor for electrical power engineering, Bulletin Of The Polish Academy Of Sciences-Technical Sciences, 59(4), pp. 409-414 (2011).

Model of the broadband interferometric optical biosensor in the planar configuration

M.BŁAHUT

Optoelectronics Department, Silesian University of Technology, 2 Krzywoustego Str. 44-100 Gliwice, Poland
e-mail address: marek.blahut@polsl.pl

Optical configuration of examined sensor is shown in Fig.1. It consists of a single-mode waveguide, a multimode section and a single-mode output waveguide. The refractive index variation of measured external surrounding affects the modal properties of multimode waveguide and the field distribution of the output signal. The image variations are registered by the single-mode output waveguide. The structure is excited by a broadband light source from the range of 0.5-0.75μm. Material parameters shown in the Fig.1 concern to the polymer SU8 waveguide on SiO_2 substrate. Their dispersion characteristics were determined in the paper [1]. It is assumed that the optical system will be used to the analysis of biological substances. Hence the suggested refractive index changes of the cover n_c for examined characteristics is in the limit of 1.33-1.35.

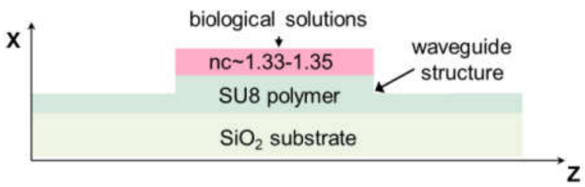

Fig.1. The geometry of one dimensional waveguide structure in step-index configuration.

The thickness of the input and the output waveguide for the single-mode operation amounts to 400nm and the thickness WM of a few-mode multimode section is changed from 700nm to 1000nm.

The operation principle of examined optical structure can be determined by the modal field analysis. Taking into account results of the paper [2], the power P at the output of the structure can be expressed by the equation (1), where $\phi_0(x)$ is the wave function of single-mode waveguide and $\phi_l^M(x)$ are the wave functions of multimode section of an order l with propagation constants β_l

$$P \sim \left| \int_{-\infty}^{+\infty} \phi_0(x) \sum_{l=0}^{N-1} \phi_l^M(x) \cdot e^{-j\beta_l z} dx \right|^2 \tag{1}$$

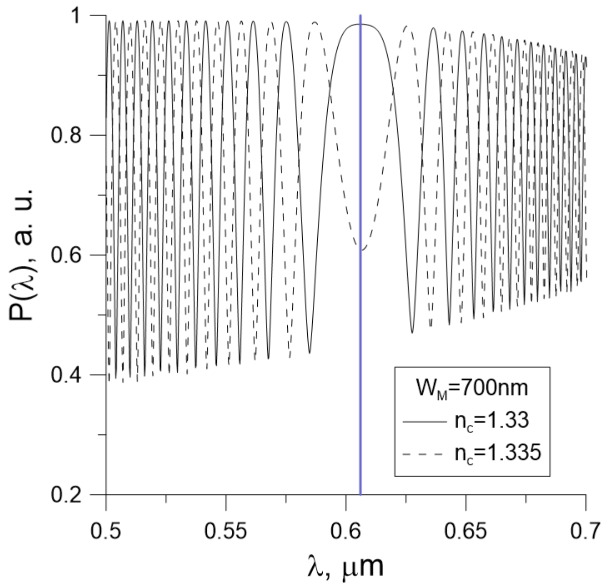

Fig. 2 Output power P(λ) distribution for the different refractive indices of the biological cover n_c. The width of the multimode section W_M=700nm.

This dependency has been examined for different geometries of the structure excited by the white light of wavelengths range from 0.5-0.7μm. Fig.2 shows typical output spectral characteristics P(λ) for the two different values of the refractive index of the cover – n_c=1.33 and n_c=1.335. The length of analyzed multimode section L is equal to 2000μm and its thickness amounts to 700nm. The length of input and output waveguides amounts to 5000μm.

One can see characteristic effects which occur near the wavelength of 0.608μm, shown in the Fig.2 by vertical line. This wavelength defines the short range inside of which propagation constants difference of modes and in connection with it the phase of the signal change very slowly with the wavelength, for the assumed geometry of the structure.

For the waves of the shorter wavelengths (below 0.59μm) the signal extremes shift towards longer waves with the increase of the refractive index of the cover. On the other hand for the waves of longer wavelengths (over 0.62μm) the signal extremes shift towards shorter waves, with the increase of the refractive index of the cover. Similar effects have been observed in the case of differential interferometers [3].

Application of broadband source gives the possibility of the direct detection of refractive index of the cover by the measurement of the spectral characteristics of the output signal.

References:

[1] K. Gut, Z. Opilski, Bull. Pol. Acad. Sci. Tech. 63(2), 349, (2015).

[2] M.Błahut. Proc. SPIE, 1045503, (2017)

[3] K.Gut, Optic Express, 25, 31111,(2017)

Optical properties of achromatic flat-surface gradient index microlenses

R. BUCZYNSKI[1,2], A. FILIPKOWSKI[1,2], H. T. NGUYEN [1,2], D. PYSZ[2], R. STEPIEN[2], A. WADDIE[3], M. R. TAGHIZADEH[3], R. KASZTELANIC[1,2]

[1]University of Warsaw, Faculty of Physics, Pasteura 5, 02-093 Warszawa
[2]Łukasiewicz -Institute of Electronic Materials Technology, Wólczynska 133, 01-919 Warszawa
[3]Heriot-Watt University, Department of Physics, School of Engineering and Physical Sciences, Scottish Universities Physics Alliance, Edinburgh, EH14 4AS, UK.
e-mail address: *ryszard.buczynski@fuw.edu.pl*

Achromatic lenses are highly desirable for both imaging systems and beam manipulation tasks. It is well known that singlet refractive lenses cannot be achromatic (Fig. 1(a)) due to the dispersive nature of all known glass materials the chromatic aberrations cannot be compensated by any shape of lens. The standard solutions to eliminate chromatic aberrations are based on multi-element lens systems. However, a few works have discussed methods to create singlet-type achromatic lenses. Flynn et al. proposed to fabricate a hybrid diffractive-refractive achromatic lens, where a refractive lens made of homogenous material, is combined with an additional diffractive Fresnel lens [1]. Other solutions show a feasibility of development lenses made of 2 materials with spherical surfaces [2] or lenses made of 3 components with spherical or flat surfaces [3].

We proposed a fully flat-parallel gradient index (GRIN) microlens, which can be easily integrated as part of the optical fiber line. In order to design and fabricate a nanostructured GRIN lenses, it is necessary to use pair of glasses with good rheological properties and similar expansion coefficients as well as thermal properties, which allow joint thermal processing in a fiber drawing tower. To ensure achromatic properties of lenses, the first derivative of the difference between the material dispersion of the glasses has to cross a zero. We have developed in-house a pair of borosilicate glasses labelled as NC34 and NC21A which fulfils these requirements for the development of achromatic nGRIN microlenses.

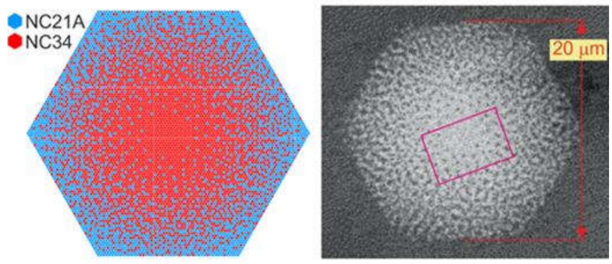

Fig. 1. Internal structure of the achromatic nanostructured GRIN microlens composed of NC21A and NC34 glass nanorods: a cross-section of design and fabricated component.

The NC21A/NC34 pair of glasses has an expansion coefficient difference of $\Delta\alpha$=0.4×10-7·K-1, which is sufficiently small for joint thermal processing. During the drawing in the fiber drawing tower the glasses are kept at a temperature between the curvature and sphere points. For NC21A/NC34 the difference in the curvature temperature is ΔT_c=50°C and difference in sphere temperature is ΔT_{sph}=35°C.

The nanostructure of the proposed GRIN lens has been designed so the effective refractive index would change parabolically between these two refractive indices, from the maximum at the optical axis to the minimum on the edge of the aperture. We have used a standard stack and draw method commonly used for photonic crystal fiber fabrication to develop achromatic nGRIN microlenses. The preform was formed with 0.6 mm diameter NC21A and NC34 glass rods. A hexagonal structural preform was then stacked layer by layer, according to the calculated pattern (Fig. 1). A total of 7651 glass rods were used and the final element had 101 rods on the diagonal. The preform was drawn into sub-preforms of diameters 5 mm. A 30 mm outer diameter NC21A glass tube was used to create sub-preform and finally achieve a 125 µm diameter fiber with a 20 µm nanostructured lens structure in the middle [4,5].

The light propagation through the lens has been characterized using the imaging setup. It was illuminated by a collimated beam from continuous-wave laser sources at wavelengths in the range 532 nm - 1550 nm. The beam formed by the nanostructured lens was imaged by a microscope lens onto a camera. For each laser source, CCD, CMOS, and phosphate enhanced CCD cameras with appropriate sensitivities were used. The images of the beam cross-sections were collected on the CCD continuously by the translation of the structured lens. A series of images were taken at different distances from the lens facet with the distance changing with a step of 1 µm and then combined to give the plot of the beam FWHM and the longitudinal profile of the beam formed by the measured lens.

The focal spot was observed at a distance of 34.1 – 35.6 µm over a wavelength range of an octave between 600 nm and 1550 nm. It is nearly wavelength independent, however axial achromatic behavior is clearly observed. A maximum working distance, defined as the distance from the final lens facet to the focal plane, of 35.6 µm was observed for 980 nm illumination. For the remaining longer and shorter wavelengths the working distance is shorter. The measured beam diameter at the focal plane with FWHM criterion is equal to 2.1 µm – 4.1 µm in the considered wavelength range.

Acknowledgments: This work was supported by This work was supported by the project TEAM TECH/2016-1/1 (POIR.04.04.00-1C74/16) operated within the Foundation for Polish Science Team Programme co-financed by the European Regional Development Fund under Smart Growth Operational Programme (SG OP), Priority Axis IV.

References:

[1] N. Davidson et al., Appl. Opt. 32(25), 4770–4774 (1993).
[2] J. N. Mait et al., Opt. Express 23(17), 243268 (2015).
[3] G. Beadie at al., Proc. SPIE 10181, 1018108 (2017).
[4] A. Filipkowski et al., Opt. Lett. 40(22), 5200–5203 (2015).
[5] R. Buczynski et al., Opt. Express 27(7), 9588-9600 (2019).

Spectral properties of photonic crystal fibers infiltrated with nanoparticles-doped ferroelectric liquid crystals

D.BUDASZEWSKI[1], K. WOLIŃSKA[1], B. JANKIEWICZ[2], B. BARTOSEWICZ[2], and T. R. WOLIŃSKI[1]

[1]Faculty of Physics Warsaw University of Technology, Koszykowa 75, 00-662 Warsaw, Poland
[2]Military University of Technology, Gen. S. Kaliskiego 2, 00-908 Warsaw, Poland
e-mail address: *daniel.budaszewski@pw.edu.pl*

Photonic crystal fibers (PCFs) infiltrated with liquid crystals (LCs) have been a research hotspot in recent decades mainly due to their high sensitivity to external physical factors.
In order to further improve spectral parameters of photonic liquid crystal fibers (PLCFs), various methods have been adopted. Aligning materials [1] and metallic nanoparticles (NPs) [2] have been used to enhance spectral and electro-optical parameters of PLCFs.
Recently, ferroelectric liquid crystals (FLCs) have been employed to infiltrate PCF structures resulting in faster switching times than for commonly used nematic LCs [3].

In this work we have focused on investigations of switching times and temperature dependence of clearing point of an isotropic PCF infiltrated with a mixture of FLC and gold NPs in different concentrations. As it was reported elsewhere [4], doping FLCs with metallic NPs can further enhance switching times and luminescent properties.

We have used an isotropic LMA-10 PCF which was infiltrated with a mixture of W-212 FLC (MUT Warsaw, Poland) doped with 2-nm gold NPs in concentration of 0.1%, 0.2% and 0.3 % wt.
We have observed a shift of transition temperature towards higher values that depends on concentration of gold NPs in FLC. Simultaneously a slight improvement in switching time was registered for the investigated PLCF sample under the influence of an external electric field. This behavior can be attributed to inhomogeneous alignment of FLC-NPs mixture inside PCF micro-channels resulting in increased attenuation of the PLCF sample.

Acknowledgments: This work was supported by National Science Center under the Grant No. 2015/19/B/ST7/03650

References:

[1] D. Budaszewski et. al., Optics Letters 39, 16 (2014)
[2] D. Budaszewski et. al., Optics Express 27, 10 (2019)
[3] D. Budaszewski et. al., Liquid Crystals 46, 2 (2019)
[4] S. K. Gupta et. al., Adv. Mater. Lett 6, 1 (2015)

Influence of electric field frequency on optical response of photonic crystal fibers infiltrated with NP-doped liquid crystals

M.S. CHYCHŁOWSKI[1], B. BARTOSEWICZ[2], B. JANKIEWICZ[2], T.R. WOLIŃSKI[1]

[1]Faculty of Physics, Warsaw University of Technology, Koszykowa 75, 00-662, Warsaw, Poland
[2]Institute of Optoelectronics, Military University of Technology, Kaliskiego 2, 00-908, Warsaw, Poland
e-mail address: milosz.chychlowski@pw.edu.pl

A typical method for modification of material properties is to introduce a small amount of additives to a host structure as e.g. in composites materials that can reduce weight and maintain the same durability or in civil engineering where metal rods added to concrete greatly increase its resistance to stresses. Our recent research efforts with liquid crystals doped with Ag/Au nanoparticles and infiltrated photonic crystal fibers were focused on two electro-optical parameters – switching times and reduction of threshold voltages needed for reorientation[1-3]. In this work we have investigated an influence of electric field frequency on optical response of photonic crystal fibers infiltrated with two nematic liquid crystals doped with different concentrations of Au NPs.

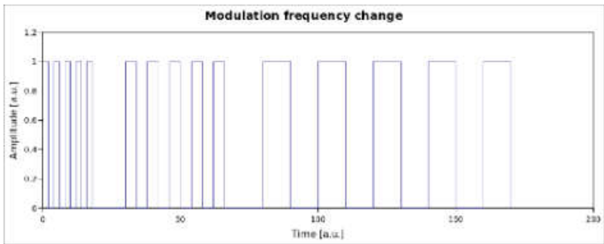

Fig. 1. Electric field frequency change

Acknowledgments: This work was supported by the Grant NCN 2015/19/B/ST7/03650 from the Polish National Science Center

References:

[1] A. Siarkowska et. al., “Thermo- and electro-optical properties of photonic liquid crystal fibers doped with gold nanoparticles”, Beilstein J. Nanotechnol., 8, 2790–2801 (2017)
[2] D. Budaszewski et. al., "Enhanced efficiency of electric field tunability in photonic liquid crystal fibers doped with gold nanoparticles", Opt. Express 27, 14260-14269 (2019)
[3] D. Budaszewski et al., "Nanoparticles-enhanced photonic liquid crystal fibers", Journal of Molecular Liquids 267, 271-278 (2018)

The influence of selected gases on reduced graphene oxides

S. DREWNIAK [1], M. PROCEK [1], R. MUZYKA [2]

[1] Department of Optoelectronics, Faculty of Electrical Engineering, Silesian University of Technology, 2 Krzywoustego Str., 44-100 Gliwice, Poland.

[2] Institute for Chemical Processing of Coal; 1 Zamkowa St., 41-803 Zabrze, Poland

e-mail address: sabina.drewniak@polsl.pl

The reduced graphene oxide is the material which is mainly built of carbon and to a lesser extent, of the residual functional groups. This material could be used as a receptor layer in the gas sensing structures.

We applied reduced graphene oxide on the transducer and performed the investigations using various gases; hydrogen, nitrogen dioxide and ammonia. The reaction of the sample was checked (we measured the resistance) during contact of the structure with different atmospheres (different concentration of H_2, NO_2 and NH_3 in a carrier gas).

As the results show, the sample reacts on various gas in different way (it is selective). The hydrogen caused an increase in resistance while nitrogen dioxide a decrease. There was no reaction (no changes of resistance) when ammonia was dosed.

Purification of tellurite glasses for mid-infrared applications

X. FORESTIER[1, 2], M. KLIMCZAK[1, 2], R. BUCZYŃSKI[1, 2]

[1]Institute of Electronic Material Technology (ITME), Wólczyńska 133, 01-919 Warszawa, Poland
[2]University of Warsaw, Faculty of Physics, Pasteura 5, 02-093 Warsaw, Poland
e-mail address: *rbuczyns@igf.fuw.edu.pl*

Production of optical elements for near and mid-infrared applications such as food safety, defense industry or medicine is of increased interest. Glasses developed for those applications have to present good mechanical and physicochemical properties. They also need to be thermally stable to avoid crystallization during the thermal treatments involved in the production of optical elements such as fiber optics by the stack and draw method[1].

Absorption due to free water and hydroxyl group bonded to the glass network is critical for applications beyond 3 µm. Water contained in the raw materials and in the atmosphere is detrimental to the transmission of tellurite glasses. Indeed water hydrolyses the glass network following the reaction:

$$\equiv Te-O-Te\equiv + H_2O \rightleftharpoons 2|\equiv Te-OH|$$

Recent research [2-4] shows that a low OH content is achievable in tellurite glasses in order to reduce the large absorption band around 3 µm using various purification methods described below. Different synthesis conditions and compositions using fluorides and chlorides were investigated as a preliminary study. Transmission measurements were conducted to study the impact on the water content.
To reduce the water content, 3 solutions:

- Make the synthesis under dry and oxidizing or protected atmosphere to limit the reduction of tellurium oxide and the concentration of hydroxyl groups.
- Make the synthesis using reactive atmosphere processing (RAP) such as CCl_4 or Cl_2.
- Make the synthesis using solid-state dehydrating agents. In this case, replacing part of the oxides by their chlorides or fluorides compounds. Reactions with halides react with water as follow:

$$TeCl_4 + 2H_2O \rightleftharpoons TeO_2 + 4HCl$$
$$TeCl_4 + 4|\equiv Te-OH| \rightleftharpoons 2|\equiv Te-O-Te\equiv| + TeO_2 + 4HCl$$

We report the purification of tellurite glasses under the TeO_2-ZnO-ZnF_2-Na_2O glass system. A drastic reduction of the absorption band due to free water, weakly and strongly bonded hydroxyl group was observed, as shown on figure 1, allowing a transmission up to 5.5 µm for long optical element such as optical fibers (Fig. 1).

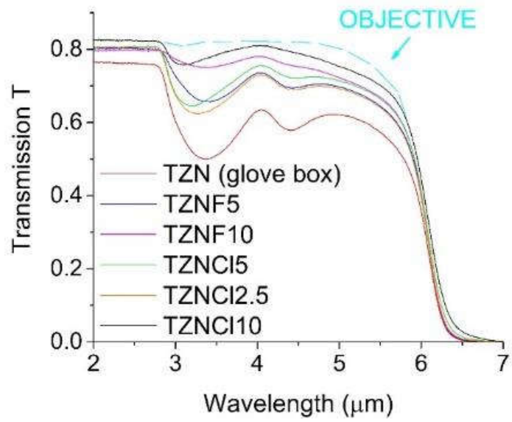

Fig. 1. Transmission spectra of the investigated glasses (sample thickness=2mm)

Acknowledgments: This work was supported by European Training Network H2020-MSCA-ITN-2016 Grant No 722380, SUPUVIR: Supercontinuum broadband light sources covering UV to IR applications.

References:
[1] D. Pysz, I. Kujawa, R. Stępień, M. Klimczak, A. Filipkowski, M. Franczyk, L. Kociszewski, J. Buźniak, K. Haraśny and R. Buczyński, "Stack and draw fabrication of soft glass microstructured fiber optics", Bull. Pol. Acad. Sci. Tech. Sci., volume 62(4), pp. 667-682 (2014).

[2] A. Lin, A. Ryasnyanskiy, J. Toulouse, "Fabrication and characterization of a water-free midinfrared fluorotellurite glass." Opt. Lett. 36, 740-742 (2011)
[3] M. Boivin, M. El-Amraoui, S. Poliquin, R. Vallee, Y. Messaddeq, "Advances in methods of purification and dispersion measurement applicable to tellurite-based glasses," Opt. Mater. Express 6, 1079-1086 (2016)
[4] X. Feng, J. Shi, M.Segura, N.M. White, P. Kannan, L. Calvez, X. Zhang, L. Brilland, W.H. Loh, "Towards Water-Free Tellurite Glass Fiber for 2-5 um Nonlinear Applications.", Fibers 1, 70-81 (2013)

Optimization of PMMA and PS granulates extrusion process for polymer optical fiber technology

M. JÓŹWICKI[1], M. GIL – KOWALCZYK[2]*, M. GARGOL[1], P.MERGO[2]

[1] Department of Polymer Chemistry,
[2] Optical Fiber Technology Laboratory,
Maria Curie-Skłodowska University, M. Curie-Skłodowska Sq. 5, 20-031 Lublin, POLAND
e-mail address: *malgorzata.gil@poczta.umcs.lublin.pl*

The most commonly used material for preparation of optical fibers is vitreous silica dioxide. Through the doping with different inorganic substances several properties of pure silica dioxide can be improved, e.g. refractive index. However, mechanical strength or rigidity of silica fibers still not satisfactory [1]. At this point, polymer optical fibers (POF's) should be mention. These fibers are attractive materials thanks to their great flexibility and high resistance to external factors. It should be noted that the POF's are not deprived limitations and problems. These fibers are characterize by high signal attenuations according to silica fibres. Other limitations are: glass transition temperature, melting temperature, refractive index, thermo-optic coefficient [2,3].

Polymer materials can be relatively easily modified with the help of organic or inorganic additives, by diffusion process or during bulk polymerization. An important advantage of polymer fibers is their biocompatibility. Thanks to their specific properties, they have been used as elements of optical fiber sensors, in local telecommunications networks and in the field of biomedical applications (diagnostics) [4,5]. In this regard, the most popular polymeric materials used to produce POF's are commercially available polymers like: polycarbonates, poly (methyl methacrylate), polystyrene, cyclic olefin copolymers and amorphous fluoropolymers. Poly (methyl methacrylate) (PMMA) is a transparent thermoplastic widely used in various industries. It is characterized by good resistance to UV radiation, easy polishing and tensile and flexural strength. In addition, PMMA production is cheap. The thermal stability of PMMA is better compared to other plastics, e.g. polystyrene or polyethylene, which is a desirable feature in POF's preparation. Furthermore, PMMA is resistant to water, diluted acids, alkalis and mineral oils. For PMMA, the refractive index is 1.49 at 589.2 nm and range of the glass transition temperature is from 105 to 120 ^{o}C [6,7].

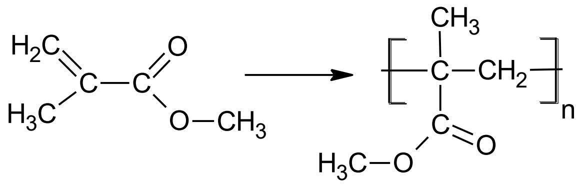

Fig. 1. The scheme of polymerization of methyl methacrylate

Polystyrene is a polymer having an aromatic ring. In its pure form, it is a hard, brittle and colorless thermoplastic material. The use of additives allows to obtain polystyrene with much better elasticity. This polymer, next to PMMA, is the most commonly used material for the production of POF's. The refractive index for PS is higher than for PMMA and is 1.59. The glass transition temperature is between 90 and 100 ^{o}C [8].

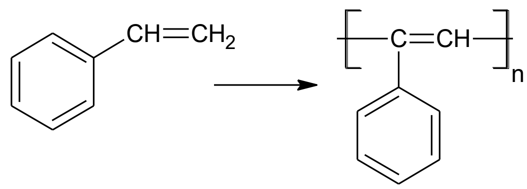

Fig. 2. The scheme of polymerization of styrene

The aim of this work was to determine the optimal extrusion temperature for polymer optical fibers from PMMA and PS. Commercial granules of both polymers were used in the studies. The samples were subjected to several different temperatures in which they were kept in an oven for different periods of time. In order to analyze the changes that the tested samples could undergo, thermal (TG/DTG) and spectroscopic (ATR/FT-IR) tests were performed. Based on FT-IR spectra's of the liquid monomers, it was also possible to calculate the double bond conversion, which gave us a picture of the degree of monomer conversion.

References:

[1] S.K. Shukla et al. Optics and Laser Technology 115, 404–432, (2019).

[2] K. Peters, Smart Mater. Struct. 20, 2281, (2010).

[3] Y. Luo et al. Sensors 17, 511, (2017).

[4] T. Wang, et al. Opt. Commun. 307, 5–8, (2013).

[5] P. Stajanca et al. Opt. Fiber Technol. 41, 227-234, (2018).).

[6] F. Namouchi et al. J. Alloys Compd. 469 (1-2), 197–202, (2009).

[7] M.C.J. Large, J. Moran, L. Ye, Meas. Sci. Technol. 20, (2009).

[8] J. Scheirs, D.B. Priddy, „Modern Styrenic Polymers: Polystyrenes and Styrenic Copolymers", John Wiley & Sons, Ltd, (2003).

The direct laser writing system for mask-based lithography based on confocal microscopy

K.GUT[1], S. STUDENT[2]

[1] Department of Optoelectronics, Silesian University of Technology, 2 Krzywoustego Str., 44-100 Gliwice, POLAND

[2] Institute of Automatic, Silesian University of Technology, 8 Krzywoustego Str. 44-100 Gliwice, POLAND

e-mail address: *kazimierz.gut@polsl.pl*

A new method of the direct laser writing system is described in which a confocal microscopy laser system is used to create transparency photomask in lithography. The system was tested with negative SU-8 photoresist. The photolithography is the most used technique in polydimethylsiloxane microfluidic prototyping. However, if the features are smaller than 20 µm it is very difficult to prepare the photomasks. Even though very often used glass photomasks are commercially available, the high cost of such masks is a significant problem to the use of photolithography in the prototyping of PDMS devices. In our solution, we use confocal microscopy system which is a common equipment in biomedical laboratories to produce precise microfluidic masters. Our system provides a fast and high precision technique which can be used without additional costs in biomedical centres with microscopy laboratories.

Novel directional coupler utilizing hyperbolic metamaterial: coupled mode formulation by reciprocity

A.TYSZKA-ZAWADZKA[1], B JANASZEK[1], M. KIELISZCZYK[1], P.SZCZEPAŃSKI[1,2]

[1]Institute of Microelectronics and Optoelectronics, Warsaw University of Technology, Koszykowa 75, 00-662 Warsaw, Poland

[2]National Institute of Telecommunications, Szachowa 1, 04-894, Warsaw, Poland

e-mail address: *a.tyszka@elka.pw.edu.pl*

Over the past decade, media exhibiting hyperbolic dispersion, known as hyperbolic metamaterials (HMMs), have been used in the design of waveguides. The study of such anisotropic waveguiding structures has proved guided waves as well as plasmonic propagation, field enhancement, sign-varying energy flux, and light slowing or stopping [1-6]. However, despite a number of prospective applications, modal coupling in HMM-based waveguide systems have not been yet investigated.

Within this work we analyze controlled mode coupling in a waveguide system based on tunable hyperbolic metamaterial (THMM). The analyzed system consists of two parallel planar waveguides with core layers formed by a dielectric (described by electric permittivity ε_a) and a THMM structure (described by electric permittivity tensor ε_b), respectively, Fig. 1.

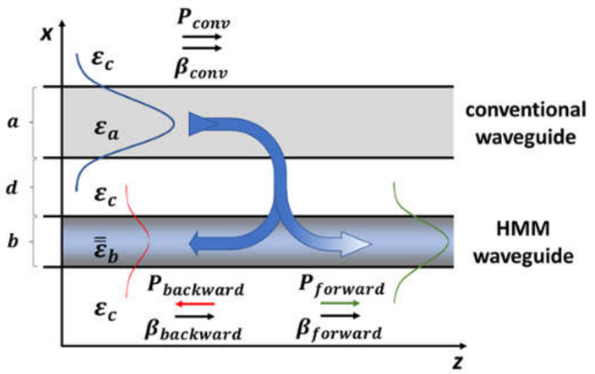

Fig. 1. Scheme of analyzed structure.

Considered THMM waveguide supports two TM modes of different propagation constants, i.e., forward mode, whose energy flow and wave vector are in the same directions, and backward mode, whose energy flow and wave vector are in the opposite directions.

In the case of HMM waveguide (which is anisotropic), the standard coupled mode theory (CMT) based on a perturbation approach as well as CMT derived from a variational principle are not applicable, due to the broken link between the forward- and backward-propagating modes [7]. Thus, to study the modal coupling of the TM mode of dielectric waveguide with the backward and forward TM modes of HMM waveguide, the generalized coupled mode formulation by reciprocity is required [8].

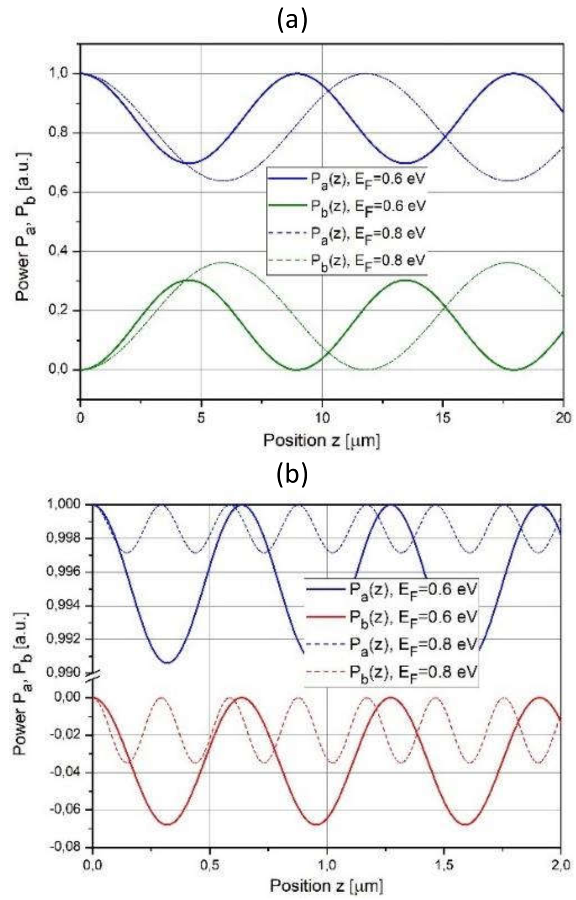

Fig. 2. Power of TM0 mode of dielectric waveguide with power of forward- (a) and backward (b) modes of HMM waveguide as a function of "z" direction for two values of Fermi energy.

For this purpose, we developed an rigorous analytical approach towards controlled mode coupling in THMM based two-waveguide system, with coupled mode equations derived from generalized reciprocity relation. The characteristics illustrating the power of TM modes of conventional and HMM waveguides as a function of “z” direction, reveal the power transfer between the conventional (forward) mode and the forward- and backward (HMM) modes, see Fig.2. Moreover, the coupling between the guided modes can be controlled with an external parameter, here the Fermi energy.
As we can see, for given “z” position we can obtain the minimum or maximum of power depending on the Fermi energy level.
We believe that developed approach allows for proper design of efficient planar waveguide couplers of tailorable and tunable properties.

Acknowledgments: This work was supported by The National Centre for Research and Development (NCBiR) under grant No. TECHMATSTRATEG1/347012/3 /NCBR/2017 (HYPERMAT).

References:
[1] M. Ishii et al., Optics Letters 39, 16, (2014)
[2] E. I. Lyashko et al., Quantum Electronics 45, 11, (2015)
[3] Y. He et al., Optics Letters 37, 14, (2015)
[4] B. Li et al., Applied Physics Express 8, 8, (2015)
[5] H. Hu et al., Scientific Reports 3, (2013)
[6] A. Tyszka-Zawadzka et al., Optics Express 25, 7, (2017)
[7] W. Chen et al., Physical Review B 99, 195307, (2019)
[8] I. Tsang et al., Journal of Lightwave Technology 6, 2 (1988)

Study of sensing properties of UV activated organic-inorganic blend of graft comb copolymer and ZnO nanomaterial for room temperature NO_2 gas sensing applications in ppm and sub-ppm range

P. KAŁUŻYŃSKI[1], M. PROCEK[1], A. STOLARCZYK[2]

[1] Department of Optoelectronics, Silesian University of Technology, 2 Krzywoustego Str, Gliwice, Poland ;
[2] Department of Physical Chemistry and Technology of Polymers, Silesian University of Technology, 9 Strzody St., 44-100 Gliwice, Poland;
e-mail address: Piotr.kaluzynski@polsl.pl

In this work, we present our recent research on a novel organic-inorganic sensing layer resulting from the combination of two materials, graft com copolymer PEGSil (based on poly(3-hexylotiophene)) mixed with zinc oxide nanomaterial for (NO_2) resistance gas sensor application. Organic-inorganic blends were deposited on interdigital transducers (Au on Si/SiO_2) by drop coating method. Sensor response characteristics were measured for different concentrations of NO_2 in N_2 carrier gas from 50 ppb up to 1 ppm. Measurements were carried out at room temperatures with UV light irradiation on sensing structures, as a charge carriers activation factor. Obtained results show that the change in sensitivity for NO_2 detection of elaborated sensors is significant and is about 9% per 1ppb in concentration range from 50 to 200 ppb of NO_2 in N_2 carrier gas. These results show great potential of these materials as a sensing layer for NO_x gas sensing.

Optical fiber sensors for rotational seismology – field measurements for data comparability analysis

A.T. KURZYCH[1], L.R. JAROSZEWICZ[1], M. DUDEK[1], J.K. KOWALSKI[2]

[1] Institute of Technical Physics, Military University of Technology,
Gen. S. Kaliskiego St.2, 00-908 Warsaw, Poland
[2] Elproma Elektronika Ltd., Szymanowskiego St. 13, 05-092 Łomianki, Poland
e-mail address: *anna.kurzych@wat.edu.pl*

Seismological research requires data about translational ground displacements and strain measurements. Nowadays, it turned out that three rotational components which have been often neglected, can provide additional valuable information. According to recent developing interest of rotational seismology there is significant need for research both theoretical but mostly experimental one. It affects growth of rotational sensors technology which have to meet strict technical requirements. The very wide measuring range is the most crucial parameter (signals amplitude from 10^{-7} rad/s to 10 rad/s, frequency from 0.01 Hz to 100 Hz). One can distinguish three basic groups of rotational sensors: mechanical such as TAPS (by Polish Academy of Science), Rotaphone (by Czech Academy of Science), MEMS technology – Horizon (EMCORE); electromechanical - R1, R2 (Eentec) and optical: RLG (by LMU, Germany), blueSeis-3A (iXblue), SRS-5000 (Optolink). However, total insensitivity to linear motion, wide measuring range, high sensitivity, portability make systems based on FOGs the most appropriate sensors for rotational seismology.

In order to fulfill all technical requirements for rotational sensors we designed and constructed device based on an closed-loop FOG – a Fibre-Optic System for Rotational Events & phenomena Monitoring (FOSREM version FOS5 – Fig.1). It is a an interferometric optical fiber sensor designed to continuously observe rotational effects. It uses closed-loop configuration which is based on the compensatory phase measurement method as well as specific electronic system. In this paper we present laboratory investigation of FOS5 including Allan variance analysis indicating that Angle Random Walk is equal to 10^{-7} rad/s. Expect laboratory verification of proper FOS5 devices operation we carried out field tests in order to analyze FOS5 devices data reliability by their data comparability as well as consistency.

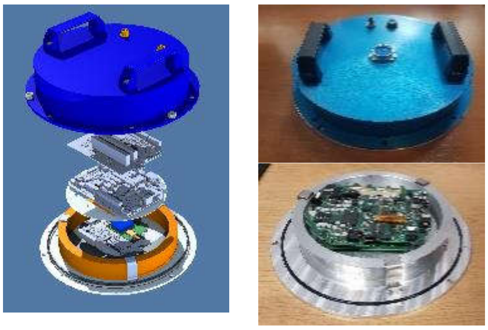

Fig. 1. FOS5: 3D project (left), technical realization (right).

Acknowledgments: This work was supported by the National Science Centre, Poland - project 2016/23/N/ST10/02508 and program POIR 04.02.00-14-A003/16 “EPOS – System Obser-wacji Płyty Europejskiej”.

Bending loss analysis in silica hollow core antiresonant fibers fabricated with single capillary or nested capillary claddings

B. LOU[1], G. STĘPNIEWSKI[2,3], D. PYSZ[2], L. ZHAO[1], R. BUCZYŃSKI[2,3], M. KLIMCZAK[2,3]

[1]Jiangsu Normal University, School of Physics and Electronic Engineering, Xuzhou 221116, Jiangsu, China
[2]Łukasiewicz Research Network Institute of Electronic Materials Technology, Wólczyńska 133, 01-919 Warsaw, Poland
[3]University of Warsaw, Faculty of Physics, Pasteura 5, 02-093 Warsaw, Poland
e-mail address: *mariusz.klimczak@fuw.edu.pl*

Hollow core anti-resonant fibers (ARF) are a novel class of optical fibers, which guide light in an air core due to the anti-resonance of the guided mode with the cladding [1]. Cladding in these fibers, composed most typically of one ring of circular, non-touching capillaries can be considered a simplification of a more complex, "cob-web" structure of the Kagome fibers [2]. ARFs hold the promise of the ultra-low loss for future low-latency telecommunications [3], as well as for ultra-high peak power laser pulse transmission [4]. Optical properties of ARFs can be easily modified by infiltration with gases, enabling ultrashort laser pulse synthesis and mid-infrared gas lasers [5,6]. Bending loss is a challenge in these structures. Nested capillary cladding structure has been proposed for ARFs to alleviate this problem [7].

Here, we study experimentally bend loss performance of two ARF test series, one with a single capillary ring cladding, and one with nested capillaries. Both fiber types have been investigated in context of bend loss performance before, including bend-induced mode-structure control in femtosecond laser pulse transmission and in bend loss performance at mid-infrared wavelengths [8,9]. Despite this, no direct comparison of bending loss has been performed for physical structures. In this work, we focus on the near-infrared wavelength range specifically around 1560 nm and 1900 nm corresponding to erbium or thulium doped ultrafast fiber oscillators, which would both benefit from availability of pulse delivery fibers. The geometric parameters of the developed ARFs are summarized in Table 1 and Fig. 1 shows their structures in Scanning Electron Microscopy (SEM) images.

Tab. 1. Geometric parameters of ARFs used in this study.

Parameter	Single ring ARF	Nested ARF
Outer diameter	164 µm	161 µm
Capillary diameter	24 µm	25 µm
Capillary wall thickness	1.8 µm	1.8 µm
Inner capillary diameter	-	15 µm
Inner cap. wall thickness	-	0.8 µm
Core diameter	66 µm	65 µm

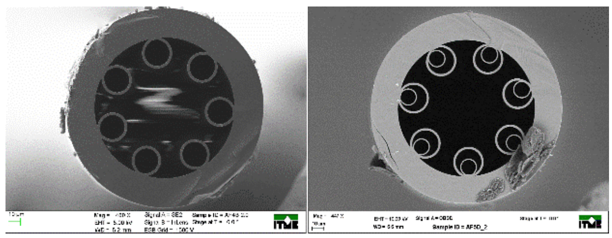

Fig. 1. SEM images of the reference, single capillary ring ARF and the nested capillary ring ARF used in this work.

The structures of both fibers are reasonably comparable with the nested capillaries used in one of the fibers being the primary difference. This cladding modification avoids introduction of new nodes into the fiber layout, which is at the core of the ARF advantage over the Kagome fibers [3,7]. Bending loss measurements with our fibers have been performed with 2 m long samples, and a full loop (full turn) has been introduced at around half-length of the samples. Aspheric lenses have been used to couple in and out the light from a compact supercontinuum source (Leukos) and transmission spectra have been recorded with an optical spectrum analyzer (Yokogawa, 1200-2400 nm). Full turns have been applied with radii from 8 cm down to 1.75 cm. Experimental results for both fibers are summarized in Fig. 2 and show a clear advantage of the nested capillary concept over the single capillary ring fiber. Notably, this result has been achieved with the nested capillary ARF with inner and outer capillary walls of different thickness. This is detrimental, because it gives raise to additional resonances and loss [1]. Despite this our experiment revealed, that in the 1900-2000 nm wavelength window, compatible with the new ultrafast Tm+Ho doped fiber lasers and amplifiers, introduction of nested capillaries into the cladding pushes bend loss down from around 6-7 dB/full turn to about 1 dB/full turn for as small as a 5 cm diameter. Technological fiber imperfections of this test series can be solved with additional technological runs of fiber drawing.

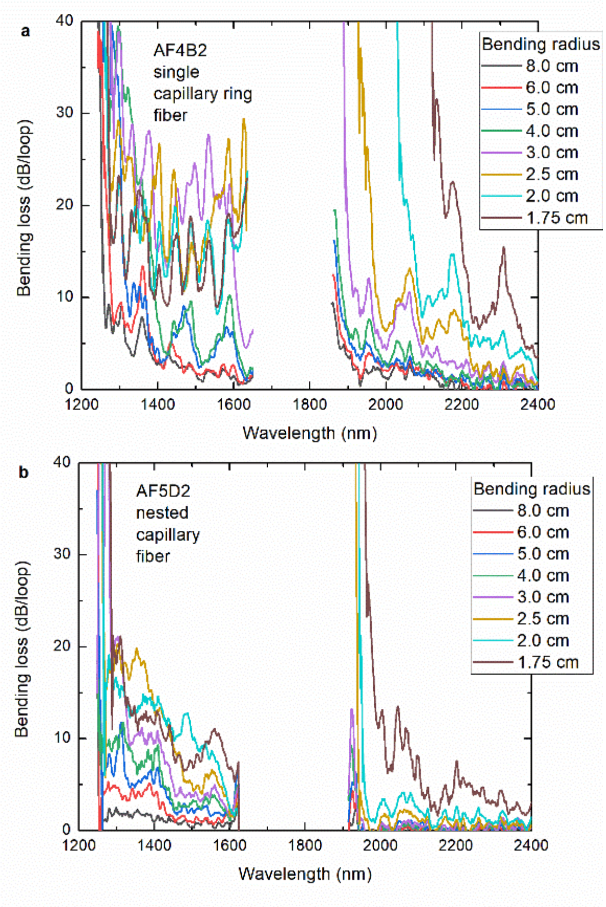

Fig. 2. Measured bending loss characteristics of the single capillary ring ARF (a) and the nested capillary ARF (b) over one full loop and at near-infrared wavelengths.

References:

[1] F. Poletti, Opt. Express 22, 23807
[2] F. Benabid et al. Science 298, 399
[3] D. Bradley et al. 2018 European Conference on Optical Communication
[4] P. Jaworski et al. Opt. Express 21, 22742
[5] U. Elu et al. Optica 4, 1024 (2017).
[6] M. R. A. Hassan et al. Optica 3, 218
[7] W. Belardi et al., Opt. Lett. 39, 1853
[8] D. Dobrakowski et al. JOSA B 36, 3030
[9] M. Klimczak et al. Opt. Lett. 44, 4395

Perimeter protection of east EU border rivers

N. PAŁKA[1], J. MŁYŃCZAK[1], M. ŻYCZKOWSKI[1], M. KAROL[1], M. MACIEJEWSKI[1], M. KOWALSKI[1], P. MARKOWSKI[1], M. SZUSTAKOWSKI, K. CICHULSKI[1]
S. BRAWATA[2], G. GRZECZKA[3], A. ADAMCZYK[3]

[1]Military University of Technology, 2 Kaliski Str., 00-908 Warsaw, POLAND
[2]Vortex Sp. z o.o., Al. Grunwaldzka 28/6 , 80-229 Gdańsk, POLAND
[3]Polish Navy Academy, Śmidowicza Street 69, 81-127 Gdynia, POLAND
e-mail address: *norbert.palka@wat.edu.pl*

The eastern border of the European Union often runs through wild rivers located in wooded or mountainous areas. These rivers are not only a natural border but also a place of frequent smuggling people, drugs and cigarettes into the EU. Smuggling of cigarettes usually takes place with the use of several-meter long inflatable boats driven by oars, on which 1-2 people transport several about 20-kg packages.

A modern system for detecting and visualizing people, means of transportation and smuggled goods to solve the problem of detection of events related to illegal crossing of the state border in wetlands, coastal areas and rivers was proposed. The system is based on the fusion of data from a variety of sensors for perimeter protection (acoustic, magnetic, microwave, pyroelectric) and optoelectronic observation systems (thermal imaging cameras and visible radiation cameras).

The developed system is characterized by autonomy, the ability to adapt to the ambient conditions and is resistant to possible attempts to emulate the sensors as well as the interference of unauthorized persons.

Acknowledgments: This work was supported by the National Centre for Research and Development under project DOB-BIO9/25/2018.

Design of Displacement Sensor Based on Fiber Bragg Grating for long-range extension measurement of pipeline compensators

E. MACIAK[1], W. KOSTOWSKI[2], G. GŁUSZEK[3], D. ADAMECKI[3], Z. OPILSKI[1], T. PUSTELNY[1]

[1] Department of Optoelectronics, Silesian University of Technology, 2 Krzywoustego St., 44-100 Gliwice, POLAND

[2] Department of Thermal Technology, Silesian University of Technology, 18 Konarskiego St., 44-100 Gliwice, POLAND

[3] Department of Mining Mechanization and Robotisation, Silesian University of Technology, 2 Akademicka St., 44-100 Gliwice, POLAND

e-mail address: erwin.maciak@polsl.pl

The expander is a maintenance-free compensator, which is designed as a freely movable construction for compensation of length changes to pipelines. The expander can be used for various pipes, including gas pipelines in subsidence areas, unstable areas, and mining areas, etc.

The objective of the work is to develop an effective and safe system for measurement extension and/or shortening expander in natural gas transmission pipelines by applying a non-invasive measurement and data transmission system based on fiber optic sensing technique, Fiber Bragg Grating (FBG) sensors. A special mechanical transducer have been applied onto conversion mechanism to transfer displacement to the deflection of the sensing element (cantilever), and the deflection-induced strain is exerted on FBGs. The system will improve the operational safety of gas transmission pipelines. It will also reduce the environmental footprint and decrease the cost of emergency pipeline works by minimizing the risk of a pipeline failure. The use of the fiber optic technology is the only solution suitable to meet the highest safety standards of the gas transmission network operator.

Fusion splicing and termination of silica hollow core anti-resonant fibers with single mode fibers

Y. MIN[1], A. FILIPKOWSKI[2,3], G. STĘPNIEWSKI[2,3], M. KLIMCZAK[2,3], L. ZHAO[1], R. BUCZYŃSKI[2,3]

[1] Jiangsu Normal University, School of Physics and Electronic Engineering, Xuzhou 221116, Jiangsu, China
[2] Łukasiewicz Research Network Institute of Electronic Materials Technology, Wólczyńska 133, 01-919 Warsaw, Poland
[3] University of Warsaw, Faculty of Physics, Pasteura 5, 02-093 Warsaw, Poland
e-mail address: *ryszard.buczynski@fuw.edu.pl*

Hollow-core fibers (HCF) have ultra-low Rayleigh scattering and nonlinear coefficients due to the use of air-guiding light mechanism which reduces the overlap of modes propagating in the core and in the cladding. Inhibited coupling fibers (ICF) and anti-resonant hollow core fibres (ARF) are two examples that are especially interesting. The first published information about ICFs involves the Kagomé fibers, developed in 2002 [1]. The principle of conducting light in ICF was described in [2] and showed a fundamental difference between guiding light using inhibited coupling and photonic bandgap (PBG).

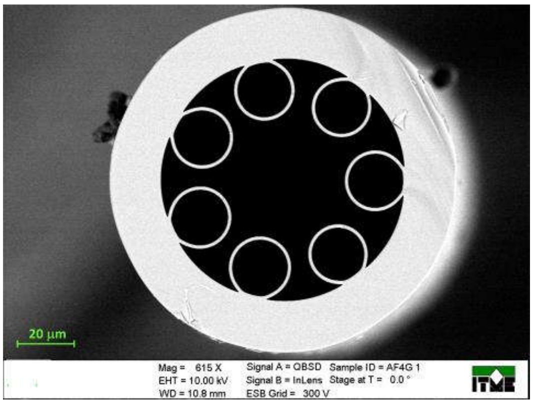

Fig. 1. SEM image of the ARF used in the experiment.

ARFs were demonstrated in 2011 [3] and can be considered as simplified ICF fibres, which consist of one ring of circular capillaries in the cladding (Fig. 1).

Over the past few years, several examples of the use of ARF for laser spectroscopy have been presented. Laser gas detection plays a large role in applications such as environment monitoring [4], medical sciences [5] or in controlling industrial processes [6]. In most gas detection techniques, sensitivity can be improved by increasing the length of the effective detection path, which can be done with hollow core fibers (HCF) filled with the gas being the subject of the study [7].

To efficiently use ARF in sensor devices, it is necessary to integrate these fibers with single or multimode fibers supplying light from lasers. Since ARFs have fine structure sensitive to thermal damage, their fusion splicing is non-trivial.

We performed a series of splices of SMF28 fiber to and in-house developed AR-HCF. For splicing we used the LDS 3sae “ring of fire” splicer which enables advanced control of splicing parameters, including arc duration at various temperatures, heating area offset from the splicing point, and distance of the fibers before splicing. It was observed that increasing the arc power and reducing the arc duration can easily damage the AR-HCF cladding capillaries. Additionally, the strength of the fiber depends on the softening time [8]. Decreasing arc power and increasing arc duration enables more durable splices. One of obtained splices is shown in Fig. 2.

Fig. 2. ARF-SMF splice observed under a microscope.

Tab.1. Splice parameters (LDS 3Sae)

Prefuse Duration	**Push Time**	**Fuse Time**	**ROF Splice Offset**
0.5s	0.3s	0.5s	145
Prefuse Power	**Push Power**	**Fuse Power**	**Push time**
600mW	750mW	790mW	45µm

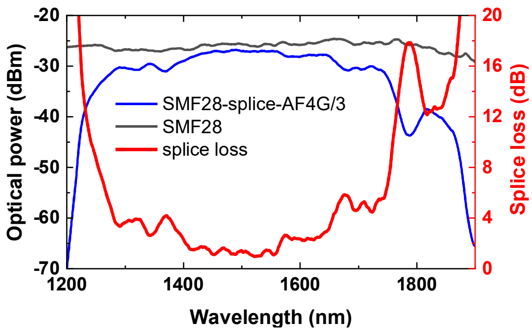

Fig. 3. Transmittance through SMF28 fiber (black line) and through spliced fibers SMF28 – AF4G/3 (blue line). Splice loss measured while light was coupled to SMF28 (red line).

To estimate coupling efficiency and splice loss for SMF28 to ARF splices, transmittance measurements were performed in a spectral range of 1200 – 2200 nm with use a supercontinuum source (Leukos) and an optical spectrum analyzer (Yokogawa). Measurement of the spliced fibers SMF28 – ARF labelled AF4G/3 showed loss of about 1.5 dB for the maximum of transmission window of the used ARF (1400 – 1600 nm). This result, shown in Fig. 3, was achieved while the SMF28 fiber was used as the input fiber. For the opposite direction of propagation, when ARF was the input fiber, the splice loss reached 10 dB (Fig. 4). This high loss results from low coupling efficiency (weak mode overlap) when light goes from 40 µm core of ARF to 9 µm core of SMF28, as well as from numerical aperture mismatch (ARF has several time smaller NA than SMF28).

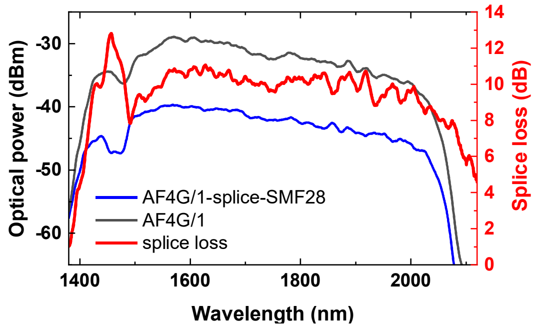

Fig. 4. Transmittance through ARF AF4G/1 (black line) and through spliced fibers AF4G/1 - SMF28 (blue line). Splice loss measured while light was coupled to ARF (red line).

Our preliminary tests have revealed that we were able to obtain reasonable quality of splice of ARFs and SMFs with loss below 1.5 dB.

References:

[1] F. Benabid et al. Science 298, 399 (2002).
[2] F. Couny et al. Science 318, 1118 (2007).
[3] A. D. Pryamikov et al., Opt. Express 19, 1441
[4] F. Köttig et al. Nature Commun. 8, 813 (2017).
[5] A. I. Adamu et al. Sci. Rep. 9, 4446 (2019).
[6] A. N. Kolyadi et al. Opt. Express 21, 9514 (2013).
[7] F. Yu et al. Opt. Express 20, 11153 (2012).
[8] J. H. Chong and M. K. Rao, Opt. Express 11, 1365

Effects of cladding modification tapered optical fiber on optical properties of propagated light

J.MOŚ[1], K. A. STASIEWICZ[1], L.R. JAROSZEWICZ[1]

[1] Military University of Technology, Institute of Technical Physics,
gen. Sylwestra Kaliskiego 2, 00-908 Warsaw, Poland
e-mail address: *joanna.mos@wat.edu.pl*

One of very important physical phenomenon for tapered optical fiber is evanescent wave [1-2]. Nowadays, it is widely described and used for sensor application. It due to with change in the optical properties of light propagated in taper waist area which is strongly dependent on the refractive index of the environment or surrounding material. Development of that device determine a connection of optical fiber technology with special material. Properties of this material should enable control refractive index for external factor – temperature, pressure, humidity etc. [3-8].

In this research, the sensing area of tapered optical fiber was surrounded by mixtures of liquid crystal and 0,1% wt. nanoparticles of gold. The refractive index can be controlled by temperature, electric or magnetic field. Cell was built by special glasses with ITO layer and alignment of liquid crystal layer. Twist orientation on molecules of liquid crystal was applied. Optical spectrum analysis for the wavelength range of 550–1200 nm and time-courses at the temperature range of T = 25–60 °C for a steering voltage in the range of 0–200 V were provided.

Acknowledgments: This work was supported by the National Science Centre, grant number UMO-2018/29/N/ST7/02347

References:

[1] Zhili Li et. al., Sensors and Actuators B: Chemical 248, (2017)
[2] Gilberto Brambilla, Journal of Optics, 12, (2010)
[3] Shan Zhu et. al., Proc. of SPIE 8311, (2011)
[4] Cándido Bariáin et. al., Sensors and Actuators B Chemical, 69, 1-2, (2000)
[5] Candido Bariain et. al., Optical Engineering 39,8, (2000)
[6] Limin Tong et. al., Optics Express 12, 6, (2004)
[7] Hamid Lati et. al., Photonic Sensors 2,4, (2012)
[8] Pavel Polynkin et. al., Optics Letters, 30, 11, (2005)

The use of silk fibroin in a fiber optic humidity sensor

Z. OPILSKI [1], M. PROCEK [1], S. AZNAR-CERVANTES [2], L. CENIS [2], , M. BARBEL [3]

[1] Silesian University of Technology, Department of Optoelectronics, 2 Krzywoustego Str., 44-100 Gliwice, Poland

[2] Inst. Murciano Invest. & Desarrollo Agr. & Alimentar, La Alberca 30150, Murcia, Spain

[3] CSIC, Inst. Microelect. Barcelona, CNM, Bellaterra 08193, Barcelona, Spain

e-mail address: zbigniew.opilski@polsl.pl

The article presents the properties of silk fibroin (SF), which enabled the construction of a fiber optic relative humidity sensor. The presented sensor operates based on the Fabry-Perot interferometer built at the end of a standard multimode telecommunications fiber. In research, a broadband light source (xenon lamp) was used to illuminate the interferometer. This allowed the study of the spectral characteristics of the sensor and their changes due to changes in ambient humidity causing changes in the optical path in the resonator. The technology of preparing sensing layer was presented. Then, work focused on choosing the method of detecting the measurement signal and measuring selected sensor measurement characteristics. Moisture sensitivity characteristics as well as the measured response and sensor regeneration times were selected for the presentation.

The importance of monitoring the vergence eye movements for solutions using virtual technologies

M. PISZCZEK[1], M. POMIANEK[1], M. MACIEJEWSKI[1], L. JODŁOWSKI[1], P. KRUKOWSKI[2]

[1] Institute of Optoelectronics, Military University of Technology,
2 Kaliski Str., 00-908 Warsaw, POLAND
[2] RemmedVR sp. z o.o., 47/10 Domaniewska Str., 02-672 Warsaw, POLAND
e-mail address: marek.piszczek@wat.edu.pl

The human eye has several features that enable it to perform its basic functions: shape recognition, color differentiation and stereoscopic vision that enables the assessment of the position of objects in space.
Recently, a special interest of researchers has been focused on eye-tracking due to the possibility of amblyopia treatment or communication with a computer using sight.

The basis for solving the above problems is to monitor the convergence of vision. From the point of view of the human visual system, the eye's vergence movements are closely linked to accommodation. This fact has a very important meaning and implications. Therefore, research on vergence may concern physiological, technical and functional aspects.

The physiological aspect is, above all, the ability to correctly reproduce the mechanism of spatial vision in virtuality. Unfortunately, the majority of commercially available 3D VR/AR goggles are solutions that use only the vergence mechanism. In the literature, this phenomenon is known as the Vergence-Accommodation Conflict. Incorrect functioning of the accommodation mechanism causes discomfort in the reception of virtual space. This problem becomes particularly important for the development of VR goggles dedicated to the therapy of amblyopia when the patient's involvement in computer games is used.[1]. Therefore, one of the essential elements of the works conducted by the authors is the possibility of monitoring eye vergence and confronting it with the "accommodation distance".

The technical aspect is mainly hardware and software ways of measuring eye vergence. The most popular solution today is eye-tracking based on the analysis of images from the video system. For this purpose, the eye is illuminated with infrared light, and on the basis of the analysis of the illuminators' reflections on the surface of the eyeball, the gaze point is calculated[2]. More complex systems consist of up to 3 cameras observing the eye, which is illuminated by a 6-10 point source[3]. Such methods require high computing power and thus become difficult to implement in mobile devices.
One possibility to solve this problem is to delegate complex tasks to external computing units as well as to use other measurement methods. In the field of eye vergence monitoring, this alternative can be, among others, position-sensitive detectors or optical scanning systems based on 2D mirror MEMS. The above-mentioned solutions can offer high speed of operation with a significant reduction of calculation requirements.
An important element of the work carried out by the authors is the comparison of the measurement and implementation capabilities of the above-mentioned solutions with the classic vision eye-tracking.

The utility aspect is an indication of new functionalities resulting from the knowledge of momentary values of the eye fixation point. First of all, this expansion of the HMI in the field of interactive possibilities. In a virtual environment, we are able to imitate the activities performed by a human in the physical world and even expand them, including just through visual interaction.

Monitoring of eye vergence movements is crucial for developing this type of HMI. If we interact with virtual objects, we can trigger their specific reactions. e.g. display information about them, and if they are elements of a GIU program, you can affect the functioning of such an application.[4].

You can also explore the real world using the "eye-gaze" HMI. The integration of a stereoscopic vision system with a virtual environment allows, for example, to perform spatial analysis of objects of the physical world. One of the areas of work carried out by the authors is the expansion of the HMI interface arsenal based on the use of virtual technologies.

The above examples show how important optoelectronic systems are for virtual technologies. At the same time, they point to the importance and multi-facetedity of issues regarding monitoring of eye vergence movements.

Acknowledgments: This work was supported by Project "RemmedVR device for home vision therapy".

References:

[1] Jessica D. Bayliss et. al., Lazy Eye Shooter: a Novel Game Therapy for Visual Recovery in Adult Amblyopia,2012 IEEE International Games Innovation Conference,

[2] Patent US 2008/0049185 A1, EYE LOCATION AND GAZE DETECTION, Feb. 28, 2008

[3] Patent US 8,929,589 B2, SYSTEMS AND METHODS FOR HIGH-RESOLUTION GAZE TRACKING, Jan. 6, 2015

[4] Thomas E. Hutchinson, Human- Computer Interaction Using Eye-Gaze Input, IEEE TRANSACTIONS ON SYSTEMS, MAN, AND CYBERNETICS, VOL. 19, NO. 6, NOVEMBER/DECEMBER 1989 pp 1527-1534

The stability of the MEMS 2D mirror's operating point in terms of eye tracking systems

M. POMIANEK[1], M. PISZCZEK[1], M. MACIEJEWSKI[1], L. JODŁOWSKI[1], P. KRUKOWSKI[2]

[1] Institute of Optoelectronics, Military University of Technology,
2 Kaliski Str., 00-908 Warsaw, POLAND
[2] RemmedVR sp. z o.o., 47/10 Domaniewska Str., 02-672 Warsaw, POLAND
e-mail address: *mateusz.pomianek@wat.edu.pl*

Eye tracking systems are now largely based on video analysis. In the case of mobile devices, however, this solution is proving to be quite a burden for the stand-alone computing units that exist there. One of the trends in solving this problem is to develop other eye tracking methods. One of them is 2D MEMS mirror. They allow for high angle measurement accuracy[1]. An example of such a mirror by OPUS Microsystems (model OP-6111) is shown in Figure 1.

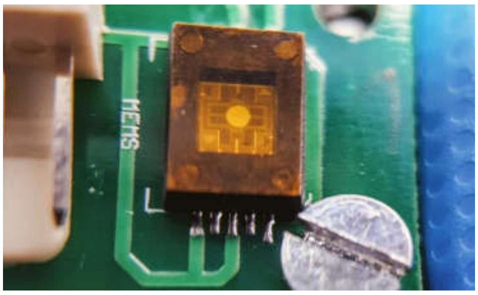

Fig.1. OP-6111 mirror by OPUS

The module is designed to scan in Lissojous mode on two frequencies 22 and 1.4 kHz, providing scanning at +- 20 and 15 angles[2]. It scans the eye area with a laser beam. The laser is picked up by the detector after the reflection from the eye surface. Depending on the level of the return signal, the position of the eye pupil (the lowest signal) is determined. For such a system to work optimally, it is necessary to select the scanning field in a way that it covers the full area of the human eye. Improper selection of these parameters results in reduced resolution of the pupil position detection and increased scanning time.

To determine the optimum operating point for MEMS 2D mirrors, it is necessary to determine the stability of the system. An example of the OP-6111 stability chart at 3316Hz slow axis frequency is shown in Figure 2.

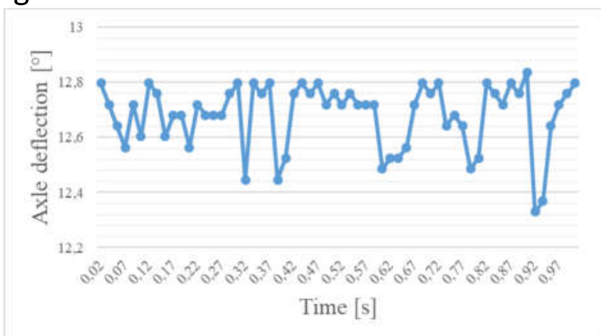

Fig.2. Stability of the slow axle

This publication is focused on the stability research of the OP-6111 mirror. The aim of the studies is to determine the scope of optimal work for eye tracking systems.

Acknowledgments: This work was supported by Project "RemmedVR device for home vision therapy".

References:

[1] Junya Wang et. al., “UKF-based MEMS micromirror angle estimation for LiDAR” J. Micromech. Microeng. 29 (2019) 035005 (9pp).
[2] http://www.opusmicro.com/products.html

Sensing applications of LC:PDMS photonic systems

K.A. RUTKOWSKA[1], P. SOBOTKA[1], SZ. BACZYŃSKI[1], K. MARCHLEWICZ[2], A. DYBKO[2]

[1]Faculty of Physics, Warsaw University of Technology, Koszykowa 75, 00-662 Warszawa
[2]Faculty of Chemistry, Warsaw University of Technology, Noakowskiego 3, 00-664 Warszawa
e-mail address: *katarzyna.rutkowska@pw.edu.pl*

Polydimethylsiloxane (PDMS), also known as dimethylpolysiloxane, is characterized by high optical transparency and low surface energy. Therefore it is widely recognized as a functional, high-quality organic material for optofluidic systems [1]. The most important advantage of PDMS in terms of practical implementation is its cheap and easy processing. Actually, PDMS-based photonic devices are usually fabricated with use of replica molding techniques. Superior rheological properties of PDMS in a liquid form allows for copying and reproducing fine-sized features. In this way, complex microstructures can be successfully manufactured in such flexible polymeric substrates at much lower cost in comparison to traditional glass- or semiconductor-based components for integrated optical systems.

In principle, air-channels formed in PDMS material can be additionally filled with other liquid materials. In this work traditional fluids employed in optofluidics is replaced with liquid crystals (LCs). Advantage of proposed solution stems from application of such strongly anisotropic and hi-tech materials, whose properties can be easily tuned by external electric field. In this context electrical tuning along with specific polarization properties of LC:PDMS elements are easy to be demonstrated, what means that prospective devices of this type can find their potential use as threshold sensors of the electric field.

In this communication different cheap and efficient methods for mold fabrication are presented and compared. In addition, possibility of eutectic liquid electrodes application is shown.

References:

[1] A.R. Hawkins, H. Schmidt, Handbook of Optofluidics, CRC Press 2010.

Methodology for assessing near-infrared absorption properties of historical materials and microorganisms from objects in the collections of the Auschwitz-Birkenau State Museum in Oświęcim

D. RYBITWA[1], E. MACIAK[2], M. PROCEK[2], P. KAŁUŻYŃSKI[2], A. WAWRZYK[1]

[1] Auschwitz-Birkenau State Museum, Więźniów Oświęcimia 20, 32-603 Oświęcim, Poland
[2] Department of Optoelectronics, Silesian University of Technology,
2 Krzywoustego St., 44-100 Gliwice, POLAND

The Auschwitz-Birkenau State Museum in Oświęcim, Poland (A-BSM), a former German Nazi Concentration and Extermination Camp, collects and protects thousands of movable objects of special nature, purport and symbolism. These are mainly personal possessions brought by prisoners sentenced to extermination and found at the campsite after liberation, such as: shoes, clothes, tallisim, suitcases, kitchen utensils, prostheses and brushes. The collections include also objects related to the everyday existence of prisoners in the camp, e.g. striped camp garments, clogs, patches, pots, bunks and boards, and items connected with the SS crew, e.g. helmets, guard boots, collar patches, whips, clubs and camp records. The post-camp relics are made of different materials, both natural of plant and animal origin (fabric, leather, wood) as well as artificial (vulcanised fibre, cardboard, paper, artificial leather) or synthetic (rubber, metal). Due to the low quality of these objects, and damages associated with their usage, they are often torn and patched, and therefore extremely susceptible to deterioration caused by process of natural ageing and growth of microorganisms. Metabolites produced by microorganisms inhabiting historical objects may also contribute to discoloration of materials and weakening of their mechanical properties, so one of the conservation issues is the adaptation of appropriate disinfection techniques.

In order to disinfect very small surfaces which were microbiologically contaminated and limiting unnecessary disinfection of the whole object, a new research has been started on the suitability of a medical diode laser with a wavelength of 810 nm for disinfection of historical objects from the A-BSM. This study aims to assess near-infrared absorption properties of the most common historical materials in A-BSM, as well as microorganisms found on their surfaces.

Fabrication aspects of silicon nitride photonics integrated circuits

M. SŁOWIKOWSKI[1.2], M. LELIT[1,2], M. JUCHNIEWICZ[1], B. STONIO[1,2], B. MICHALAK[1], M. FILIPIAK[1], K. PAVŁOV[1], P. WIŚNIEWSKI[1,2], S. STOPIŃSKI[2], R. PIRAMIDOWICZ[2], R. B. BECK[1,2]

[1] Warsaw University of Technology, Centre for Advanced Materials and Technologies CEZAMAT, Poleczki 19, 02-822 Warsaw, Poland

[2] Warsaw University of Technology, Institute of Microelectronics and Optoelectronics, Koszykowa 75, 00-662 Warsaw, Poland

e-mail address: *mateusz.slowikowski@pw.edu.pl*

Photonic integrated circuits (PICs) have been present for a significant time in telecom and sensing applications [1,2]. Nowadays, the majority of the PIC-based systems operate in the wavelength range around 1550 nm. However, for some applications, such as lab-on-chip or bio-photonics, visible wavelengths are more adequate [3]. In such applications, the silicon platform, in which the signal transmission range starts from 1100 nm, is not useful, unlike the silicon nitride platform, which has a transmission window starting from 400 nm.

Silicon nitride has a refractive index of ca. 2.0, compared to silicon with an index of ca. 3.5. This results in a smaller difference of refractive indices comparing to silicon oxide ($n \approx 1.5$) and bigger footprints of designed elements, which projects directly on final dimensions of the photonic circuits. On the other hand, such circuits are more immune to inaccuracies and imperfections of the manufacturing process, which allows using less sophisticated and less expensive technological processes for their fabrication.

In this work we present and discuss the selected aspects of manufacturing integrated photonic elements using silicon nitride technological platform, being currently developed in CEZAMAT laboratories. A first series of testing structures has been successfully designed and manufactured to verify the potential of the developed technology.

All fabricated chips were designed as multimode, which resulted in larger dimensions of the waveguide cross-section. The Film Mode Matching (FMM) and Finite Difference (FD) methods were used for the simulations. Based on the results of simulations layouts of test structures were designed.

A library of technological processes has been developed with the use of designed layouts, which allows the fabrication of core passive photonic components: waveguides, multimode interferometers (MMI) and arrayed waveguide gratings (AWG). The dedicated process flow based on standard CMOS processes has been developed, consisting of the following steps: wafer surface preparation, oxide growth, silicon nitride deposition, resist application, lithography, development, dry etching, oxide deposition and separation of chips. The SEM image of the cross-section of a fabricated waveguide is shown in Fig. 1.

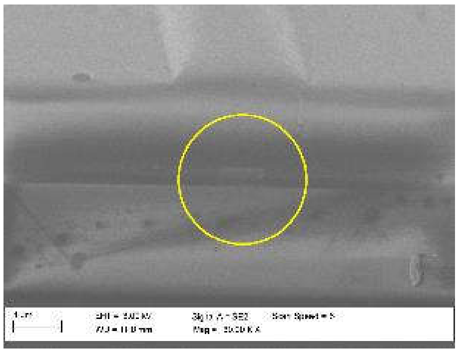

Fig. 1. SEM image of waveguide cross-section, marked silicon nitride part.

The composition and thickness of the layers in the cross-section starting from the bottom is as follows: silicon substrate, 2.3 µm thick silicon oxide, 320 nm of silicon nitride (guiding layer) and 2.3 µm of silicon oxide. Due to the use of low pressure chemical vapor deposition (LPCVD) for bottom silicon oxide and silicon nitride, and plasma-enhanced chemical vapor deposition (PECVD) for top silicon oxide, it was possible to shape the thickness of these layers with a nanometer resolution. The use of the electron beam lithography allowed transfer of the layout to the resist with a similar accuracy. Nevertheless, it is still possible to improve these results by further optimization of electron beam lithography and plasma etching processes. The exemplary results are shown in Fig. 2.

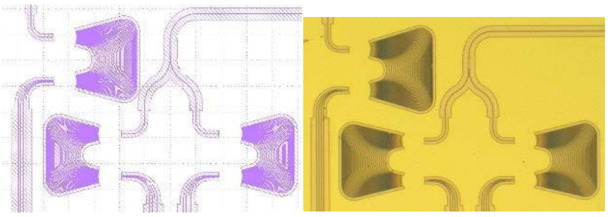

Fig. 2. Top – part of designed layout, bottom - fabricated AWGs.

Testing showed average optical power losses in waveguides between 1.7 and 3.7 dB/cm. For the 1×2 MMI, the distribution of optical power between the outputs is comparable and the level of loss for a single output is not higher than 6 dB. Fabricated AWGs have cyclic spectral characteristics, the measured channel spacing and free spectral range are close to the design values.

The obtained results are considered promising and current work is focused on development of light coupling gratings, thermal modulators and trenches for microfluidics. Further optimization of previously developed processes is carried out in parallel.

Acknowledgments: This work was supported by the National Centre for Research and Development (project OPTO-SPARE, grant agreement PBS3/B9/41/2015).

References:

[1] Doerr, C. R. Silicon photonic integration in telecommunications. Front. Phys. 3, 1–16 (2015).

[2] Welch, D. F. et al. Large-scale InP photonic integrated circuits: Enabling efficient scaling of optical transport networks. IEEE J. Sel. Top. Quantum Electron. 13, 22–29 (2007).

[3] Porcel, M. A. G. et al. Silicon nitride photonic integration for visible light applications. Opt. Laser Technol. 112, 299–306 (2019).

Optical properties of one-dimensional tin oxide nanostructures

W.SMOK[1], W.MATYSIAK[1], T. TAŃSKI

[1]Department of Engineering Materials and Biomaterials, ul. Konarskiego 18A, 44-100 Gliwice, Poland
e-mail address: *weronika.smok@polsl.pl*

Gas sensors based on semiconductor metal oxides (MOS) are widely used in many areas, which include the control of chemical pollution in the air and rooms, alarms of hazardous substances, and even medical diagnostics based on the patient's breathing. The popularity of this type of sensors is due to their high sensitivity, low cost and simplicity of manufacture, as well as compatibility with modern electronic devices. One of the most commonly considered MOS is tin dioxide, which is characterized by simultaneous optical transparency and electrical conductivity, an energy gap width of approx. 3.6 kV and high sensitivity. In recent years, many attempts have been made to improve the SnO2 sensory properties, including design of sensors based on one-dimensional nanostructures of this material, such as nanofibers, nanotubes or nanowires. One of the simpler methods of producing one-dimensional tin oxide nanomaterials is to combine the solution electrospinning method with a sol-gel process [1-4].

Zhang et al. he used the electrospinning process to produce PVA/SnCl4 nanofibers which, after calcining in the form of SnO2 nanofibers, was used to build the ethanol sensor. The tests showed high sensitivity, fast response time and high repeatability [5]. Sensors based on coreless SnO2 nanofibers manufactured by W. Q. Li et al. Also showed high sensitivity to detect ethanol, acetone, methanol and acetic acid [6].

The purpose of this work was to produce SnO2 nanowires using a hybrid electrospinning method combined with the sol-gel process and to analyze the morphology, structure and optical properties of one-dimensional nanomaterials produced in this way.

First, solution of PVP/DMF/EtOH/SnCl4·5H2O was prepared, with a weight ratio of PVP:SnCl4·5H2O equal to 1:3. Then the obtained solution was directly subjected to the electrospinning process with constant parameters shown in Tab. 1.

Tab. 1. Electrospinning parameters.

Parameter	Value
Flow rate [ml/h]	0.25
Voltage [kV]	24
Distance between the electrodes [cm]	15

The composite nanofiber polymer-precursor mat obtained in this way was subjected to a calcination process at 600 °C for 10 hours to degrade the organic phase as presented in the Fig. 1.

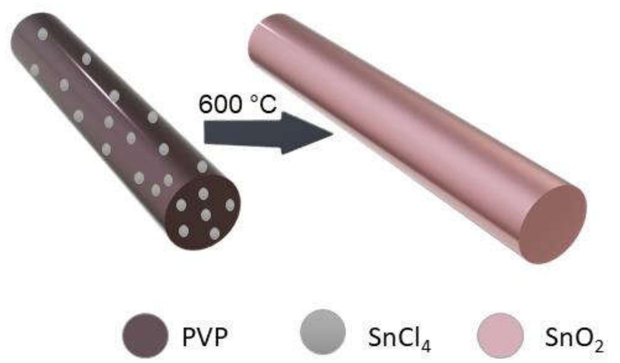

Fig. 1. Schematic representation of the temperature effect on the morphology of nanofibers

Morphology analysis using SEM showed that composite PVP/SnCl4 nanofibers were obtained as a result of electrospinning (Fig. 2).

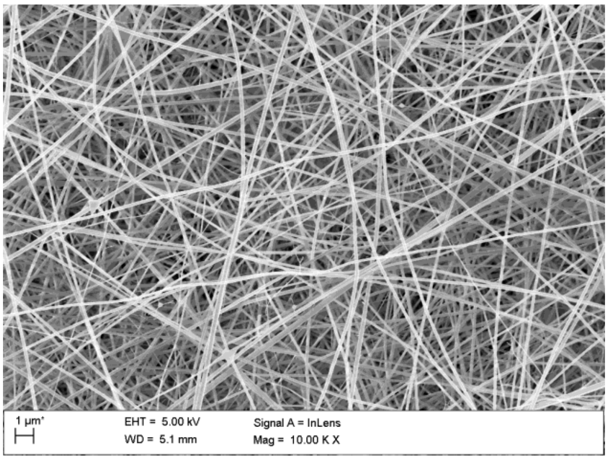

Observation of nanofibers after calcination showed that smooth, defect-free SnO_2 nanotubes were obtained as presented in the Fig. 3.

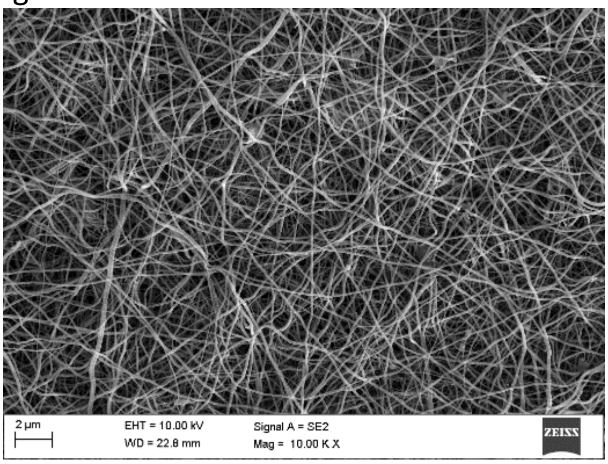

Summing up, using the electrospinning method, PVP/$SnCl_4$ composite nanofiber mats were produced from the solution, which were transformed into SnO_2 nanofibers as a result of heat treatment.

Acknowledgments: This work was supported by the National Science Centre, Poland based on the decision number 2016/23/B/ST8/02045.

References:

[1] B. Bahrami et. al., Sensors and Actuators B: Chemical 133, 1, (2008)
[2] X. Gao et. al., Sensors and Actuators B: Chemical, 277, 20, (2018)
[3] W. Ge et. al., Journal of Alloys and Compounds, 746, (2018)
[4] M. Zhang et. al., Materials Science and Engineering: B, 209, (2016)
[5] Y. Zhang et. al., Sensors and Actuators B: Chemical, 141, 1, (2009)
[6] W. Q. Li et. al., Materials Letters, 132, (2014)

Numerical analysis of integrated photonics structures obtained by FDTD method

P. STRUK[1]

[1] Department of Optoelectronics, Faculty of Electrical Engineering, Silesian University of Technology, 2 Krzywoustego Str., 44-100 Gliwice, Poland.
e-mail address: Przemyslaw.Struk@polsl.pl

The Author presents theoretical analysis focused on optimization of the integrated photonics structure for sensors applications. The numerical analysis were focused on design of grating coupler for applications in sensor structure intended for determination of physical properties of biological liquids materials - refractive index. The analysis were focused on determination of optimal parameters of the grating coupler in particular spatial period L and depth of grooves d_G for obtain maximum sensitivity of refractive index detection as well as for optimization of uncoupling the light out of the structure towards the detector.

The numerical analysis of the sensor structure with grating coupler was carried out by Finite Difference Time Domain method (FDTD).

Acknowledgments: This work was supported by grant 05/040/RGJ20/2003 (pro-quality grant) financed by Silesian University of Technology in Gliwice, Poland.

References:

[1] Struk, P., Materials 12(1), 175, 1-15 (2019).
[2] P. Struk, Proc. of SPIE, Vol. 11204 1120402-1 (2019)

Evanescent wave transducers based on grating couplers embossed in silica-titania waveguide films

C.TYSZKIEWICZ[1], P. KARASIŃSKI[1], A. KAŹMIERCZAK[2]

[1] Department of Optoelectronics, Silesian University of Technology,
2 Krzywoustego Str. 44-100 Gliwice, Poland
[2] Institute of Microelectronics and Optoelectronics, Warsaw University of Technology, 75 Koszykowa Str. 00-662 Warszawa, Poland
e-mail address: cuma.tyszkiewicz@polsl.pl

The fast development of planar evanescent waveguide sensors can be mainly attributed to the research team of W. Lukosz. Among the others, they developed planar sensor structures using grating couplers [1]. A number of other research groups were inspired by the results obtained by Lukosz, to initiate studies on planar waveguide sensors. Apart from a contribution of the research team led by Lukosz to the development of planar evanescent wave sensors, contributions given by Kunz [2], Brandenburger [3], Szendrõ [4] and Lambeck [5] are noteworthy. In Poland, the research works involving planar evanescent wave sensors have been concentrated at the Silesian University of Technology [6]. This work concerns planar waveguide evanescent wave transducers using grating couplers embossed in SiO_2:TiO_2 waveguide films. These films have high refractive index (~1.8) and their perfect optical properties make them suitable for application in the technology of planar optical waveguide sensors. It has been shown that using grating couplers having a period of Λ=800 nm it is possible to excite the fundamental waveguide mode in the first, second and even third diffraction order. The excitation in the second and third diffraction order is taking place with the negative coupling angles, and in the first diffraction order the structure is excited with the positive angle. It was shown that it is possible to excite the waveguide mode in the second diffraction order for two incoupling angles of the same magnitude but the opposite sign and in the first diffraction order for one incoupling angle. This way, exploiting symmetry, it is possible to determine precisely the location of the zero angle on coupling characteristics, and thereby from the position of a coupling peak corresponding to the first diffraction order one can determine refractive index of the medium covering the structure.

Acknowledgments: This work was supported by National Centre for Research and Development in Poland under Grant 05/040/TAN19/0031

References:

[1] Embossing technique for fabricating integrated optical components in hard inorganic waveguiding materials, Opt. Lett. 8 (1983) pp. 537-539.
[2] R.E. Kunz, J. Dübendorfer, R.H. Morf, Finite grating depth effects for integrated optical sensors with high sensitivity, Biosens. Bioelectron. 11 (1996) pp. 653-667.
[3] A. Brandenburg, R. Polzius, F. Bier, U. Bliltewski, E. Wagner, Direct observation of affinity of reactions by reflected mode operation of integrated optical grating coupler, Sensor and Actuators B 30 (1996) pp. 55-59.
[4] I. Szendrõ, Art and practice to emboss gratings into sol-gel waveguides, Proc. SPIE 4284 (2001) pp.80-87.
[5] P.V. Lambeck, "Integrated optical sensors for the chemical domain", Meas. Sci. Technol. 17 (2006) pp. R93-R116.
[6] P. Karasiński, "Embossable grating couplers for planar evanescent wave sensors", Opto-Electron. Rev., 19(1) (2011) pp. 10-21

Chromatic dispersion engineering in nanostructured graded-index silica fiber tapers for supercontinuum generation

J. ZHOU[1], A. FILIPKOWSKI[2,3], G. STĘPNIEWSKI[2,3], D. MICHALIK[2,3], M. KLIMCZAK[2,3], L. ZHAO[1], R. BUCZYŃSKI[2,3]

[1] Jiangsu Normal University, School of Physics and Electronic Engineering, Xuzhou 221116, Jiangsu, China
[2] Łukasiewicz Research Network Institute of Electronic Materials Technology, Wólczyńska 133, 01-919 Warsaw, Poland
[3] University of Warsaw, Faculty of Physics, Pasteura 5, 02-093 Warsaw, Poland
e-mail address: *ryszard.buczynski@fuw.edu.pl*

There is a demand for new types of optical fibers with enhanced bandwidth for telecommunications or for designing new types of sensors with superior sensitivity compared to existing solutions [1]. Currently, fiber optics fabrication is dominated and determined by performance of Modified Chemical Vapor Deposition (MCVD) and other variations of CVD preform fabrication [2]. These techniques limit the design flexibility for fibers to rotational (or elliptical) symmetry [3]. In MCVD processes, the usable materials and dopant levels of silica glass are very narrow, which limits obtaining fibers with arbitrary refractive index profile [4]. Because of these limitations, single-mode graded-index fibers have never been considered as a viable dispersion engineered medium.

In nonlinear fiber optics, an intriguing design methodology for chromatic dispersion and mode properties exists in the form of tapering [5]. Here, we take a previously demonstrated nanostructured, graded-index silica single mode fiber and taper it using a computer-controlled splicing/tapering rig (LDS 3 Sae) [6].

The fiber sample used in this study is an all-solid silica fiber with a homogeneous cladding and a nanostructured graded index (nGRIN) core, as shown in scanning electron microscopy image in Fig. 1. The refractive index profile of the core has been designed by a stacking silica and Ge-doped silica rods in predetermined pattern, with a refractive index contrast of $\Delta n = 12 \times 10^{-3}$. The geometric dimensions of the used nGRIN fiber were also comparable to the SMF-28, with 9 µm core diameter and 125 µm outer diameter. The fiber sample used in this work was uncoated for easy of processing at the tapering rig.

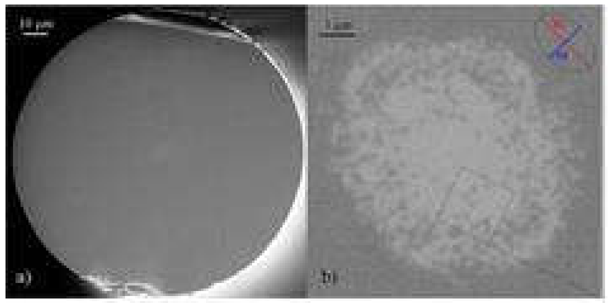

Fig. 1. (a) SEM image of the fabricated fiber, (b) SEM image of the fiber core.

Despite complex internal structure, the fiber subjects to mechanical cleaving, using standard tools. Cleaved fiber samples of 20 cm length were placed in the tapering rig and tapered around the middle length point. The tapered section was 1 cm long, excluding the down- and up-tapered sections, which were about 2.5 mm each, as shown in Fig. 2. Three taper structures were fabricated, with the taper waists of 100 µm (sample 1), 70 µm (sample 2) and 40 µm (sample 3). The length of the entire sample was selected both for the ease of handling, as well as in order to facilitate chromatic dispersion measurement using a Mach-Zehnder interferometer.

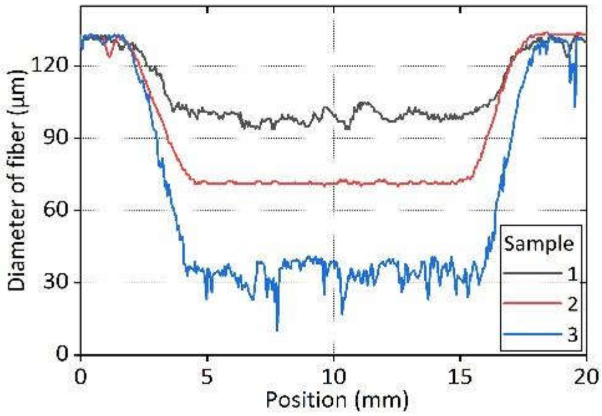

Fig. 2. Fabricated taper samples geometry, as measured at the tapering rig.

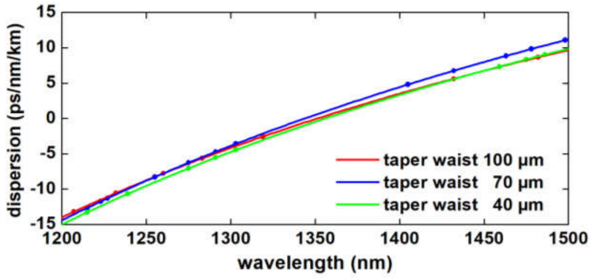

Fig. 3. Measured chromatic dispersion profiles of the nGRIN fiber tapers.

Results of these measurements are shown in Fig. 3. Each of the structures shows a zero dispersion (ZDW) wavelength around 1300 nm, because the SMF-28 dispersion dominates the structure, while the taper section strongly modifies it only over a short sample length. Next, we performed supercontinuum generation experiments with the tapers. Short sample lengths motivated femtosecond pumping, and a Menlo Systems Blue Cut laser has been used (400 fs, 1030 nm center wavelength, 10 MHz). Results are shown in Fig. 4. Spectral broadening has been observed only in the smallest waist tapered section, which we preliminarily attribute to enhanced nonlinearity of the structure. Limited spectral broadening stems from unfavorable dispersion conditions.

Obtained initial results confirm, that the nGRIN fibers reported earlier [6] can be successfully tapered despite their structural complexity, and that they can be used in nonlinear optics experiments. Longer taper sections are planned to better control dispersion profile and enhance nonlinear optics performance in operation with erbium fiber-based femtosecond lasers.

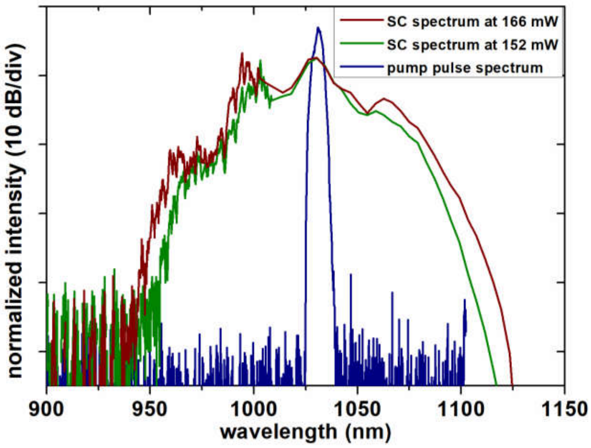

Fig. 4. Pump pulse and SC spectra recorded in experiment with the 40 μm waist taper.

References:

[1] M. Ferreira et al. Optical Fibers: Technology, Communications and Recent Advances Nova Science Publishers, Inc, London, 2017.
[2] K. Oh & U.-C. Paek, Silica Optical Fiber Technology for Devices and Components: Design, Fabrication, and International Standards, Wiley; 1 edition, USA (2012).
[3] H. Okazaki et al. Commun. Jpn 65-C (1982).
[4] K. Himeno et al. J. Lightw. Technol. 23, 3494 (2005).
[5] P. Falk et al. Optics Express 13, 7535 (2005)
[6] A. Anuszkiewicz et al., Sci. Rep. 8, 12329 (2018).

TABLE OF CONTENTS